



LAWRENCE  
LIVERMORE  
NATIONAL  
LABORATORY

# Non-cratonic diamonds from UHP metamorphic terranes

L. F. Dobrzhinetskaya, E. F. OBannon, H. Sumino

August 24, 2020

Reviews in Mineralogy and Geochemistry

## **Disclaimer**

---

This document was prepared as an account of work sponsored by an agency of the United States government. Neither the United States government nor Lawrence Livermore National Security, LLC, nor any of their employees makes any warranty, expressed or implied, or assumes any legal liability or responsibility for the accuracy, completeness, or usefulness of any information, apparatus, product, or process disclosed, or represents that its use would not infringe privately owned rights. Reference herein to any specific commercial product, process, or service by trade name, trademark, manufacturer, or otherwise does not necessarily constitute or imply its endorsement, recommendation, or favoring by the United States government or Lawrence Livermore National Security, LLC. The views and opinions of authors expressed herein do not necessarily state or reflect those of the United States government or Lawrence Livermore National Security, LLC, and shall not be used for advertising or product endorsement purposes.

1 **Reviews in Mineralogy & Geochemistry**

2

3 **Non-cratonic diamonds from UHP metamorphic terranes**

4

5

**Larissa Dobrzhinetskaya**

6

*Department of Earth and Planetary Sciences, the University of California at Riverside,*

7

*900 University Ave, Riverside, CA 92521, USA*

8

*larissa@ucr.edu*

9

10

**Earl F. O'Bannon III**

11

*Physical and Life Sciences, Physics Division, Lawrence Livermore National Laboratory,*

12

*Livermore, CA 94550, USA*

13

14

**Hirochika Sumino**

15

*Department of General Systems Studies, Graduate School of Arts and Science,*

16

*the University of Tokyo, 3-8-1 Komaba, Tokyo, Japan*

17

18

19 **Contents**

20

21 **ABSTRACT**

22 **INTRODUCTION**

23 **DIAMONDS FROM ULTRAHIGH PRESSURE METAMORPHIC TERRANES**

- 24 • **The history of microdiamond discoveries in the Kokchetav massif,**  
25 **Kazakhstan**
- 26 • **New microdiamond localities discovered between 2011-2020**
- 27 ○ *Ceské Stredohorí, Stráž nad Ohří, Plesovice and Gfohl areas of*  
28 *Bohemian massif, Central Europe*
- 29 ○ *Microdiamonds in detrital garnets from Erzgebirge, Germany*
- 30 ○ *The Betic and Rif Cordilleras, NW Africa and SE Spain*
- 31 ○ *Straumen localiy of Western Gneiss Region, Norway*
- 32 ○ *Tonsvika area, Tromso nappe, the northern Norwegian Caledonides*
- 33 ○ *Jämtland and Årescutan areas, the Sweden Caledonides*
- 34 ○ *Diamonds from Lago di Cignana, Italy, Western Alps*
- 35 ○ *Diamonds from Pohorje (Slovenia) in the Austro-Alpine UHPM terrane,*  
36 *Eastern Alps*
- 37 ○ *More diamonds from Qinling region, China*
- 38 ○ *Graphitized diamond in West Greenland UHPM terrane*
- 39 ○ *The Western Mediterranean orogen – the Edough Massif, NE Algeria,*  
40 *new UHPM terrane*
- 41 ○ *Diamonds from Nishisonogi unit, Nagasaki metamorphic complex,*  
42 *western Kyushu, Japan*
- 43 • **Lonsdaleite from WGR, Norway and Kokchetav massif, Kazakhstan and a**  
44 **problem with its identification**
- 45

46 **ISOTOPIC STUDIES OF UHPM DIAMONDS**

- 47 • **Carbon and nitrogen isotopes, and nitrogen contents in UHPM diamonds**
- 48 ○ *Carbon isotopes characteristics of the Kokchetav diamonds*
- 49 ○ *Carbon isotope characteristics of the Erzgebirge diamonds*
- 50 • **Noble gas isotopes in diamonds from UHPM terranes**
- 51 ○ *“Unprecedentedly” high helium-3 content in the Kokchetav diamonds:*  
52 *myth or reality?*
- 53

54 **MECHANISMS OF METAMORPHIC DIAMOND FORMATION**

- 55 • **UHPM diamonds crystallized from a multicomponent supercritical C-O-H**  
56 **fluid or a hydrous silicate melt**
- 57 • **Oxidation state of UHPM diamond crystallization**
- 58 • **UHPM diamond formation under metastable conditions**
- 59 • **Comet impact hypothesis for the origin of diamonds from Kundy Kol Lake,**  
60 **Kokchetav Massif**
- 61

62 **MISIDENTIFICATION OF MICRODIAMONDS DUE TO CONTAMINATION**  
63 **FROM SAMPLE PREPARATION**

- 64 • **General precautions and examples**

- 65 • **Raman spectroscopy: indigenous diamond vs its synthetic counterpart**
- 66 • **How to prove that microdiamond is indigenous**

67 **FUTURE DIRECTIONS**

68

69 **ACKNOWLEDGEMENTS**

70

71 **REFERENCES**

72

73 **ABSTRACT**

74

75         The discovery of diamonds in metamorphic rocks of continental affinities  
76 occurred shortly after the discovery of coesite in similar rocks. These important  
77 discoveries led to a revolution in our understanding of the subduction and exhumation of  
78 continental materials and the establishment of a new discipline, ultra-high-pressure  
79 metamorphism (UHPM). After these discoveries more ultra-high pressure (UHP)  
80 minerals were found and dozens of UHPM terranes were established. Diamond is a  
81 remarkable material which is chemically inert and stable over geological timescales  
82 making it the perfect “geological container” where gas, fluid, and solid inclusions can be  
83 preserved. Moreover, its presence is indicative of specific pressure and temperature  
84 conditions which implicate subduction to a minimum depth of ~120 km. The inclusions  
85 trapped inside these diamonds can shed light on the composition, redox state, and  
86 evolution of the fluids related to UHPM diamond formation while the carbon isotope  
87 ratios of the diamond itself can inform us about the source of carbon. The purpose of this  
88 review is to provide a brief history on the discovery of microdiamonds starting with work  
89 that began in the mid 1960’s in Kokchetav massif, Kazakhstan, through to the present  
90 day. Particular attention will be on more recent micro-diamond discoveries in the last  
91 decade. The current state of understanding of the mechanisms of UHPM diamond  
92 formation, the misidentification of microdiamonds due to contamination from sample  
93 extraction/preparation, and the future of UHPM diamond research are discussed. The  
94 paper also considers the controversial topic of the occurrence of lonsdaleite within the  
95 population of microdiamonds from UHPM terranes.

96

97 **INTRODUCTION**

98 A multitude of geological and geodynamic events are recorded in collisional  
99 orogens where large-scale processes such as deep subduction of lithospheric plates,  
100 mantle convection, and mountain building occur. Continental collision is accompanied by  
101 the subduction of continental materials into the Earth's deep interior. The exhumation of  
102 these materials back to the Earth's surface is one of the largest natural processes that  
103 occur on the Earth. These rocks contain minerals formed under pressures that are higher  
104 than the pressures that occur within the crust and they provide a considerable amount of  
105 information about processes that occur in the Earth's mantle. Evidence of mineral  
106 reactions and deformation, fluid and melt migrations, phase transformations, and  
107 geochemical recycling are recorded in these rocks. On a regional scale continental  
108 collision zones release "energy" through earthquakes and volcanic eruptions.

109 In the early stages of the theory of plate tectonics several concepts were  
110 established; one such concept was that the continental crust is buoyant and will always  
111 remain floating above the oceanic crust. Therefore, this early version of plate tectonic  
112 theory did not provide a mechanism for the subduction of continental crust into the  
113 Earth's deep interior. This paradigm was significantly challenged in 1984 with two  
114 discoveries of coesite, first in the Dora Maira, Alps (Chopin 1984) and the second,  
115 published only three months later, in the Western Gneiss Region, Norway (Smith 1984).  
116 Soon after these exciting discoveries, microdiamonds were discovered in the Kokchetav  
117 massif, Kazakhstan (Sobolev and Shatsky 1990). These startling revelations ushered in an  
118 entirely new discipline, ultrahigh pressure metamorphism (UHPM).

119           Crustal rocks of that have experienced recrystallization within or above the  
120 coesite and diamond stability fields ( $\geq 2.7 - 4.0$  GPa,  $\sim 700 - 1000$  ° C) implying  
121 subduction to a depth of  $\geq 90-120$  km are considered as UHPM rocks. The presence of  
122 coesite and/or diamond in metamorphic rocks of continental affinities has become the  
123 standard for defining UHPM terranes. UHPM researches flourished due to the detailed  
124 studies of outcrops and mineral/rock thin-sections in laboratories with the aid of  
125 advanced state-of-art analytical and synchrotron assisted instruments and technologies.  
126 This led to the establishment of more than 20 coesite- and 9 diamond-bearing localities  
127 (Fig. 1) (e.g. Ogasawara 2005; Dobrzhinetskaya 2012; Schertl and Sobolev 2013; Liou et  
128 al. 2014 and here in). By combining all the results of these researches an integrated  
129 picture of the processes operating in the deep Earth at converging plate boundaries is  
130 realized. Moreover, a greater understanding of how crustal materials are recycled into the  
131 deep mantle environment and incorporated into large-scale mantle dynamics is also  
132 gained from these studies.

133           Diamond is an important index-mineral of UHPM events. Since diamond is  
134 chemically inert and stable over geological timescales it is the perfect “geological  
135 container” where gas, fluid, and solid inclusions can be preserved. These inclusions can  
136 provide detailed information about the conditions and chemistry of diamond forming  
137 media as well as mantle mineralogy and geochemistry. Moreover, diamond, which is  
138 often included in zircon, can be a precise geochronological indicator of the peak of UHP  
139 metamorphism. Aside from the inclusions,  $\delta^{13}\text{C}$  isotope characteristics of the diamond  
140 itself can provide information about the carbon reservoir from which it crystallized. The

141 type of nitrogen aggregation in diamond can shed light on the residence time of diamond  
142 in the environment where the diamond crystallized.

143         There are dozens reviews published in international forums that discuss impact of  
144 UHP mineralogy and UHP metamorphism studies on refining thermobarometry and plate  
145 tectonic modelling (e.g. Ernst and Liou 2000; 2008; Chopin 2003; Liou et al. 2004; 2009;  
146 2014; Green 2005; Zhang RY et al. 2007; Gerya 2010; Beltrando et al. 2010; Green et al  
147 2010; Guillot et al 2008; Zhang G et al. 2013; Schertl and Sobolev 2013). However,  
148 comprehensive reviews of the studies of UHPM diamonds as well as their detailed  
149 studies with modern state-of-art instruments and technologies are still scarce (e.g.  
150 Ogasawara 2005; Dobrzhinetskaya 2011).

151         The goal of this review is to provide an update of new diamond discoveries that  
152 led to the establishment of new UHPM terranes, and to summarize and critically analyze  
153 existing concepts of diamond formation. An additional objective is to specifically  
154 emphasize certain aspects of knowledge from studies of diamonds which have been  
155 missed before and/or less highlighted in current research projects. The review outlines  
156 new constraints from many well-known collisional orogens which will lead to the  
157 improvement of geotectonic modelling that is currently being developed for very deep  
158 subduction of continental rocks, and their exhumation.

159

## 160 **DIAMONDS FROM ULTRAHIGH PRESSURE METAMORPHIC TERRANES**

### 161 **The history of microdiamond discoveries in the Kokchetav massif, Kazakhstan**

162         In the mid 1960's several detrital grains of diamond ranging in size from 7 to 200  
163 microns were found in the Tertiary detrital deposits of titaniferous sands in the vicinity of

164 the Kokchetav massif, northern Kazakhstan (Kashkarov and Polkanov 1964). The alleged  
165 source of the detrital material was determined to be the Precambrian metamorphic rocks  
166 of the Kokchetav massif (Essenov et al. 1968). By the 1970's extensive geological  
167 mapping and exploration for mineral resources began in Kazakhstan, led by A. A.  
168 Zaychkovsky from the Kokchetav Geological Survey. They collected nearly 10 m<sup>3</sup> of  
169 rocks from the eclogite lenses enclosed in garnet-biotite gneisses that were exposed at the  
170 shore of Kundy Kol lake, Akmola Region, Kazakhstan. After crushing the rocks, the  
171 heavy minerals separation and flotation techniques were applied and, several  
172 microdiamonds were recovered from the residua (Rozen et al. 1972). It was concluded  
173 that these diamonds had formed under unusual crustal metamorphic conditions (Rozen et  
174 al. 1979).

175         The first detailed geological and petrographic descriptions of microdiamonds  
176 found *in situ* together with their host minerals was reported by Sobolev and Shatsky in  
177 Russian publications (1987; 1988). However, these unusual diamonds remained unknown  
178 to Western scientists until Sobolev and Shatsky (1990) published their results in *Nature*.  
179 They provided a detailed description of diamond morphologies and presented credible  
180 and convincing images of diamonds *in situ*. They were the first who postulated that these  
181 diamonds had formed in metamorphic rocks of continental affinities during deep  
182 subduction. They emphasized that new models are needed to explain how crustal rocks  
183 can be subducted to depths >~100-120 km and subsequently returned to the Earth's  
184 surface with preserved mineralogical relicts of ultrahigh pressure metamorphic (UHPM)  
185 events.

186           Following the efforts of the international community, the Kokchetav diamond-  
187 bearing metamorphic terrane became the “classic locality” of ultrahigh pressure  
188 metamorphism (e.g. Ernst and Liou 1999; Ogasawara 2005; Dobrzhinetskaya 2012;  
189 Schertl and Sobolev 2013; Liou et al. 2014). The “classic UHP rocks” of Kokchetav  
190 massif include metamorphic rocks with sedimentary and volcanic protholiths. They  
191 consist of varying lithologies of felsic gneisses, calc-silicate rocks, schists, quartzites,  
192 marbles, eclogites and garnet pyroxenites. Microdiamonds ranging in size from ~10 to  
193 100  $\mu\text{m}$  with an average size ~40-50  $\mu\text{m}$  occur in all the above mentioned lithologies  
194 (Fig. 2) in high concentrations. According to Pechnikov and Letnikov (2008) the  
195 Kokchetav microdiamond reserves are calculated to be as large as ~2.5 billion carats,  
196 with the average content of ~20 carats per ton. The Kokchetav diamonds have varying  
197 morphologies such as rose-like and dendritic-like crystals (Fig. 3 A), platy skeletal-like  
198 and shapeless single crystals (Fig. 3 B, C), or polycrystalline aggregates (Fig. 2 D),  
199 hopper-like cuboidal, or cuboidal and octahedral- like with truncated corners, and  
200 sometimes slightly rounded single crystals (Fig. 3 E, F). They are often observed as  
201 inclusions in refractory minerals such as zircon and garnet where they remain well-  
202 preserved and protected from complete transformation to graphite during exhumation of  
203 the UHPM rocks accompanied by retrograde metamorphism. Peak metamorphic  
204 conditions of these UHP rocks is estimated by thermobarometry of the rock forming  
205 minerals to be  $P\sim 4.5$  GPa and  $T=950-1000$  °C (e.g. Ogasawara 2005). Studies of  
206 nanoinclusions in these diamonds suggest that the Kokchetav diamonds formed at a  
207 pressure range of 6-9 GPa, and a temperature range of 980-1200 °C (e.g. Dorzhinetskaya

208 et al. 2006). The age of the UHPM event is Cambrian ~531 Ma whereas the protoliths of  
209 diamond-bearing rocks are as old as Precambrian ~2100–2700 Ma (Table 1).

210         Soon after Kazakhstan, similar microdiamonds (Fig. 4) were found in the Western  
211 Gneiss Region (WGR), Norway (Dobrzhinetskaya et al. 1995; van Roermund et al.  
212 2002), the Erzgebirge Massif of Germany (Massonne 1999), in China in the metamorphic  
213 rocks of the Dabie mountains, (Xu et al. 1992, 2003) and Qinling region (Yang et al.  
214 2003, and the Kimi complex of the Greek Rhodope (Mposkos and Kostopoulos 2001,  
215 Perraki et al. 2006). Microdiamonds have also been discovered in UHP oceanic floor  
216 metasediments at Lago di Cignana, the western Alps, Italy (Frezzotti et al. 2011; 2014).  
217 The above-mentioned localities are unconditionally classified as UHPM terranes because  
218 aside from diamond other ultrahigh pressure minerals have been discovered there such as  
219 coesite, TiO<sub>2</sub>-II (rutile with  $\alpha$ -PbO<sub>2</sub> structure), majoritic garnet, Ca-Esk-rich  
220 clinopyroxene and others. Since the detailed reviews on UHPM diamonds were published  
221 by Ogasawara (2005), Dobrzhinetskaya (2012) and Liou et al. (2014) several new  
222 diamond-bearing metamorphic rock localities have been reported.

223         Table 1 summarizes the occurrences of microdiamonds in metamorphic rocks  
224 starting from their earlier descriptions (e.g. Dobrzhinetskaya 2012) to present. Within  
225 them are new diamond localities reported from granulite and garnet peridotites from the  
226 northern part of the Bohemian massive (Kotková et al. 2011; Naemura et al. 2011;  
227 Perraki and Faryad 2014), detrital diamonds from Erzgebirge (Schönig et al. 2019), from  
228 felsic granulites of the Betic Rif Cordillera, NW Africa and SE Spain (Ruiz-Cruz and  
229 Sanz de Galdeano 2012; 2013; 2014), from Straumen area of Western Gneiss Region,  
230 Norway (Smith and Godard 2013), from gneisses and eclogites of the Tromsø Nappe of

231 Caledonides (Janák et al. 2013), from gneisses of Seve Nappe of Caledonides, Sweden  
232 (Majka et al. 2014; Klonowska et al. 2017), from oceanic metasediments of Lago di  
233 Cignana, Western Alps, Italy (Frezzotti et al. 2011; 2014; Frezzotti 2019), from garnet-  
234 kyanite-quartz-feldspathic gneisses of Pohorje, Eastern Alps (Janák et al. 2015), from  
235 amphibolites of Quinling region, China (Wang et al. 2014), from West Greenland  
236 (Glassley et al. 2014), and from garnet megacryst in mélangé of the Edough Massif, NE  
237 Algeria (Bruguier et al. 2017).

238 **New microdiamond localities discovered between 2011-2020**

239 ***Ceské Stredohorí, Stráž nad Ohří, Plesovice and Gfohl areas of Bohemian massif,***  
240 ***Central Europe***

241 The first *in situ* microdiamonds were reported as inclusions in garnet from felsic  
242 gneisses exposed in vicinities of Erzgebirge, northwestern part of the Bohemian Massif,  
243 Germany (Massonne 1999). The Erzgebirge locality became the second classical example  
244 of an UHPM terrane supported by extensive studies and publications (e.g. Nasdala and  
245 Massonne 2000; Stöckhert et al. 2001, 2009; Massonne 2003; Massonne and Tu 2007;  
246 Massonne et al. 2007; Dobrzhinetskaya et al. 2003; 2006a; 2013). Since 2011 several  
247 new microdiamonds localities (Table 1) in the northern part of the Bohemian massif have  
248 also been reported (Kotková et al. 2011; Perraki and Faryad 2014).

249 Kotková et al. (2011) unambiguously documented microdiamonds ranging in size  
250 from 5 – 30  $\mu\text{m}$  *in situ* in thin sections (Fig. 5) prepared from drill cores' of felsic  
251 granulites extracted from two boreholes at the České Stredohorí Mountains and from an  
252 outcrop in Stráž nad Ohří (Czech Republic). These felsic granulites are like the granulite  
253 facies metamorphic rocks that formed in the core of the Bohemian massif during the

254 Variscan orogeny, 340 - 380 Ma (e.g. Kröner and Willner 1998; Massonne and O'Brien  
255 2003). Microdiamonds from the granulites of these new localities occur as inclusions in  
256 Grt, Zr, and in Ky included in garnet. The correctly performed polishing technique  
257 provided indisputable evidence that the microdiamonds are *in situ* (Fig 5). The  
258 microphotographs show that diamond inclusions “protrude” above the host minerals  
259 (zircon and/or garnet) well-polished surface. Kotková et al. (2011) proposed that  
260 diamond formation took place during UHP metamorphism due to the deep subduction of  
261 continental materials followed by exhumation accompanied by high-T granulite  
262 metamorphism at shallower depths. The authors hypothesized that during subduction (>  
263 120-150 km) the K-Fsp-Qtz rich continental crust had “amalgamated” with small  
264 fragments of mantle materials and the latter are now presented as sparse lenses of the  
265 garnet peridotite containing relicts of Cr-spinel. The novelty of this study is that if we  
266 connect all three new microdiamond localities to the UHPM Erzgebirge domain and  
267 assume that all granulites have the similar deep subduction, exhumation and metamorphic  
268 history, they encompass an area of > 1000 km<sup>2</sup> (Kotková et al. 2011).

269 Perraki and Faryad (2014) discovered diamond, coesite, and moissanite inside of  
270 polished zircon grains. The zircons were extracted from the heavy minerals fraction that  
271 was separated from the crushed kyanite-bearing Gföhl granulite samples (the  
272 Moldanubian Zone of the Bohemian massif). The Gföhl kyanite-bearing granulites contain  
273 lenses and boudins of eclogites, garnet peridotites, and garnet pyroxenites. The  
274 thermobarometric calculations suggest that UHP metamorphism occurred at P >4 GPa  
275 and T = 680 °C followed by granulite facies metamorphism and partial melting at P < 2

276 GPa and  $T = 850\text{--}950$  °C. Perraki and Faryad (2014) agreed with Kotková et al. (2011)  
277 that the diamonds crystallized during UHP metamorphism of the Variscan Orogeny.

278 One novel aspect of the study of Perraki and Faryad (2014) is that they found  
279  $\text{SiO}_2$  (coesite) coexisting with diamond and moissanite (SiC). Moissanite formation  
280 requires extremely reducing conditions, e.g. 4.5–6 log units below the iron-wustite (IW)  
281 buffer, whereas diamond and  $\text{SiO}_2$  (coesite) may coexist at an oxygen fugacity close to  
282 the diamond + CO fluid buffer (CCO) and the fayalite-magnetite-quartz (FMQ) oxygen  
283 buffers (e.g. Mathez et al. 1995; Frost BR and Frost CD 2014). Additional studies of the  
284 coexisting diamond, coesite, and moissanite inclusions in zircons from Gföhl granulites  
285 should be a high priority for future investigations, since such a study would shed light on  
286 the redox conditions of fluid-rock interactions and microdiamond formation in UHPM  
287 terranes.

### 288 *Microdiamonds in detrital garnets from Erzgebirge, Germany*

289 After several decades of the intensive studies motivated by the first discoveries of  
290 coesite and microdiamonds in rocks of continental affinities, it was shown that UHP  
291 metamorphism is not a rare phenomenon. However, despite the widespread exposure of  
292 presumably UHPM rocks in the continent-continent collisional orogens the mineralogical  
293 evidence of ultra-high-pressure metamorphism remains scarce, since during exhumation  
294 UHP minerals are typically overprinted with lower-grade metamorphism and partial  
295 melting. Schönig et al. (2019) proposed to study the distribution and characteristics of  
296 UHPM rocks by analyzing detrital garnets that have accumulated in surface sediments.

297 They collected detrital garnets from loose sediments deposited near the  
298 Erzgebirge massif where diamonds were described as inclusions in garnets and zircons

299 (e.g. Nasdala and Massonne 2000; Dobrzhinetskaya et al 2003; Kotková et al. 2011;  
300 Naemura et al. 2011; Perraki and Faryad 2014). The sediments consist of sand from the  
301 creeks around the Saidenbach reservoir that have been draining the Erzgebirge UHPM  
302 rocks for a long time. After heavy mineral separation and examination of the residua with  
303 optical microscopy about 700 grains of garnets were chosen for further research. Out of  
304 the 700 inclusion bearing garnets they found 26 garnets containing 46 inclusions of  
305 monomineralic coesite, and 22 garnets containing 41 diamond inclusions, and they  
306 examined them with Raman spectroscopy (Schönig et al. 2019). These results provide  
307 undisputable evidence that the processes of erosion and weathering of UHPM rocks can  
308 relocate UHP minerals to sediments scattered around the hard rock exposures. Therefore,  
309 this method may be used as an additional technique for discovering new UHPM terranes.  
310 Similar methodology has been successfully applied to single zircon grains that were  
311 separated from UHPM rocks and has been successfully used for more than a decade to  
312 identify microdiamonds and other UHPM mineral inclusions.

### 313 *The Betic and Rif Cordilleras, NW Africa and SE Spain*

314 Recently a microdiamond-bearing locality was discovered within the felsic  
315 gneisses of granulite facies in the Betic-Rif arc (NW Africa) and in the SE of Spain  
316 (Ruiz-Cruz and Sanz de Galdeano 2012). This tectonically complicated domain belongs  
317 to the pre-Mediterranean Alpine orogenic zone formed during the Africa-Eurasia  
318 collision (e.g. Platt et al. 2013). Octahedral, cuboid and cubo-octahedral microdiamonds  
319 of <5 x 10-15 µm size (Table 1) were reported as inclusions in garnet, kyanite, and quartz  
320 with relicts of coesite from felsic granulites exposed in the Ceuta area of the Northern  
321 Rif, NWAfrica (Ruiz-Cruz and Sanz de Galdeano 2012). The authors have estimated the

322 metamorphic conditions of the Ceuta granulites as  $P=4.3$  GPa and  $T=1100^{\circ}\text{C}$   
323 (corresponding to a depth of  $>150$  km) and suggested that the diamond-bearing crustal  
324 rocks and peridotites experienced a similar UHP metamorphic condition. The also  
325 suggested that the UHP metamorphism occurred  $\sim 330$  Ma ago followed by partial  
326 melting and migmatization at  $\sim 265$  Ma (Ruiz-Cruz and Sanz de Galdeano 2013). Given  
327 that the diamond-bearing garnet from felsic gneiss contains apatite' exsolution lamella  
328 and clusters, the authors calculated the phosphorous solubility in garnet and compared it  
329 with those obtained in high-pressure and high temperature experiments (Konzett and  
330 Frost 2009; Konzett et al. 2012). Based on such a comparative analysis they concluded  
331 that the highest pressure reached during UHPM was 7 GPa, and temperature  $\sim 1150^{\circ}\text{C}$   
332 (Ruiz-Cruz and Sanz de Galdeano 2013).

333 ***Straumen localiy, Western Gneiss Region, Norway***

334 After the discovery of coesite inclusions in clinopyroxene occurring in the  
335 dolomite-eclogites from Grytting, Norway (Smith 1984) the Geological Survey of  
336 Norway (NGU) initiated a search in 1992 for possible microdiamonds in the WGR.  
337 Garnet-kyanite-phlogopite gneisses were collected at Fjørtoft island of WGR and crushed  
338 at the NGU laboratory. Several grains of microdiamonds (30-45  $\mu\text{m}$  size) were separated  
339 from the heavy mineral concentrates extracted at the NGU laboratory using a  
340 thermochemical decomposition method (Dobrzhinetskaya et al. 1995). Later  
341 microdiamonds were found *in situ* in garnet peridotite from Fjørtoft (van Roermund et al.  
342 2002), and in Fe-Ti garnet peridotite from Svartberget (Vrijmoed et al. 2008).

343 *In situ* diamond has also been reported from two more localities in the central and  
344 northern parts of WGR, Norway (Smith and Godard 2013; Janák et al. 2013). Smith and

345 Godard (2013) conducted Raman spectral point analysis and Raman mapping of the  
346 carbon-bearing inclusions in zircon from kyanite-phengite-coesite eclogites from the  
347 Straumen eclogite pod in the WGR, and they identified two graphitized diamonds. The  
348 authors noticed that the position 1<sup>st</sup> order Raman mode of the diamond inclusions varies  
349 from 1332 cm<sup>-1</sup> (ambient value for single crystal diamond) down to as low as 1322 cm<sup>-1</sup>.  
350 They observed additional features in the Raman spectra of these diamonds (doublets with  
351 peaks at 1328 cm<sup>-1</sup> and 1322 cm<sup>-1</sup>) which are like the Raman spectra of diamonds from  
352 the Kokchetav Massif. Given the Raman results and the *in situ* nature of the diamonds the  
353 geological origin of the Straumen diamonds is indisputable.

354 ***Tonsvika area, Tromsø nappe, the northern Norwegian Caledonides***

355 Janák et al. (2013) documented microdiamonds (~10 μm) *in situ* in kyanite-  
356 garnet-biotite-gneisses exposed near Tonsvika, Tromsø nappe (452 Ma), in the northern  
357 part of the Norwegian Caledonides territory (Table 1). Microdiamonds were observed in  
358 thin sections with optical microscopy and confirmed with Raman spectroscopy.  
359 Microdiamonds occur as single crystals as well as multiphase inclusions of diamond +  
360 MgCO<sub>3</sub> and/or diamond + CaCO<sub>3</sub> in garnet. In addition to the diamond and diamond-  
361 carbonate inclusions, monocrystalline quartz with radial fractures was observed  
362 suggesting that this quartz is a product of decompression of coesite. Most of the Raman  
363 spectra collected from 21 microdiamonds in two petrographic thin sections have peaks  
364 that are observed between 1332 and 1330 cm<sup>-1</sup> suggesting the presence of *sp*<sup>3</sup>-hybridized  
365 carbon bonding (diamond). The presence of G bands (1580 cm<sup>-1</sup>) in Raman spectra  
366 indicate that *sp*<sup>2</sup> hybridized carbon bonding (graphite) is also present. The  
367 thermodynamic calculations reported by Janák et al. (2013) suggest that diamond

368 crystallization took place at  $P = 3.5 \pm 0.5$  GPa and  $T = 770 \pm 50$  °C. The microdiamond  
369 discovery in Tromsø nappe combined with the previous discoveries of coesite,  
370 microdiamonds, majoritic garnets in the neighboring Western Gneiss Region extends this  
371 UHPM terrane by >100 - 120 km.

### 372 *Jämtland and Årescutan areas, the Sweden Caledonides*

373 Diamond inclusions are documented in 2014 for the first time in porphyroblastic  
374 garnets from garnet-sillimanite-biotite gneisses in the Seve Nappe Complex of northern  
375 Jämtland, Swedish Caledonides (Majka et al. 2014). Diamonds ranging in size from 4 to  
376 7  $\mu\text{m}$  with spheroidal and bleb-like forms occurring inside of a multiphase assemblage of  
377 carbonate, quartz, and rutile that were identified using optical microscopy (Fig. 6). The  
378 presence of  $sp^3$  carbon bonding was confirmed with Raman spectroscopy, and scanning  
379 electron microscope (SEM) images acquired in secondary electron (SE) mode reveal  
380 negative relief of diamond inclusions with respect to the very flat, perfectly polished  
381 surface of the host garnet (Majka et al. 2014).

382 Klonowska et al. (2017) discovered another microdiamond locality approximately  
383 50 km from the locality described by Majka et al. (2014). Microdiamonds ( $\sim 5$   $\mu\text{m}$  size)  
384 are found *in situ* as single and composite (diamond + carbonate) inclusions in garnet from  
385 garnet-phengite-kyanite-rutile gneisses in the Åreskutan area of the Seve Nappe  
386 Complex. Raman modes were observed at  $1328\text{ cm}^{-1}$  and  $1331\text{ cm}^{-1}$  confirming the  
387 presence of diamond (Solin and Ramdas 1970). Moreover, besides these diamonds, the  
388 gneisses contain textural relicts of decompressed coesite, observed as polycrystalline  
389 quartz surrounded by radial cracks. Thermodynamic calculations suggest that diamond  
390 crystallization took place at  $P = 4.1\text{--}4.2$  GPa and  $T = 830\text{--}840$  °C (Klonowska et al.

391 2017). The mineral assemblages of the UHP metamorphism were later overprinted under  
392 amphibolite and granulite facies conditions. The age of the UHP metamorphism recorded  
393 in the Åreskutan diamond-bearing gneisses occurred before ~ 445 Ma (Klonowska et al.  
394 2017).

### 395 *Diamonds from Lago di Cignana, Italy, Western Alps*

396 Although UHP metamorphism in the Western Alps was proposed in the mid  
397 1980's when coesite was discovered (Chopin 1984), diamonds were not found in the  
398 Western Alps until almost two decades later (Frezzotti et al. 2011; 2014; Frezzotti 2019).  
399 Frezzotti et al. (2011) discovered microdiamond inclusions ranging from <2 -30 micron  
400 in size in Mn-rich garnets from garnetite nodules and boudins enclosed within mica-  
401 schists and quartzites that are spatially associated with eclogite facies metabasites. The  
402 upper part of this metamorphosed ophiolitic section belongs to the Lago di Cignana  
403 tectonic unit of the Western Alps and appears to be the first recognized UHPM terrane  
404 which originated as a fragment of the Thetyan oceanic lithosphere. The tiny diamond  
405 inclusions are closely associated with C-O-H fluid inclusions, and tiny inclusions of  
406 magnesite and SiO<sub>2</sub> (quartz). There is no evidence that the quartz is a product of  
407 decompression of coesite during exhumation. Instead, the SiO<sub>2</sub> clusters are products of  
408 lower temperature post-metamorphic reactions that occurred in adjacent layers of the  
409 mica-schists (Frezzotti et al. 2011; 2014).

410 Detailed studies of diamond and C-O-H fluid enclosed in garnets using Raman  
411 spectroscopy and  $\delta^{13}\text{C}$  and  $\delta^{18}\text{O}$  isotope geochemistry revealed that organic carbon  
412 dissolved in hydrous fluids was transported to a depth ~ 110 km together with oceanic  
413 sediments during Alpine oceanic subduction about 35 Ma ago. Frezzotti et al. (2011,

414 2014) and Frezzotti (2019) concluded that during subduction the UHP metamorphism led  
415 to diamond crystallization from C-O-H fluid at respectively high oxidation state [ $fO_2 = 0$   
416  $- 1.5$  log units higher than the Fayalite-Magnetite-Quartz (FMQ) buffer]. This UHP  
417 metamorphism took place at  $P \geq 3.2$  GPa and  $T \leq 600$  °C and is classified as a cold  
418 subduction metamorphism (e.g. Frezzotti 2019).

#### 419 *Diamonds from Pohorje (Slovenia) in the Austro-Alpine UHPM terrane, Eastern Alps*

420 The Pohorje Mountains have been considered as an UHPM terrane since Janák et  
421 al (2004, 2006) constrained the pressure and temperature ( $P \geq 3.5$  GPa and  $T = 800$ -  
422  $850$ °C) for eclogite and peridotites enclosed in meta-carbonaceous rocks, although at that  
423 time no UHP index minerals had been known in this locality. Later, Janák et al. (2015)  
424 discovered microdiamond ( $\sim 10$   $\mu\text{m}$  size) inclusions in garnets from metapelitic gneisses  
425 that consist of layers rich in biotite, white mica, garnet and kyanite alternating with felsic  
426 layers, veins and segregations of quartz and feldspar. Inside of the host-garnets diamond  
427 occurs as single cubic or cubo-octahedral crystals and as a part of composite inclusions  
428 where it is associated with moissanite (SiC) and fluid inclusions containing abundant  $\text{CO}_2$   
429 and traces of  $\text{CH}_4$ . Diamonds, associated minerals, and fluid inclusions were confirmed  
430 with Raman spectroscopy. The authors concluded that diamond formed at depth  $> 100$   
431 km during Late Cretaceous (ca. 92-95 Ma) subduction of the continental slab from  
432 reduced supercritical fluids that formed during UHP metamorphism of carbonaceous  
433 sediments. This diamond-forming media is similar to that reported by Perraki and Faryad  
434 (2014) in the Gföhl granulites of the Moldanubian Zone of the Bohemian massif, where  
435 they documented polyphase inclusions of diamond+moissanite+coesite in zircon.

#### 436 *More diamonds from Qinling region, China*

437           Though the Chinese Orogenic belt (COB) is a well-established UHPM terrane  
438 where coesite (e.g. Okay et al. 1988) as well as relicts of stishovite (Liu et al. 2007) and  
439 majoritic garnet with lamella exsolution of ortho- and clinopyroxenes (Ye et al. 2000) are  
440 well-documented, the diamonds in these rocks are scarce. There are two reports of  
441 diamond occurrences in the Dabie mountains (Xu et al. 1992, 2003) and the Qinling  
442 region of China as inclusions in zircons (Yang et al. 2003). However, these reports were  
443 not confirmed by others for more than a decade.

444           In 2014, Wang et al. (2014) documented more microdiamonds as inclusions in  
445 zircons that had been separated from amphibolite rocks from the North Qinling region.  
446 To date, all microdiamonds reported from the COB have only been confirmed with  
447 Raman spectroscopy. Advanced electron microscopy studies of these diamonds such as  
448 FIB and TEM have not yet been reported. Nevertheless, both FIB and TEM research on  
449 these unusual diamonds is very important since it would likely shed light onto the  
450 geochemical conditions under which these diamonds crystallized. Considering that very  
451 few microdiamonds have been documented in the UHPM rocks of the COB it is  
452 understandable that researchers may be skeptical of these reports. It is possible that the  
453 low concentration of diamonds in the COB may be explained by geochemical conditions  
454 that would impede diamond crystallization. Hypothetically, such conditions could be: (i)  
455 low concentration of carbon in the bulk rocks and/or in small amounts of fluid/hydrous  
456 melt that can penetrate subducting slabs during UHP metamorphism; (ii) perhaps the  
457 concentration of carbon was high enough to start diamond nucleation, but the oxygen  
458 fugacity was extremely high which would prevent diamond crystallization; (iii) or all the

459 diamonds were replaced by graphite during slow exhumation of the UHPM rocks  
460 accompanied by low pressure and high temperature regional metamorphism.

461 ***Graphitized diamond in West Greenland UHPM terrane***

462 A new UHPM terrane was documented by Glassley et al (2014) within the  
463 Nagssugtoqidian Orogen (Proterozoic age, ca. 1.8 Gy) of western Greenland. The  
464 mineralogical confirmation of different UHP events includes (i) the presence of relicts of  
465 orthopyroxene exsolved from a supersilicic garnet precursor, (ii) exsolution lamella of  
466 rutile from garnet and pyroxenes, (iii) exsolution lamella of magnetite from olivine, and  
467 (iv) unusual quartz needles exsolved from olivine – a hypothetical ringwoodite. Glassley  
468 et al (2014) showed that the Raman spectra of three micron-sized carbon-bearing  
469 inclusions in garnet exhibit modes at  $1335\text{ cm}^{-1}$ , which unambiguously suggests the  
470 presence of  $sp^3$ -carbon bonds, e.g. the diamond structure. Broad peaks at  $\sim 1420$  - $1450$   
471  $\text{cm}^{-1}$  which are consistent with hydrogenated carbon on the diamond surfaces and well-  
472 pronounced Raman bands of graphite at  $1580\text{ cm}^{-1}$  suggest that diamond probably  
473 gradually transformed to graphite. The authors hypothesized that these diamonds were  
474 encapsulated in the garnet during their growth and were transformed to graphite during  
475 decompression accompanied by metamorphism to granulite facies. The UHP  
476 metamorphism conditions suggest a pressure of  $\sim 7\text{ GPa}$  and a temperature of  $\sim 975\text{ }^\circ\text{C}$ .

477 ***The Western Mediterranean orogen – the Edough Massif, NE Algeria, new UHPM***  
478 ***terrane***

479 Bruguier et al. (2017) reported the first find of a diamond inclusion in a garnet  
480 megacryst from a mélange exposed at the northern margin of Africa (Edough massif, NE  
481 Algeria). A single diamond crystal approximately  $50\text{ }\mu\text{m}$  in size inter-grown with rutile

482 was found as an inclusion in an almandine-rich garnet. The garnet was found within  
483 weathered actinolite-rich mylonites. The SE SEM image presented in Figure 3a from  
484 Bruguier et al. (2017) is unequivocal evidence that the diamond-rutile inclusion is  
485 indigenous to the Edough massif. The image shows that the diamond is clearly  
486 “protruding above” the perfectly polished surface of the host mineral, which is very  
487 typical for a diamond – garnet interface. The contact zone between the diamond – garnet  
488 interface, appears intact which strongly suggests that the diamond is naturally occurring  
489 and not contamination from a cutting with a diamond-saw and/or polishing with  
490 diamond-grit. Other garnets from the same area contain rutile, zircon, apatite, and  
491 plagioclase inclusions.

492 Thermodynamic calculations suggest that an UHP metamorphic event took place  
493 at  $P \geq 3.6$  GPa and  $T = 750$  °C (Bruguier et al. 2017; Caby et al. 2014). Studies of the  
494 zircon inclusions suggest that the Alpine age of UHP metamorphism of the West  
495 Mediterranean Orogen is between  $32.4 \pm 3.3$  Ma and  $20.7 \pm 2.3$  Ma (Bruguier et al.  
496 2017). This was followed by exhumation as slab rollback occurred in the Oligocene  
497 (Brun and Faccenna 2008; Tirel et al. 2013). Additional studies of this locality should  
498 find more evidence of UHPM, such as UHP minerals and/or traces of their  
499 decompression products and/or proof of retrograde metamorphism.

500 *Diamonds from Nishisonogi unit, Nagasaki metamorphic complex, western Kyushu,*  
501 *Japan*

502 Nishiyama et al. (2020) report the discovery of microdiamond aggregates in the  
503 matrix of a metapelite from the Nishisonogi unit, Nagasaki metamorphic complex,  
504 western Kyushu, Japan. The Nishisonogi unit represents a Cretaceous subduction

505 complex which has been considered as an epidote–blueschist subfacies metamorphic unit,  
506 and the metapelite is a member of a serpentinite mélangé in the Nishisonogi unit  
507 (Nishiyama et al. 2020). The glaucophane and phengite ages are reported to be 95-90 Ma  
508 using the  $^{40}\text{Ar}/^{39}\text{Ar}$  method (Faure et al. 1988) and 85-60 Ma using the K-Ar method  
509 (Hattori and Shibata 1982). The aggregates of diamonds range in size from 10-50  $\mu\text{m}$  and  
510 they are embedded in dolomite, phengite, and albite (see Fig 4 in Nishiyama et al. 2020).  
511 The diamonds are not sticking out above the polished surface of the sample. However, it  
512 should be noted that they are surrounded by soft minerals. Using SiC and  $\text{Al}_2\text{O}_3$  abrasives  
513 as the main polishing abrasives, one would expect to see the diamonds “standing above”  
514 the flat surface of the surrounding softer minerals (see Fig 4 in Nishiyama et al. 2020).  
515 This is because of the hardness of diamond itself, and it would not be “eroded” or  
516 ‘flattened” by either SiC or  $\text{Al}_2\text{O}_3$  abrasives since these abrasives are not as hard as  
517 diamond. Unfortunately, images where the diamonds are completely enclosed by the host  
518 minerals are not presented in this publication.

519 The authors characterized the microdiamonds with electron diffraction and  
520 Raman spectroscopy. They report from Raman micro-spectroscopy of graphite that the  
521 temperature of this unit is 450 °C, and that the co-existence of microdiamond and Mg-  
522 carbonates suggests the precipitation of diamond from a C-O-H fluid under pressures  
523 higher than 2.8 GPa. Due to the relatively low temperature found for these rocks they  
524 discuss the possible metastable growth of diamonds found in metapelites from a  
525 Cretaceous subduction complex in Western Kyushu, Japan. However, the authors present  
526 several lines of evidence for HP to UHP conditions, (i) pseudomorph after coesite, (ii)  
527 high Si content in phengite, (iii) pseudomorph after titanite, and (4) the possibility of

528 nearby lawsonite-garnet assemblages. Ultimately these authors seem to prefer a stable  
529 formation of diamond from a C-O-H fluid at pressures > 2.8 GPa and temperatures of  
530 ~450 °C. While the authors did specify that they used Al<sub>2</sub>O<sub>3</sub> and SiC for polishing of the  
531 samples they do not specify if diamond tools were used to extract or cut the samples for  
532 polishing. Importantly, they also did not employ high resolution techniques (e.g. FIB  
533 assisted TEM) to carefully examine the diamond-host mineral(s) interface. To  
534 unambiguously classify the metapelites from a Cretaceous subduction complex in  
535 Western Kyushu, Japan as a new UHPM terrane more FIB-TEM research is required on  
536 the existing samples or new samples from this locality to confirm that these diamonds are  
537 indigenous.

538 **Lonsdaleite from WGR, Norway and Kokchetav massif, Kazakhstan and a problem**  
539 **with its identification**

540         Since lonsdaleite, a hexagonal polymorph of diamond, has been reported to occur  
541 in UHPM terranes a short discussion is warranted. At General Electric Company Bundy  
542 and Kasper (1967) synthesized a wurtzite like polymorph of carbon at P=13 GPa and  
543 T=1000 °C, and they named it hexagonal diamond. In nature hexagonal diamond was first  
544 identified from the Canyon Diablo iron meteorite and Goalpara ureilite (e.g. Frondel and  
545 Marvin 1967; Hanneman et al. 1967). It was named lonsdaleite in honor of the  
546 distinguished crystallographer Professor Kathleen Lonsdale (FrondeL and Marvin 1967).  
547 Lonsdaleite has since been found in many other meteorites (e.g. Daulton et al. 1996). It  
548 has also been reported to occur in terrestrial impact craters, Ries Crater, Germany (e.g.  
549 Rost et al. 1978), Popigai impact structure (e.g. Masaitis et al. 1972; Koeberl et al. 1997),  
550 Sudbury impact structure, Ontario, Canada (e.g. Masaitis et al. 1997), and Lappajärvi

551 structure, Finland (e.g. Masaitis et al. 1998). There is also one report of lonsdaleite  
552 occurrence in nodules from Pipe 50, Fuxian kimberlite field, China (Leung and Winston  
553 2002). These discoveries led to the hypothesis that lonsdaleite forms during impact  
554 events and very high pressure and temperatures are needed. However, it has also been  
555 reported to occur in UHPM rocks which would require alternative hypothesis to explain  
556 their existence.

557 Lonsdaleite has been reported in WGR, Norway (Godard et al. 2003; Godard et  
558 al. 2004; Smith et al. 2004) and in Kundy Kol, Kokchetav massif, Kazakhstan (Smith  
559 2004; Smith et al. 2004; Dubinchuk et al. 2009; Smith et al. 2011, Shumilova et al. 2011).  
560 Since these localities have been proven to be UHPM terranes by numerous studies, and it  
561 is known that they did not form during impact events, alternative hypotheses are required  
562 to explain the existence of lonsdaleite in these rocks. One hypothesis is that the formation  
563 of hexagonal polytypes such as lonsdaleite could be cumulative with the metamictization  
564 of diamond (Smith et al. 2011; Smith and Godard 2013). Another hypothesis, which will  
565 be discussed in greater detail below is that they formed during an impact event with a  
566 comet (Tretiakova and Luykin 2016; 2017).

567 Raman spectroscopy has been one of the most common techniques for confirming  
568 the presence of natural lonsdaleite since it is non-destructive, and micron sized samples  
569 can be studied *in situ* (Smith and Godard 2009; Shumilova et al. 2011; Goryainov et al.  
570 2014). Lonsdaleite has a 2H structure (spacegroup  $P6_3/mmc$ ) which has three  
571 theoretically predicted Raman active modes, the transverse optical oscillations of the  $E_{2g}$   
572 mode, and the longitudinal  $A_{1g}$  and transverse  $E_{1g}$  optical modes. Wu and Xu (1998)  
573 report the following theoretically predicted active modes  $E_{2g}$  1193  $\text{cm}^{-1}$ ,  $A_{1g}$  1312  $\text{cm}^{-1}$ ,

574 and the  $E_{1g}$   $1305\text{ cm}^{-1}$ , while Denisov et al. (2011) predict them to be at 1221, 1280, and  
575  $1338\text{ cm}^{-1}$  respectively. The  $E_{2g}$  mode is predicted to have very low intensity so the  $A_{1g}$   
576 and  $E_{1g}$  modes are typically used to identify lonsdaleite. Since the predicted lonsdaleite  
577 modes occur near the cubic diamond Raman active  $T_{2g}$  mode it should be noted that the  
578 peak position and width of the cubic diamond mode can vary significantly. As discussed  
579 by Nasdala et al. (2016) the peak position of the Raman active diamond mode can be  
580 downshifted and broadened by local heating through absorption of the laser (Herchen and  
581 Cappelli 1991), nanometer sized crystals (Lipp et al. 1997), substitution of  $^{13}\text{C}$  for  $^{12}\text{C}$   
582 (Anthony and Banholzer 1992), incorporation of B impurities (Pedroza-Montero et al.  
583 2005) and accumulation of structural damage from nearby radioactive phases (Nasdala et  
584 al. 2013). Hence, one needs to be cautious when interpreting Raman spectra of natural  
585 diamonds since shifts in the cubic diamond Raman peak position and peak width could be  
586 misinterpreted as lonsdaleite.

587 Notably, there appears to be no consensus on the existence of lonsdaleite as a  
588 discrete mineral (e.g. Németh et al. 2014). Németh et al. (2014) point out that despite  
589 extensive efforts lonsdaleite has never been produced as a pure material and they show  
590 that defects in cubic diamond provide an explanation for the characteristic  $d$ -spacings and  
591 reflections reported for lonsdaleite. Natural lonsdaleite has been described as stacking  
592 disordered diamond where cubic and hexagonal sequences are interlaced in a complex  
593 way (e.g. Salzmann et al. 2015; Murri et al. 2019). Thus, while numerous studies of  
594 lonsdaleite have been reported from UHPM terranes more studies of natural lonsdaleite  
595 using high resolution techniques are needed to resolve this controversy.

596

597 **ISOTOPIC STUDIES OF UHPM DIAMONDS**

598 **Carbon and nitrogen isotopes, and nitrogen content in UHPM diamonds**

599 Carbon isotopic composition (expressed as  $\delta^{13}\text{C}_{\text{PDB}}$ ) is a key parameter used to  
600 constrain the origin and formation environment of a diamond. Since UHPM diamonds  
601 formed in situ in subducted continental lithologies, their carbon isotope ratios should  
602 reveal the origin of carbon, and the isotope fractionation of the C-O-H fluids from which  
603 UHPM diamond formed. These carbon isotope ratios record the formation conditions  
604 both before and during diamond crystallization.

605 Among the reports on carbon isotopic compositions, E-type (eclogitic) and P-type  
606 (peridotitic) diamonds (e.g. Harris et al. 1975; Cartigny 2005) found in kimberlites  
607 clearly show some similarities; both types of diamonds have a peak at approximately  
608  $-5\text{‰}$ , which is similar to mantle-derived carbon observed in mid-ocean ridge basalts  
609 (MORBs), carbonatites, and kimberlites (Table 2, Fig. 7) . While E-type diamond  
610 isotopes are also spread towards lighter carbon to approximately  $-30\text{‰}$ , suggesting their  
611 sedimentary origin (Fig. 7). However, it must be noted that linking light carbon isotope  
612 ratios of diamonds to their origin from sedimentary organic carbon with long-time  
613 averaged  $\delta^{13}\text{C}_{\text{PDB}}$  value of  $-25\text{‰}$  requires; (i) unusually low temperature (below  $700^{\circ}\text{C}$ )  
614 in the mantle to avoid homogenization with sedimentary carbonate (average  $\delta^{13}\text{C}_{\text{PDB}} =$   
615  $0\text{‰}$ ), or (ii) absence of carbonate in the subducted sediment in which the diamond  
616 formed, which would be unusual since carbonates makes up about 80% of subducted  
617 carbon (Cartigny et al. 2014).

618 The concentration of nitrogen, which is the main substitutional diamond impurity,  
619 is also an important parameter when combined with  $\delta^{13}\text{C}_{\text{PDB}}$  to constrain the origin of  
620 metasomatic C-O-H fluids and therefore diamonds formation (Table 2, Fig. 8). As noted

621 by Cartigny et al. (2014), the behavior of nitrogen during diamond formation is unclear  
622 since nitrogen in diamond may be both compatible and incompatible (Smart et al. 2011,  
623 Palot 2013). On the contrary, if nitrogen compatibility is experimentally constrained, it  
624 would shed light on the composition, redox state, and evolution of the fluids related to  
625 UHPM diamond formation.

626 Nitrogen isotope ratios also provide a clue to the origin of diamonds,  
627 crustal/sedimentary nitrogen is enriched in  $^{15}\text{N}$ , by approximately +5‰ compared with  
628 the atmosphere ( $\delta^{15}\text{N} = 0\text{‰}$ ), whereas mantle nitrogen is depleted in  $^{15}\text{N}$  by  
629 approximately -5‰. Being different to carbon, nitrogen isotopes are fractionated by only  
630 a few per mill during their incorporation into diamond, so nitrogen that is incorporated  
631 into diamond during crystallization is representative of the growth medium. Most E-type  
632 diamonds have a mantle-like  $\delta^{15}\text{N}$ , which is inconsistent with their origin from subducted  
633 organic carbon. On the other hand, UHPM diamonds systematically exhibit heavy  $^{15}\text{N}$   
634 values ranging from +2 to +12 ‰ (Cartigny et al. 2001; 2014), suggesting their  
635 sedimentary source because devolatilization during sediment subduction would  
636 preferentially release  $^{14}\text{N}$ , resulting in further enrichment of subducted material in  $^{15}\text{N}$   
637 (Bebout and Fogel 1992; Busigny et al. 2003).

### 638 *Carbon isotopes characteristics of the Kokchetav diamonds*

639 Carbon isotopic composition studies of UHPM diamonds are limited due to their  
640 micron-size. One approach involves separating and grouping tens of thousands of  
641 microdiamonds and processing them together so that there is enough  $\text{CO}_2$  to be analyzed  
642 with a mass spectrometer providing average  $\delta^{13}\text{C}$  ratios. For instance, Cartigny et al.  
643 (2001) reported  $\delta^{13}\text{C}_{\text{PDB}} = -11 \text{‰}$  to  $-10 \text{‰}$  in diamonds from garnet-clinopyroxene

644 rocks and nitrogen contents 11,150 ppm, and  $\delta^{13}\text{C}_{\text{PDB}} = -10.19\text{‰}$  to  $-8.5\text{‰}$  and 2650  
645 ppm of nitrogen content in diamonds from marble of the Kokchetav massif, Kazakhstan  
646 (Table 2, Fig. 8). Based on possible carbon isotope fractionation between coexisting  
647 carbonate and diamond, Cartigny et al. (2001) estimated diamonds crystallization  
648 conditions as  $T \leq 700^\circ\text{C}$  and  $P=3$  GPa, e.g. slightly below the peak of UHPM, and  
649 concluded carbon and nitrogen stable isotopes strongly support their metasedimentary  
650 origin. If combine Cartigny et al. (2001) data with earlier  $\delta^{13}\text{C}_{\text{PDB}}$  bulk measurements of  
651 the Kokchetav diamonds, they fall in range of  $-10.2 \text{‰}$  to  $-26.9 \text{‰}$  (e.g. Lavrova et al.  
652 1997; Chopin and Sobolev 1995; review - Ogasawara 2005).

653         Later, Imamura et al. (2013) using Secondary Ion Mass Spectrometry (SIMS)  
654 technique analyzed carbon isotopes in diamonds (10–25  $\mu\text{m}$  in size) included in garnet  
655 from dolomite marble of the Kokchetav Massif. These diamonds were subdivided on to  
656 morphological types: S-type consisting of single-crystal core and polycrystalline rim, and  
657 R-type presented by single crystal with rugged surfaces. In S-type diamonds the rim  
658 exhibits lighter  $\delta^{13}\text{C}_{\text{PDB}} = -17$  to  $-27\text{‰}$ , whereas the core is much heavier, with  $\delta^{13}\text{C}_{\text{PDB}} =$   
659  $-9$  to  $-13\text{‰}$ . The R-type diamonds fall into narrow ranges of  $\delta^{13}\text{C}_{\text{PDB}} = -8$  to  $-15\text{‰}$ ,  
660 which are like those in the core of the S-type diamond. This suggests that the R-type  
661 diamonds probably formed at the same stage as the core of the S-type, whereas rim  
662 growth during the second stage did not occur, or occurred, very weakly in R-type  
663 microdiamonds. Therefore, carbon isotopic data corroborate the two-stage growth of the  
664 Kokchetav microdiamonds.

665         Interestingly, the  $\delta^{13}\text{C}_{\text{PDB}}$  value of dolomite from the host rocks ranges from  $-4$  to  
666  $-7\text{‰}$ , whereas the bulk dolomitic marble exhibits  $\delta^{13}\text{C}_{\text{PDB}} = -2\text{‰}$  (Ohta et al. 2003). The

667 marginal range of  $\delta^{13}\text{C}_{\text{PDB}} = -8$  to  $-27\text{‰}$  in S-type and R-type diamonds is different than  
668 that in mineral dolomite ( $\delta^{13}\text{C}_{\text{PDB}} = -4$  to  $-7\text{‰}$ ) and dolomitic marble host rock ( $\delta^{13}\text{C}_{\text{PDB}} =$   
669  $-2\text{‰}$ ). It is difficult to attribute these differences to isotopic fractionation considering that  
670 the metamorphic temperature was very high ( $\sim 1000^\circ\text{C}$ ; e.g. Ogasawara et al. 2000).  
671 Under such conditions, the diamonds in dolomitic marble would not have been in carbon  
672 isotopic equilibrium with the dolomite. There appears to be no good candidate material or  
673 process that could occur in the dolomitic marble that would explain the origin of the very  
674 light  $\delta^{13}\text{C}_{\text{PDB}} = -17$  to  $-27\text{‰}$  values, measured in the rim of the S-type diamonds.  
675 Imamura et al. (2013) speculated that perhaps a fluid with a light carbon isotope ratio  
676 infiltrated into the dolomite marble from the surrounding gneisses, which might contain  
677 light carbon of organic origin. With regards to this explanation, it will be discussed below  
678 that the Erzgebirge microdiamonds from felsic gneiss have a similar light carbon, e.g.  
679  $\delta^{13}\text{C}_{\text{PDB}} = -17$  to  $-27\text{‰}$  (Dobrzhinetskaya et al. 2010). However, Imamura et al. (2013)  
680 have not discussed these data because no carbon isotope measurements in diamonds from  
681 felsic gneisses of the Kokchetav massif have been reported.

### 682 *Carbon isotope characteristics of the Erzgebirge diamonds*

683 Massonne and Tu (2007) used a bulk analysis approach to obtain the carbon  
684 isotope ratios of diamond inclusions in zircons from the Erzgebirge UHPM terrane, and  
685 they reported that lighter carbon was involved ( $\delta^{13}\text{C}_{\text{PDB}} = -24\text{‰}$  to  $-33\text{‰}$ ) in the  
686 diamond-graphite formation.

687 Dobrzhinetskaya et al. (2010) used SIMS to analyze the  $\delta^{13}\text{C}_{\text{PDB}}$  and nitrogen  
688 contents in  $\sim 5$  to  $10\ \mu\text{m}$  diameter diamonds included in garnets from the garnet-quartz-  
689 feldspathic gneisses of the Erzgebirge massif (Fig. 9). They showed that the diamonds

690 situated within the garnets closer to the garnet rim zone showed some  $\delta^{13}\text{C}_{\text{PDB}}$  variations  
691 up to 10‰, with average values ranging from  $-22$  to  $-26$ ‰ (Table 2, Fig. 9). Their  
692 nitrogen contents vary heterogeneously between each individual measurement and  
693 between all diamonds without any systematics, ranging from 240 to 4600 ppm. On the  
694 other hand, the diamonds situated closer to the central part of the zoned garnet exhibits  
695  $\delta^{13}\text{C}_{\text{PDB}} = -17$  to  $-19$ ‰, with an average value of  $-17.8$ ‰. The latter is heavier than  
696 another diamond in the intermediate zone of the same garnet ( $\delta^{13}\text{C}_{\text{PDB}} = -23$ ‰) and the  
697 other diamonds situated closer to the outer zone of the garnet (Fig. 10). Nitrogen in the  
698 diamonds from intermediate zone varies from 100 to 1200 ppm, with an average value of  
699 820 ppm; and average value of nitrogen in diamonds from outer garnet zone is 1,838. The  
700 nitrogen content data plotted versus  $\delta^{13}\text{C}_{\text{PDB}}$  show a weakly pronounced tendency to  
701 increase with the increase of lighter carbon isotope content in the diamonds (Fig. 8).

702         Based on relationships between the diamonds position in the garnet (Fig.10), the  
703 diamond formation can be constrained by the chemical zoning of the host garnet, and  
704  $\delta^{13}\text{C}_{\text{PDB}}$  values of two diamonds. Dobrzhinetskaya et al. (2010) argued that there were  
705 two stages of diamond crystallization from a C-O-H fluid rich in biogenic carbon and  
706 diverse in minor elements of crustal origin. The  $\delta^{13}\text{C}_{\text{PDB}}$  of the first stage of  
707 crystallization falls within the range of  $-17$  to  $-19$ ‰, while the second stage of  
708 crystallization is characterized by  $\delta^{13}\text{C}_{\text{PDB}} = -22$  to  $-26$ ‰. Both  $\delta^{13}\text{C}_{\text{PDB}}$  ranges strongly  
709 suggest that the carbon from which they crystallized from belongs to the same biogenic  
710 reservoir. Graphite from the 3700-Ma-old turbidite greywacke and slate from West  
711 Greenland have primary  $\delta^{13}\text{C}_{\text{PDB}} = -19$ ‰, which is similar to the range of biologically  
712 reduced carbon, and it is within the range of reduced-carbon compositions found in most

713 modern marine sediments (e.g., Rosing 1999). Dobrzhinetskaya et al. (2010) suggest that  
714 the 1st-stage of diamond crystallization was from a more reduced carbon than the second  
715 stage of crystallization. This work indicates that within Erzgebirge diamond populations  
716 there are two  $\delta^{13}\text{C}_{\text{PDB}}$  signatures which are distinguished from each other not only by  
717  $\delta^{13}\text{C}_{\text{PDB}}$  values but also by the positions of the diamond within the garnet where different  
718 zones in the garnets are related to recrystallization events during UHP metamorphism. It  
719 also suggests that the carbon-rich fluid that deeply infiltrated the subducted sediments  
720 was probably reduced during an earlier stage, producing diamonds with slightly heavier  
721 isotopes than the diamonds that crystallized during the second stage.

722 Additional carbon isotope analysis of UHPM diamonds from both Kokchetav and  
723 Erzgebirge UHPM terranes and any of the new UHPM localities at small scales ( $\mu\text{m}$  to  
724 nm) with SIMS are necessary to shed light on the evolution of carbon-bearing fluids in  
725 subducted continental lithologies before and during diamond formation.

#### 726 **Noble gas isotopes in diamonds from UHPM terranes**

727 Noble gas isotopes in mantle-derived samples are key tracers of chemical  
728 heterogeneity of the Earth's mantle and the origin of the atmosphere (e.g. Ozima and  
729 Podosek 2002; Porcelli and Ballentine 2002). Samples of MORBs and ocean island basalt  
730 (OIB) have provided the most comprehensive understanding of mantle noble gases.  
731 MORBs show relatively uniform  $^3\text{He}/^4\text{He}$  ratios around  $1.1 \times 10^{-5}$  and a trend in  
732  $^{22}\text{Ne}/^{20}\text{Ne}$ - $^{20}\text{Ne}/^{22}\text{Ne}$  ratios toward a composition more enriched in nucleogenic  $^{21}\text{Ne}$ . In  
733 contrast, OIB samples, which are derived from a deeper region of the mantle, exhibit  
734 higher  $^3\text{He}/^4\text{He}$  ratios of up to  $7 \times 10^{-5}$  and less nucleogenic Ne isotope compositions  
735 (Graham 2002; Honda et al. 1991; Trieloff et al. 2000; Stuart et al. 2003). The latter

736 characteristics are believed to be evidence for a mantle source in which primordial He,  
737 with  $^3\text{He}/^4\text{He}$  of  $(1.4\text{--}4.6) \times 10^{-4}$ , and Ne (“solar” or “Ne-B” composition, Ballentine et  
738 al. 2005; Honda et al. 1991; Trieroff et al. 2000) has been less diluted by the addition of  
739 radiogenic  $^4\text{He}$  and nucleogenic  $^{21}\text{Ne}$  produced by decay of U- and Th-series elements.  
740 The primordial noble gas source is considered to have been isolated from whole mantle  
741 convection over geological timescales and sampled by upwelling mantle plumes (Jackson  
742 et al. 2010; Mukhopadhyay 2012). However, the reasons for the less-  
743 radiogenic/nucleogenic character of the plume source are still under debate; it may be  
744 “undegassed” (e.g., Allègre et al. 1983; Kaneoka 1983; Kurz et al. 1982; Porcelli and  
745 Ballentine 2002; Porcelli and Elliott 2008; Mukhopadhyay 2012), or it may be depleted  
746 in U and Th by ancient melt extraction events (Parman 2007; Porcelli and Ballentine  
747 2002; Jackson et al. 2010). The main advantage of analyzing noble gases contained in  
748 diamonds is their great potential to constrain the noble-gas state of the deep mantle  
749 because they are formed deeper than 150 km and act as chemically/mechanically stable  
750 “capsules”. Most noble gas studies are focused on kimberlitic diamonds (e.g. review -  
751 Basu et al. 2013).

752 ***“Unprecedentedly” high Helium-3 content in the Kokchetav diamonds: myth or***  
753 ***reality?***

754 Although currently there are dozens of UHPM diamond-bearing terranes that are  
755 known, only a few noble gas studies of microdiamonds from the Kokchetav massif have  
756 been reported (Begemann 1994; Pleshakov and Shukolyukov 1994; Shukolyukov et al.  
757 1993; Verchovsky et al. 1993; Sumino et al. 2011). Due to the small (micrometer) size of  
758 UHPM diamonds, noble gas analyses were conducted using several ten-of-thousands (or

759 even a greater number) of microdiamonds that were separated from their host  
760 rocks/minerals by treatments with HF and oxidizing acids. Pleshakov and Shukolyukov  
761 (1994) and Shukolyukov et al. (1993) reported “unprecedentedly” high  $^3\text{He}/^4\text{He}$  ratio  
762 during in vacuo stepwise heating of Kokchetav microdiamonds with a maximum value of  
763 0.47 in the low temperate release, which was the highest He content known among  
764 terrestrial diamonds (Pleshakov and Shukolyukov 1994; Shukolyukov et al. 1993).  
765 Moreover, this high  $^3\text{He}/^4\text{He}$  value exceeds the maximum values reported for any  
766 terrestrial mantle-derived sample of  $\leq 7 \times 10^{-5}$  (Stuart et al. 2003) and even the primordial  
767  $^3\text{He}/^4\text{He}$  value of  $(1.7\text{--}4.6) \times 10^{-4}$  (Porcelli and Elliott 2008).

768 The most plausible source of the high  $^3\text{He}/^4\text{He}$  ratio is nucleogenic  $^3\text{He}$  production  
769 via the  $^6\text{Li} (n, \alpha) ^3\text{H} (\beta) ^3\text{He}$  reaction (Kurz et al. 1987). However, this requires an  
770 anomalously high Li content of  $\sim 100$  ppm either in the diamonds, or within a  $\sim 20 \mu\text{m}$   
771 vicinity in the host rocks (Begemann 1994; Verchovsky et al. 1993). Moreover, the host  
772 rock would need to contain 1% of U with  $\text{Th}/\text{U} = 3.3$  to provide a neutron source  
773 sufficient to produce the levels of  $^3\text{He}$  observed (Begemann 1994; Verchovsky et al.  
774 1993). An important feature of the Kokchetav diamonds was that high  $^3\text{He}/^4\text{He}$  values  
775 were obtained from gas released over a relatively low temperature range of 200-1100 °C  
776 during in vacuo heating (Pleshakov and Shukolyukov 1994; Shukolyukov et al. 1993;  
777 Verchovsky et al. 1993), and not during diamond combustion under a controlled oxygen  
778 atmosphere (Verchovsky et al. 1993). Additionally, Verchovsky et al. (1993) showed that  
779 the amount of ‘excess’  $^3\text{He}$  (as well as  $^3\text{He}/^4\text{He}$  ratio) strongly depends on the grain-size  
780 of diamond fractions: the coarser the fraction the less (by orders of magnitude) the  $^3\text{He}$   
781 concentration. These findings were interpreted to indicate that the high  $^3\text{He}/^4\text{He}$

782 component may reside in Li-rich contaminants, which are quite resistant to treatments  
783 with HF and oxidizing acids during diamond separation from their host minerals/rocks,  
784 and therefore not trapped within the diamond itself (Begemann 1994; Verchovsky et al.  
785 1993).

786 In order to clarify this “unprecedented”  $^3\text{He}/^4\text{He}$  value Sumino et al. (2011)  
787 focused their attention on the presence of abundant nanometer-sized fluid inclusions in  
788 Kokchetav microdiamonds (Dobrzhinetskaya et al. 2001, 2005, 2006a), which could  
789 provide potential sites for preserving the noble gas signature of the diamond-forming C-  
790 O-H fluid. Sumino et al. (2011) employed in vacuo sequential dynamic crushing  
791 extraction with which sample grains are mechanically crushed in vacuum in order to  
792 selectively extract noble gases from fluid/melt inclusions with significantly less noble gas  
793 release from the diamond lattice and any associated mineral inclusions (Kurz 1986; Kurz  
794 et al. 1987).

795 The crushing technique results were compared with those obtained from a  
796 conventional vacuum stepped heating method which releases noble gases from fluid and  
797 solid inclusions and the diamond lattice. According to Sumino et al. (2011) the diamond  
798 crushing process extracts most of the  $^3\text{He}$ , indicating that  $^3\text{He}$  occurs within inclusions  
799 trapped during the Kokchetav diamond formation. The inclusion-hosted  $^3\text{He}/^4\text{He}$  of (3.3–  
800 6.5)  $\times 10^{-5}$  is significantly higher than that of the MORB-source mantle ( $1.1 \times 10^{-5}$ ), but  
801 close to the maximum value observed in OIBs ( $\sim 7 \times 10^{-5}$ ) containing noble gases  
802 enriched in a primordial component and delivered from the deep mantle by plumes. On  
803 the other hand, very low  $^3\text{He}/^4\text{He}$  ( $5.0 \times 10^{-8}$ ) obtained by heating of the crushed powder  
804 supports the presence of radiogenic  $^4\text{He}$  in the diamond lattice, resulting from  $\alpha$ -particle

805 implantation from U- and Th-series radioactive elements in the diamond-bearing  
806 minerals, which is consistent with the combustion results by Verchovsky et al. (1993).  
807 The results of Sumino et al. (2011) clearly indicate that the fluid inclusions in the  
808 Kokchetav diamonds preserve primordial He similar to those observed in OIBs and that  
809 abundant He with “unprecedentedly” high  $^3\text{He}/^4\text{He}$  ratio reported by previous works  
810 (Pleshakov and Shukolyukov 1994; Shukolyukov et al. 1993) should be attributed to Li-  
811 rich contaminants resistant to separation treatments of the diamonds from their host  
812 rocks/minerals (Begemann 1994; Verchovsky et al. 1993).

813 Neon isotopes also constrain the origin of noble gases in the Kokchetav  
814 microdiamonds. Although the levels of crush-released Ne were too low for precise  
815 isotopic measurements, Ne extracted during relatively low-temperature heating steps  
816 showed an isotope composition that is on the trend defined by OIBs from hotspots  
817 (Hawaii, Iceland, and Galapagos) enriched in primordial Ne (Honda et al. 1991; Tieloff  
818 et al. 2000; Kurz et al. 2009) but plot away from MORB values (Sarda et al. 1988) (Fig.  
819 11). The Ne isotope data indicate that primordial Ne is an intrinsic feature of the  
820 microdiamonds, but at higher temperatures during diamond graphitization, the Ne  
821 released shows a nucleogenic contribution. The nucleogenic Ne resides in the diamond  
822 lattice as a result of implantation by recoiling Ne isotopes mainly produced during the  
823 reaction of  $\alpha$ -particles (from U-Th decay) with oxygen and fluorine atoms in surrounding  
824 rocks (Kurz et al. 1987; Lal 1989; Verchovsky et al. 1993). The nucleogenic Ne  
825 composition released from the microdiamonds requires a very high F/O ratio of 0.02 (Fig.  
826 11 B) compared with the average crustal values of 0.0013 (Ballentine and Burnard 2002).

827           The observation that deep-mantle-derived, plume-like noble gases are contained  
828 in the Kokchetav microdiamonds paradoxically requires that deep-mantle-derived  
829 volatiles be present in the relatively shallow mantle wedge at 190-280 km depth. To solve  
830 this paradox, Sumino et al. (2011) suggest a few possible processes which are either  
831 capable of bringing deep-mantle-derived noble gases to the relatively shallow mantle: (i)  
832 a plume tapped from the lower mantle or core-mantle boundary; and/or (ii) a large scale  
833 mantle convection cell which entrained a fragment of the deep mantle, and subsequently  
834 added it to the mantle wedge at a depth of 190-280 km.

835           To date there is no geological evidence in the vicinity of the Kokchetav massif of  
836 mantle plume activity at the time of diamond formation (~530 Ma). A plume may have  
837 interacted with the subcontinental lithosphere which was beneath metasedimentary rocks  
838 before the Kokchetav slab was subducted and microdiamonds formed. To clarify the  
839 origin of the plume-like, deep-mantle-derived noble gases in the Kokchetav  
840 microdiamonds, more investigation is required particularly on UHPM diamonds from  
841 other localities. If metasomatism by plume-derived volatiles is essential for subduction  
842 and exhumation of continental crust as proposed by Seno and Rehman (2011), and the  
843 metasomatic volatiles play an important role in UHPM diamond formation, then plume-  
844 like noble gas is expected to be observed in UHPM diamonds from other localities.

#### 845 **MECHANISMS OF METAMORPHIC DIAMOND FORMATION**

846           It is generally agreed upon that during a continental-continental collision crustal  
847 rocks can be subducted to depths of >150 km, which leads to the formation of UHPM  
848 terranes, however readers may be surprised to learn that there are countless hypotheses  
849 for the origin of microdiamonds found in these terranes. The debates are primarily

850 focused around the crystallization conditions of diamond, some of the hypotheses include  
851 (i) from carbon-rich supercritical fluids vs. hydrous silicate and/or carbonatite melts, (ii)  
852 oxidation state of the media (e.g. see reviews: Ogasawara 2005; Dobrzhinetskaya 2012;  
853 Schertl and Sobolev 2013; Liou et al. 2014; Frezzotti 2011, 2014; Frezzotti 2019; Zhang  
854 et al 2017), (iii) stable vs. metastable conditions (e.g. Simakov 2010, Pechnikov and  
855 Kaminsky 2008, 2011), and/or from meteorite impact (Tretyakova and Luykin 2016,  
856 2017). These hypotheses will be discussed individually in greater detail below.

857         During the last decade there have been attempts to resolve some of these  
858 disagreements which have resulted in considerable progress in our understanding of the  
859 formation conditions of microdiamonds. Particularly advancements in high resolution  
860 instruments such as STEM, FIB, a ‘Structural & Chemical Analyser’ (SCA) probe and  
861 ‘inVia’ Raman spectrometer combined with SEM system, micron and sub-micron  
862 monochromatic and white beam synchrotron X-ray diffraction and synchrotron infrared  
863 (IR) micro-spectroscopy have all made it possible to perform analyses at the nano-scale  
864 of solid and gas/liquid inclusions in microdiamonds. Table 3 presents summarized  
865 information on nanoscale inclusions detected in diamonds from UHPM terranes by  
866 different techniques.

867         As new instruments and technology are adopted by researchers it has led to many  
868 other important discoveries and increased our knowledge about the origins of  
869 microdiamonds. Moreover, the integration of high-pressure devices such as multianvil  
870 presses and diamond anvil cells into synchrotron X-ray facilities has enabled a wide  
871 range of experiments to study UHPM diamond crystallization at varying pressures,  
872 temperatures,  $fO_2$ ,  $X_{H_2O}$ , organic/inorganic carbon and different bulk chemistry of the

873 starting materials (e.g. Akaishi and Yamaoka 2000; Pal'yanov et al. 2002; Palynov et al.  
874 2013; Yamaoka et al. 2000; Kumar et al. 2001; Dobrzhinetskaya et al. 2004;  
875 Dobrzhinetskaya and Green 2007; Zhang et al. 2011). These experiments have  
876 demonstrated that the kinetics of diamond crystallization varies depending on different  
877 experimental conditions such as hydrous or anhydrous, oxidation states, and if the  
878 pressure and temperature are high enough to stabilize  $sp^3$  carbon bonding.

879 *UHPM diamonds crystallized from a multicomponent supercritical C-O-H fluid or a*  
880 *hydrous silicate melt*

881 Studies of nanometric fluid solid inclusions in microdiamonds (Table 3) have  
882 revealed important new information on the crystallization conditions of microdiamonds.  
883 Conventional infrared (IR) spectroscopic studies revealed the presence of molecular H<sub>2</sub>O  
884 and CO<sub>3</sub><sup>2-</sup> radical from Kokchetav microdiamonds occurred in garnet clinopyroxenite,  
885 calc-silicate, garnet-pyroxene-quartz rocks and gneisses (e.g. de Corte et al. 1998; 2002  
886 Sitnikova and Shatsky 2009). Dobrzhinetskaya et al. (2006b) carried out synchrotron IR  
887 spectroscopic studies of the Erzgebirge diamonds separated from garnet-phengite-  
888 quartz-feldspathic gneisses using a thermochemical microwave digesting method. They  
889 collected synchrotron IR spectra from two diamond crystals (Fig. 12). Both spectra (Fig.  
890 13) show the presence of nitrogen impurities, molecular H<sub>2</sub>O, OH<sup>-</sup> hydroxyl radical,  
891 CO<sub>3</sub><sup>2-</sup> radical, and silicate inclusions in addition the C-C diamond phonon absorption  
892 bonds. Dobrzhinetskaya et al. (2006b) intentionally studied the same samples with  
893 synchrotron IR that had been previously studied using FIB-TEM techniques  
894 (Dobrzhinetskaya et al. 2003). Abundant nanometric solid crystalline inclusions were  
895 found in the diamond FIB-foils some of the identified phases are: (i) SiO<sub>2</sub> containing

896 traces of K, P, Ti, Fe; (ii) inclusion of unknown stoichiometry which consists of three  
897 elements, K, P, and O, (iii) oxide  $Pb_xO_y$ , (iv) carbonate ( $Pb_2CO_3$ ), and  $Al_2SiO_5$ . However,  
898 due to the extremely small size of these inclusions and their random orientations, their  
899 lattice parameters could not be determined by selected-area electron diffraction (SAED),  
900 however, all of them yield Bragg diffraction spots confirming their crystalline nature.

901 Besides the presence of crystalline nano-inclusions a considerable amount of  
902 nanometric-size euhedral cavities representing traces of decrepit fluid were documented.  
903 Many of these cavities were associated with dislocations related to diamond growth and  
904 are evidence of diamond nucleation and growth that took place in a C-O-H fluid-rich  
905 media (Dobrzhinetskaya et al. 2003). The presence of larger scale diamond-bearing  
906 multiphase inclusions' or "pockets" inside of garnets and zircons (Fig. 14) observed in  
907 polished slides with optical microscopy and scanning electron microscopy corroborate  
908 perfectly with the nanoscale observations (Stöckhert et al. 2001; Dobrzhinetskaya et al.  
909 2003; 2006b). Moreover, direct TEM observations of fluid-filled nanometric inclusion-  
910 bubbles preserved in FIB foil prepared from the Kokchetav diamond, and the  
911 serendipitous measurement of their contents immediately after bursting, showed that the  
912 fluid consists of C, H, O, Cl, S, Ca, Fe and K (Dobrzhinetskaya et al. 2005). This well-  
913 documented direct observation of residual fluid bubbles in microdiamonds  
914 unambiguously establishes their fluid growth medium.

915 Polycrystalline microdiamonds appear to be the best samples to study nano-fluid  
916 inclusions. There are several types of polycrystalline diamonds from the Kokchetav  
917 massif: (i) "spiral diamonds" which formed from a metal-sulfur-C-O-H-silicate fluid  
918 (Hwang et al. 2003), (ii) S-type (star-shaped) and R-type (rugged face) diamonds that

919 crystallized from a fluid during two stages (Ishida et al. 2003; Ogasawara 2005), and (iii)  
920 “overgrown” diamonds which crystallized from an aqueous-carbonate and aqueous-  
921 silicate fluid/melt (Sitnikova and Shatsky 2009). Polycrystalline diamond has also been  
922 described as daughter crystals associated with larger diamonds included in garnets from  
923 Erzgebirge felsic gneisses (Stöckhert et al. 2001, 2009). Stöckhert et al. (2009) concluded  
924 that the tiny daughter crystals precipitated from a supercritical C-O-H + K-, Na-rich  
925 silicate fluid.

926 Dobrzhinetskaya et al (2013) conducted SEM and FIB-assisted TEM studies of  
927 the Erzgebirge polycrystalline diamond inclusions in zircons (Fig.15). They studied 5  
928 polycrystalline diamonds and found that they consist of 5-15 single crystals ranging in  
929 size from 0.3-5  $\mu\text{m}$  with irregular sharp-angled grain boundaries (Fig 16). Numerous  
930 triangular nanoscale voids situated along the diamond-diamond interfaces were filled  
931 with a C-O-H fluid containing traces of Al, Co, F, V, Zn, Si, Cl, S, Ca, Mg, Fe, K in  
932 varying combinations and concentrations. The latter, if considered along with the “spider-  
933 like” dislocations, sharp-angled grain boundaries, and stacking faults that were observed  
934 in these diamonds, suggests that they rapidly nucleated and grew from a fluid media  
935 under an internal stress. These observations combined with previous results provide an  
936 additional constraint for the formation conditions of these UHPM microdiamonds. They  
937 likely crystallized from a supercritical fluid with a composition that was close to one of  
938 two end members, (1) a carbon-rich hydrous-silicic fluid and (2) a hydrous-saline fluid  
939 (Dobrzhinetskaya et al. 2006a, 2013; Jacob et al. 2014).

940 Zhang et al. (2017) also conducted studies of polycrystalline diamonds in zircons  
941 separated from quartz-feldspathic gneisses at Saidenbach water reservoir, Erzgebirge,

942 Germany. Their conclusions confirm the studies by Dobrzhinetskaya et al. (2013), and  
943 unconditionally support the concept of UHPM diamond crystallization from a  
944 multicomponent C-O-H fluid or C-O-H fluid - hydrous silicate melt media.

945 Frezzotti et al. (2011) studied fluid inclusions associated with UHPM diamond  
946 formation in metamorphic schists from Lago di Cignana, Western Alps where the  
947 protolith of these rocks was oceanic sediments. Based on studies of the fluid  
948 geochemistry they concluded that the carbon was released from the subducting oceanic  
949 sediments at relatively shallow depths through the dissolution process (Frezzotti et al.  
950 2011; 2014; Frezzotti 2019). Furthermore, their detailed investigation convincingly  
951 demonstrated that deep subduction of oceanic sediments leads to a continuing saturation  
952 of the shallow fluid with carbon and precipitation of diamonds at UHP conditions  
953 occurred. The Lago di Cignana diamond's nucleation from a C-O-H fluid at UHPM  
954 conditions is unambiguously supported by the presence of coesite inclusions located in  
955 the same garnet growth zones where the primary fluid inclusions are located (Frezzotti et  
956 al. 2011; 2014; Frezzotti 2019). This is also in good agreement with thermodynamic  
957 calculations reported by Sverjensky et al. (2014) who investigated the stability of C-O-H  
958 fluids as a function of pressure, temperature, and oxidation state.

959 A literature survey on UHPM diamond crystallization reveals that sometimes  
960 discussions are oriented around "fluid vs. melt, or fluid vs. hydrous melt." Without clear  
961 a definition of how one should distinguish a silica-rich fluid from a hydrous silicate melt  
962 at high pressures and high temperatures, this controversy simply reflects a semantic issue.  
963 For example, experiments conducted by Bureau and Keppler (1999) suggest that there is  
964 a complete miscibility between silicate melt and water in most of the upper mantle,

965 except at very shallow depths. In these experiments, the hydrous melt and silicate-bearing  
966 vapor coexisted separately at low T, whereas at higher T they mixed to become a single-  
967 phase supercritical fluid that was stable at  $P=1.5\text{--}2.5$  GPa. Experiments and direct studies  
968 of fluid inclusions in natural rocks conducted by others (e.g. Akaishi and Yamaoka 2000;  
969 Pal'yanov et al. 2002; Manning 2004; Ferrando et al. 2005; Frezzotti et al. 2007) also  
970 demonstrated that at  $P \geq 4$  GPa and  $T \geq 800$  °C there is no distinction between aqueous  
971 fluids and silicate melts because volatile-rich chemical systems are in a supercritical  
972 state.

973 A melt concept for Erzgebirge diamond crystallization was nevertheless proposed  
974 by Massonne (2003) which was motivated by their studies of melting events in the bulk  
975 rocks of both Kokchetav and Erzgebirge diamond-bearing UHPM terranes which were  
976 constrained by zircon geochronology (Massonne et al. 2007; Massonne and Fockenberg  
977 2012). The cathodoluminescence images (Figs 3 and 4 from Massonne et al. 2007) clearly  
978 show that the cores of the zircons are typically eroded. The eroded zone of the zircon  
979 core is interpreted as being caused by a melting event. The second zone overgrew the  
980 eroded core and contains diamonds, while the third zone at the outer rim of the zircon  
981 grain does not contain any diamond inclusions. The authors report the following ages:  
982 metamorphic zircon core  $337.0 \pm 2.7$  Ma (21 analyses); diamond-bearing zone of zircon  
983  $336.8 \pm 2.8$  Ma (23 analyses); and the outer rim zone of zircon  $330.2 \pm 5.8$  Ma (12  
984 analyses). The zircon ages combined with petrological observations, indeed, provide  
985 some new important constraints on the pressure-time history of these rocks. However, the  
986 presence of an eroded core of zircon enveloped by diamond-bearing zircon zone does not  
987 provide any direct evidence that the diamonds originated from melt. The information

988 about the origin of the diamonds is still “hidden” inside these diamonds since Massonne  
989 et al. (2007) did not study their inclusions. Thus, the media which these diamonds  
990 crystallized from, whether it be a carbon-rich silicate melt, and/or a C-O-H fluid or a  
991 multicomponent fluid is not well constrained. Additional studies using high resolution  
992 techniques (e.g. synchrotron IR spectroscopy and FIB-assisted STEM or TEM coupled  
993 with nanoSIMS) would provide better constraints on the melt vs fluid origin of these  
994 unique microdiamonds enclosed in zoned zircons.

995         Korsakov et al. (2004) suggested that diamonds from the Kokchetav UHPM  
996 terrane should be classified as “intragranular” type A (diamonds included in garnet,  
997 clinopyroxene and zircon – e.g. high pressure minerals) and “intergranular” type B  
998 (diamonds occurring within pseudomorphs after high-pressure minerals), and  
999 “intergranular” type C which occur within the granitic-like material with a  
1000 quartz+feldspar composition. They observed that type C “intergranular” diamonds occur  
1001 in high concentrations within the quartz-feldspathic material (e.g. they could be called  
1002 “granitic melt injections” or “migmatitic material”) along the contact zone between the  
1003 garnet-biotite-quartz and clinopyroxene-calcite layers. They proposed that these  
1004 diamonds formed during the interaction of pelite-derived hydrous melt with a granitic  
1005 composition with carbonate rocks during UHPM events. Korsakov et al. (2004) suggest  
1006 that a granitic melt could act as a crystallization medium as well as a transport medium  
1007 for type C “intergranular” diamonds. If one hypothesizes that three geologic events could  
1008 have taken place, then three generations of diamonds could have formed, and they would  
1009 have different ages, formation mechanisms, and media from which they crystallized.

1010 In order to prove such a hypothesis one should collect diamonds of each type  
1011 along with: (i) geochronological data of diamond formation, (ii) type of inclusions  
1012 preserved in diamonds (fluid, gas, solid matter) and their geochemical and crystal  
1013 structure parameters, and (iii) morphology of diamonds. Until such data become  
1014 available, the “three different type of diamonds” proposed by Korsakov et al (2004) can  
1015 more straightforwardly be explained by one crystallization event that occurred during the  
1016 same geological process (supercritical fluid/melt at the peak of the UHP metamorphism)  
1017 which would imply that the diamonds all have the same age. Since diamond is chemically  
1018 stable it may survive a retrogressive metamorphic event, whereas other UHP minerals  
1019 such as coesite, majorite, phengite, super Si-titanite, high Enschlo clinopyroxene and  
1020 others can become re-equilibrated or replaced by their lower-pressure phases, e.g.  
1021 pseudomorphs. Therefore, the same diamond (type A) which formed under peak UHP  
1022 metamorphic conditions can be preserved within former UHP minerals subjected to  
1023 retrogressive metamorphism. However, in this case such a diamond would be classified  
1024 type B according to Korsakov et al. (2004). If diamonds of type C are formed due to  
1025 interaction between Si-rich and C-rich layers during their partial melting at UHPM  
1026 conditions, such diamonds are expected to contain inclusions with chemistry that would  
1027 support this origin hypothesis. Until such data are collected, the concepts of three types of  
1028 diamonds (A, B and C) crystallizing during different UHPM events remain unproven.

1029 Korsakov and Herman (2006) have also proposed that carbonate melt can be a  
1030 medium where diamond crystallization occurred in the Kokchetav dolomite marbles.  
1031 However, this hypothesis has been questioned by Imamura et al. (2013). They note that it  
1032 is difficult to explain the extremely negative  $\delta^{13}\text{C}$  values by diamond crystallization from

1033 a carbonate melt, because strong isotopic fractionation is not expected between diamond  
1034 and carbonate melt at high pressures and temperatures (Bottinga 1968; Reutsky et al.  
1035 2015).

### 1036 *Oxidation state of UHPM diamond crystallization*

1037 Another important aspect of diamond crystallization is the oxidation state of the  
1038 diamond-forming media. Association of Erzgebirge polycrystalline diamonds with  
1039 carbonate ( $\text{CaCO}_3$ ) inclusions suggests that they formed in an oxidizing environment  
1040 close to the CCO buffer (Fig. 17) (e.g. Dobrzhinetskaya et al. 2013; Jacob et al. 2014).  
1041 This is also supported by synchrotron infrared spectra of Erzgebirge diamond inclusions  
1042 which show a well pronounced absorption band at  $1430\text{ cm}^{-1}$ , which corresponds to the  
1043  $\text{CO}_3^{-2}$  radical (e.g. Dobrzhinetskaya et al. 2006a). Nanoinclusions of  $\text{MgCO}_3$  and  $\text{CaCO}_3$ -  
1044 aragonite were directly observed with TEM in diamonds from garnet–biotite gneiss of the  
1045 Kokchetav massif (Dobrzhinetskaya et al. 2001, 2005, 2006b). This allows one to  
1046 hypothesize that the Kokchetav diamonds also formed in an oxidizing environment close  
1047 to the CCO buffer (Jacob et al. 2014).

1048 Frezzotti et al. (2014) suggested that the Lago di Cignana (Western Alps)  
1049 diamond nucleation began when the  $\text{H}_2\text{O}$ -rich fluid reached the excess concentration of  
1050 carbon required for spontaneous nucleation of diamond. They showed that at high  
1051 pressures the interaction of rock buffered  $f_{\text{O}_2}$  and the prograde P-T path may control the  
1052 carbon saturation. The thermodynamic modeling (Frezzotti al. 2014) suggested that the  
1053 diamond crystallized from C-O-H fluids with a water concentration of about  $0.992 <$   
1054  $X_{\text{H}_2\text{O}} < 0.997$ , and that the  $f_{\text{O}_2}$  was at the level required for EMOD (Enstatite + Magnesite  
1055 = Olivine + Diamond) equilibrium (Fig. 17).

1056            However, there are two cases where microdiamonds were found together with SiC  
1057 as multiphase inclusions in zircon from Gföhl granulite samples of the Moldanubian  
1058 Zone, Bohemian massif (Perraki and Faryad 2014) and in garnet from metapelitic  
1059 gneisses of Pohorje, the Austro-Alpine UHPM terrane, Eastern Alps (Janák et al. 2015).  
1060 Notably, Perraki and Faryad (2014) wrote that they used SiC abrasives for one step of the  
1061 polishing procedure, but to eliminate the possibility of contamination they removed the  
1062 polish with an ultrasonic cleaner and polycrystalline-type diamond spray was used for the  
1063 polishing of the thin section surface. Additionally, the occurrence of SiC and diamond  
1064 grains beneath the polished surface was checked with both transmitted and reflected light  
1065 microscopy.

1066            Though Janák et al. (2015) hypothesized that diamond + moissanite inclusions in  
1067 garnet from metasedimentary rocks of Pohorje were crystallized from a reduced C-O-H  
1068 fluid, they concluded that further detailed studies are needed to fully understand the  
1069 oxidation state during their formation. Certainly, these unusual findings of diamond +  
1070 SiC inclusions in garnets from UHPM terranes deserve additional close attention.

#### 1071 *UHPM diamond formation under metastable conditions*

1072            Shortly after the discovery of diamonds in UHPM rocks, crystallization under  
1073 metastable conditions was considered as an alternative to the classical concept of  
1074 diamond formation in the Earth at  $P \sim 4.0\text{-}6.0$  GPa and  $T \sim 900 - 1400$  °C (Bundy 1980;  
1075 Boyd et al. 1985).

1076            Throughout the 1980's and into the mid of 1990's the concept of metastable  
1077 formation of diamonds at low pressure conditions of crustal metamorphism was proposed  
1078 (e.g. Letnikov 1983; Lavrova 1991; Ekimova et al. 1992; Lavrova et al. 1995). Even at

1079 that time it was considered controversial to the new concept of diamond crystallization  
1080 during UHP metamorphism of crustal rocks subducted to a depth  $\geq 120$  km (Sobolev and  
1081 Shatsky 1988, 1990; Shatsky and Sobolev 1993; Shatsky et al. 1995). It has since been  
1082 shown unambiguously that the Kokchetav massif is an UHPM terrane through the  
1083 documentation of numerous UHP mineral phases by hundreds of high-quality studies  
1084 involving state-of-art and synchrotron assisted instruments (see reviews: Ernst and Liou  
1085 1999; Ogasawara 2005; Dobrzhinetskaya 2012; Schertl and Sobolev 2013; Loui et al  
1086 2014). Despite all these convincing observations the concept of diamond crystallization  
1087 outside of the diamond stability field has still occasionally appealed as a formation  
1088 mechanism for diamonds found in UHPM terranes (e.g. Pechnikov and Kaminsky 2008,  
1089 Simakov 2010; 2015; 2018). Since this hypothesis has been invoked to describe the  
1090 formation conditions of microdiamonds a short discussion about what is known from  
1091 experiments on metastable diamond growth is warranted.

1092 Pechnikov and Kaminsky (2008) focused their attention on the geometry of the  
1093 “productive” diamond-bearing ore body using detailed mapping completed by the local  
1094 Kokchetav Geological Survey, and they combined this information with their  
1095 petrographic observations. They concluded that the diamonds were formed under crustal  
1096 conditions (e.g. metastable) from crustal fluid-metasomatic processes that was active  
1097 along the fault-zone superimposed on the Precambrian gneisses. They accepted the  
1098 diamond bearing zircon age of 527–537 Ma (Claoué-Long et al. 1991; Jagoutz et al.  
1099 1990; 1991; Hermann et al. 2006) as the age of diamond formation and therefore the age  
1100 of the fluid-metasomatic activities along the fault zone. The authors believe that the  
1101 micrometer size of the diamonds, along with their isotopic signatures ( $\delta^{13}\text{C} = -8.9$  ‰

1102 through  $-27\text{‰}$ ), support diamond formation under metastable crustal conditions. On the  
1103 other hand, Pechnikov and Kaminsky (2008) note that their concept does not exclude the  
1104 occurrence of episodes of UHP metamorphism and they accept the presence of coesite  
1105 and other UHP minerals in the diamond-bearing rocks. However, their concept fails to  
1106 explain when the UHP metamorphic episodes took place, and the authors did not discuss  
1107 that fact that zircons containing diamonds and/or coesite, or pyroxene with high Ca-  
1108 Eskola component and other UHP phases have the same age (e.g. Katayama et al. 2000;  
1109 2001; 2002; Ogasawara 2005). Though the prevalent light carbon isotope characteristics  
1110 of diamonds prove that such carbon has a crustal origin it doesn't reject the possibility of  
1111 the subduction of crustal rocks to a depth  $\geq 120$  -150 km where the pressure and  
1112 temperature are high enough to stabilize carbon in the form of diamond. Therefore, the  
1113 arguments of Pechnikov and Kaminsky (2008) on the metastable origin of diamonds from  
1114 Kokchetav are contrary to the conclusions reported by most other scientists who have  
1115 collected and studied diamonds from this locality

1116 Simakov (2010) report that they synthesized nano-diamonds from a water-alcohol  
1117 solution which was the source of free carbon C, in a high-pressure reactor (volume~500  
1118  $\text{cm}^3$ ) at  $P=0.1$  GPa and  $T=$  at  $500^\circ\text{C}$ . They directly applied the results of this experiment  
1119 to explain the origin of micron-sized diamonds from UHPM terrane of the Kokchetav  
1120 massif without taking into consideration all of the other UHP minerals associated with  
1121 these diamonds (e.g. Katayama et al. 2000; 2001b; 2002; Ogasawara et al. 2002;  
1122 Ogasawara 2005).

1123 Furthermore, Simakov (2015; 2018) also discussed the metastable formation of  
1124 diamond from a C-O-H-N fluid and applied this idea to explain the origin of UHPM

1125 diamonds. They discussed that nitrogen interaction decreases the total energy of  
1126 diamond nuclei formation and the equilibrated methane pressure stabilizes the diamond,  
1127 and they confirmed this by the hydrothermal synthesis of nano-diamond from nitrogen  
1128 bearing organics at metastable P-T conditions (Simakov et al. 2008). Synthesis of nano  
1129 diamonds at high temperatures and/or ambient-low pressure (e.g. metastable) are well-  
1130 known in materials sciences processes such as laser ablation, chemical vapor deposition  
1131 (CVD), autoclave synthesis from supercritical fluids, ion irradiation of graphite and  
1132 ultrasound cavitation (e.g. Krueger 2008) as well detonation techniques (e.g. Danilenko  
1133 2004), which requires extremely high pressures. However, before invoking any of the  
1134 processes mentioned above to explain how diamonds form in UHPM terranes would  
1135 require a critical evaluation of all the existing data that have been collected by many  
1136 research groups. Thermodynamic calculations for PT-conditions of diamond-bearing  
1137 rocks and the presence of UHP minerals associated with diamond are important  
1138 petrological evidence indicating that the diamonds from Kokchetav formed under UHPM  
1139 conditions and their formation does not easily fit to the models/experiments proposed by  
1140 Simakov (2010; 2015; 2018). Additionally, experiments conducted by other groups using  
1141 a starting material that is close to the bulk chemistry of the Kokchetav diamond-bearing  
1142 rocks, under both hydrous and anhydrous, and at varying oxidation states have produced  
1143 run products that are a good fit to the data collected from the rocks, diamond itself and  
1144 other associated minerals (e.g. Hong et al. 1999; Polyakov et al. 1999, 2000; Akaishi and  
1145 Yamaoka 2000; Yamaoka et al. 2000; Kumar et al. 2001; Hwang et al. 2003;  
1146 Dobrzhinetskaya et al. 2004; Dobrzhinetskaya and Green 2007a). Therefore, while the  
1147 models/experiments proposed by Simakov (2010; 2015; 2018) do, indeed, explain

1148 diamond formation outside of the diamond stability field they cannot be applied to  
1149 diamonds from the Kokchetav massif or for diamonds found in other UHPM terranes.

1150 It should be emphasized that if diamond formation under metastable conditions is  
1151 proposed the following data are expected to be presented for consideration: (i) thorough  
1152 geologic mapping of the area where the sample was collected to find any other UHP  
1153 indicator minerals that may be present; (ii) unambiguous proof of the indigenous origin  
1154 of the diamond, the diamond should be *in situ* so that the interface between the diamond  
1155 and its host mineral can be examined in detail with high resolution techniques, and (iii)  
1156 all available thermodynamic data has been reviewed.

1157 ***Comet impact hypothesis for the origin of diamonds from Kumdy Kol Lake, Kokchetav***  
1158 ***Massif***

1159 Recently a new impact-cosmic-metasomatic genesis of the Kokchetav diamond  
1160 deposit was proposed (Tretiakova and Lyukhin 2016; 2017). It was provoked by an  
1161 impact event followed by metamorphism and alteration of the rocks. The authors note  
1162 that the ring structure of Kumdy Kol Lake, where most of the diamond-bearing  
1163 metamorphic rocks of the Kokchetav massif are situated, has the form and size (~4 km  
1164 diameter) resembling a small impact crater. They suggest that the diamond-bearing  
1165 terrane formed by comet impact under an oblique angle which generated shock wave  
1166 compression with peak pressures reaching > 50 GPa.

1167 They argue that there is evidence of impact metamorphism, (1) presence of UHP  
1168 minerals diamond-lonsdaleite, coesite, omphacite, (2) the delivery by comet moissanite  
1169 (SiC) and graphite spherules as well as "meteoritic matter" such as magnetite, hematite,  
1170 iocite, troilite,  $\alpha$ -Fe, Ni-Fe, (3) annealed metallic globules are observed having various

1171 fanciful forms (globules, small dumb-bells, drops, spherules and so on) in host rock and  
1172 rock-forming minerals, and (4) dislocation and birefringence in diamonds, planar  
1173 structure in quartz, inclusions UHP minerals in rock forming minerals. The authors  
1174 suggested that collision of huge velocity comet and the Earth generated rapid shock wave  
1175 compression (pressure peak > 50 GPa) forming diamond, coesite and other UHP minerals  
1176 which later together with so-called “meteoritic matter” were subjected to regional  
1177 metamorphism and metasomatism.

1178         Additionally, they hypothesize that the “unprecedentedly” high  $^3\text{He}/^4\text{He}$  isotopic  
1179 ratios of the Kokchetav diamonds reported by (Shukolyukov et al. 1993) are indeed due  
1180 to the formation of these diamonds outside of the solar system. However, new  
1181 measurements by Sumino et al. (2011) revealed that  $^3\text{He}/^4\text{He}$  value of the Kokchetav  
1182 diamonds are close to the values found for OIB, and that the extremely high  $^3\text{He}/^4\text{He}$  ratio  
1183 likely originated from Li-rich contaminants.

1184         The “impact-cosmic-metasomatic” origin remains unproven based on the  
1185 following evidence: (i) Sumino et al. (2011) have shown that the “unprecedentedly high”  
1186  $^3\text{He}/^4\text{He}$  isotopic ratios are not likely a true feature of the Kokchetav diamonds, (ii) the  
1187 authors have not presented unambiguous evidence of the claimed “oblique” impact (e.g.  
1188 asymmetrical ejecta deposits), (iii) the authors do not propose that any of the other  
1189 dozens of similar shaped lakes around Kumdy-Kol lake were caused by impact events,  
1190 and (iv) and they do not report that the Kokchetav diamonds show unique moiré fringes  
1191 which are well-known features observed in impact-formed diamonds (e.g. Langenhorst  
1192 2003; Ohfuji et al. 2015).

1193

1194 **MISIDENTIFICATION OF MICRODIAMONDS DUE TO CONTAMINATION**  
1195 **FROM SAMPLE PREPARATION**

1196  
1197 **General precautions and examples**

1198           Since diamonds from UHPM terranes are small ranging in size from  $\leq 3 - 80 \mu\text{m}$   
1199 they can be misidentified with diamonds which were mechanically embedded into softer  
1200 minerals during sample preparation (e.g. cutting, drilling, and/or polishing with diamond  
1201 tools or abrasives). Recognition of possible contamination has been mentioned in the  
1202 scientific literature as well as in numerous instruction manuals attached to polishing  
1203 instruments. Microdiamond researchers are acutely aware that contamination from  
1204 sample preparation can occur, and that distinguishing indigenous microdiamonds from  
1205 diamonds embedded during sample preparation is not trivial.

1206           Figure 18 A-F contains a series of images showing the morphology of diamond  
1207 particles found in a typical abrasive powder and those embedded in diamond saws. Figure  
1208 18 G-H shows “loose” UHPM diamond crystals recovered from crushed rocks. If a  
1209 diamond-bearing sample is properly polished (see detailed procedure in Dobrzhinetskaya  
1210 et al. 2001), the diamonds will be elevated above the polished surface of host minerals  
1211 which is due to the difference in hardness between the diamond and host minerals (Fig  
1212 19). Visual inspection of the images, especially those acquired with an optical  
1213 microscope or SEM using low magnification, reveal that the morphology of diamonds  
1214 from abrasive grits and natural diamonds are quite similar (Fig. 18). Therefore, the  
1215 morphologies of the diamonds cannot always be used to distinguish between natural  
1216 microdiamonds and diamonds from abrasive grits.

1217 **Raman spectroscopy: indigenous diamond vs its synthetic counterpart**

1218           One should be cautious when using Raman spectroscopy as the sole diagnostic for  
1219 identifying indigenous diamonds. Diamond has a strong first order Raman mode at 1332  
1220  $\text{cm}^{-1}$ , some abrasives show broadening of this mode as well as a strong shift of this mode  
1221 to lower wavenumbers. However, Nasdala et al. (2016) show that the Raman parameters  
1222 of diamond abrasives (collected from 11 different manufacturers) widely overlap with  
1223 UHPM microdiamonds (Fig. 20 A-C, E, F) making it nearly impossible to distinguish  
1224 between a genuine UHP relict or an introduced artefact based on Raman spectroscopy  
1225 alone.

1226           The study of Menneken et al. (2007) is a prominent example of diamond  
1227 contamination during sample polishing. They reported the astonishing discovery of the  
1228 oldest microdiamonds on Earth as inclusions in zircons from the Jack-Hills conglomerate,  
1229 Australia (~ 4.2 – 3.0 Ga, Nemchin et al. 2008). They used Raman spectroscopy as their  
1230 primary diagnostic technique, particularly they relied on the FWHM of the diamond  
1231 Raman mode to distinguish their diamonds from the diamond-based abrasive used for  
1232 their sample preparation. Indeed, in Fig. 2 from Menneken et al. (2007) the plots of the  
1233 FWHM vs. Raman shift show that the Jack-Hills microdiamonds have larger FWHM's  
1234 and are shifted to lower frequency than the abrasive diamonds used during their sample  
1235 preparation. In addition to the Raman results Menneken et al. (2007) ruled out  
1236 contamination from the diamond polishing powder based on (i) some of the diamonds are  
1237 completely enclosed by zircon, and (ii) they argued that the size of the diamond  
1238 inclusions are mostly larger than the size of the diamonds in the polishing materials.

1239           However, several unreconciled discrepancies existed. One is that it does not  
1240 matter if the zircons are considered as magmatic (Hopkins et al. 2008; 2010; 2012) or as

1241 metamorphic (Rasmussen et al. 2010; 2011; 2012) the oldest Jack Hills zircons have a  
1242 shallow (<10 km) crustal origin. If diamond crystallized along with the zircon at these  
1243 shallow depths, the diamonds would have formed outside the diamond stability field.  
1244 Alternatively, the diamonds could have formed within the diamond stability field at a  
1245 depth of  $\geq 150$  km and they were later transported to these shallow depths where they  
1246 became incorporated into the zircons when they crystallized.

1247 Another discrepancy is that other high-pressure minerals or evidence of  
1248 decompression from high pressures have not been reported in the Jack Hills zircons, and  
1249 that boundary between the diamond included in zircon is highly irregular and sharp, and  
1250 even porous and filled with granular “debris” (Fig. 21 A). Such “unusual” boundaries  
1251 between two detached phases (diamond and zircon) look significantly different from the  
1252 boundaries between an indigenous diamond and its host zircon. The contact zone in many  
1253 samples generally show that the diamond is intricately intergrown with its host zircon,  
1254 which immediately makes it clear that such a diamond is indigenous (Fig. 21 B and C).

1255 Considering these inconsistencies, Dobrzhinetskaya et al. (2014) examined the  
1256 exact same diamond bearing zircon samples which were kindly provided by Menneken et  
1257 al. (2007) and Nemchin et al. (2008). The SEM (Fig. 2) and TEM studies of FIB-  
1258 prepared foils (Fig. 22) concluded that the “Jack Hills diamonds” are not indigenous, and  
1259 that they are a product of contamination from the industrial diamond abrasive used for  
1260 sample preparation (Dobrzhinetskaya et al. 2014). Dobrzhinetskaya et al. (2014) clearly  
1261 demonstrated that fragments of broken diamond’s ranging in size from  $\leq 0.10 - 0.30 \mu\text{m}$   
1262 were mechanically embedded/inserted into surficial pores and cracks (Fig. 22 A), and

1263 they eroded softer minerals together with polishing dust and petropoxy all which  
1264 occurred during sample preparation (Fig. 22 B).

1265         Later, Menneken et al. (2014) used TEM and Raman spectroscopy on FIB cut  
1266 sections of the embedded diamonds and they concluded that the embedded diamond  
1267 particles originated from the diamond polishing powder. This study is evidence that  
1268 diamonds that contaminated the sample during cutting and polishing can be misidentified  
1269 as indigenous UHPM diamonds. In the case of the Jack Hills diamonds if this  
1270 misidentification was not brought to the scientific forum, it could have had a profound  
1271 impact on our understanding of the earliest phase of Earth's history. Since it is now  
1272 known that the "Jack Hills diamonds" are not indigenous several new thorough  
1273 systematic studies of synthetic diamonds from different manufacturers and  
1274 microdiamonds from well-established UHPM terranes (Fig. 20) have been reported  
1275 (Steger et al., 2013; Nasdala et al. 2016). Raman data reported by Menneken et al. (2007)  
1276 (Fig. 20 D) fit well with the Raman data from diamond-based abrasives and tools (Fig. 20  
1277 A - C), and they partly overlap with Raman data collected from UHPM diamonds (Fig.  
1278 20 E, F). As discussed above, Nasdala et al. (2016) demonstrated that Raman  
1279 spectroscopy can be used as fast and nondestructive diagnostic method for diamond  
1280 identification. However, Raman spectroscopy cannot unambiguously differentiate  
1281 between natural diamonds and industrial diamond-abrasives. To avoid erroneous  
1282 discoveries of new microdiamond localities one should avoid using Raman spectroscopic  
1283 techniques as the *only* diagnostic for confirmation of the indigenous origin of the  
1284 diamonds.

1285 In an earlier chapter we discussed that microdiamond occurring together with SiC,  
1286 moissanite (Perraki and Farayd 2014; Janák et al. 2015) would require ultra-reduced  
1287 conditions. These samples are very important for future investigations since they imply a  
1288 specific oxidation state of the diamond-moissanite inclusions in garnet. However,  
1289 additional documentations are required that these SiC inclusions have indigenous origin.  
1290 Nasdala et al. (2016) also note that the Raman spectra of geological moissanite and the  
1291 Raman spectra of synthetic silicon carbide are not distinguishable (see their Fig. 4 d).  
1292 Consequently, the presence of moissanite in multiphase inclusions from UHPM  
1293 assemblages should be confirmed in order to exclude any misinterpretation of  
1294 contamination from SiC-based abrasives used for polishing materials.

#### 1295 **How to prove that microdiamond is indigenous**

1296 In general, we believe that it should be a mandatory for acceptance of any new  
1297 discovery of non-cratonic microdiamonds to demonstrate the nature of the diamond-host  
1298 minerals interface to avoid misidentification with remnants of diamond-based polishing  
1299 abrasives. In some cases, studies of the diamond-host mineral relationships with optical  
1300 microscopy and their documentation with high resolution SE images from an SEM can be  
1301 enough to confirm the indigenous nature of a microdiamond (e.g. Dobrzhinetskaya et al.  
1302 2001). For example, the Fig. 22 B and C present the secondary electron SEM images  
1303 which demonstrate the intergrown features of zircon–diamond interface. Such  
1304 relationships unconditionally confirm indigenous origin of the diamond inclusion in  
1305 zircon. In other cases, it is necessary to use a TEM to investigate FIB-prepared foils that  
1306 were cut through the diamond-host mineral interface (e.g. Dobrzhinetskaya et al. 2001;  
1307 2003; 2007). As an example, see Fig. 23, which demonstrates FIB-milled sample of the

1308 diamond–zircon interface. FIB-TEM techniques are the safest approach for avoiding the  
1309 misidentification of industrial diamonds-abrasive as natural diamonds, especially if the  
1310 diamond inclusions under question are smaller than 5 microns (e.g. Dobrzhinetskaya et  
1311 al. 2007).

1312 Notably one robust approach for avoiding the misidentification of diamond and  
1313 moissanite inclusions would be to not use diamond and SiC tools and abrasives during  
1314 sample extraction and preparation, one could use corundum instead. Final finishing of the  
1315 samples with colloidal SiO<sub>2</sub> liquid always provides a great polishing effect and makes  
1316 diamond inclusions more visible on the flat polished surface of the host minerals.

#### 1317 **FUTURE DIRECTIONS**

1318 Studies of UHPM microdiamonds have furthered our knowledge and  
1319 understanding of geochemical and mineralogical processes during the deep subduction of  
1320 crustal material and its interaction with the Earth's mantle. Despite their micron-size  
1321 these diamonds have preserved solid, liquid, and gas inclusions over long time periods.  
1322 These inclusions reflect pathways of the crustal rocks and organic carbon from the  
1323 Earth's surface to its interior and back to the Earth's surface. The next decade of UHPM  
1324 research should focus on the following:

1325 (i) Confirmation of the indigenous nature of microdiamonds in newly discovered  
1326 UHPM localities requires the documentation of the diamond-host mineral interface with  
1327 the aid of the high-resolution SE SEM imaging, and/or TEM imaging and crystal  
1328 structure data obtained from FIB-prepared samples.

1329 (ii) Studies of nanoscale inclusions in microdiamonds from different lithologies to  
1330 improve our understanding of geochemical environments and PT conditions of diamond  
1331 crystallization.

1332 (iii) Raman studies of anomalies in microdiamonds which are interpreted as  
1333 evidence of the “lonsdaleite structure” need to be investigated with TEM-FIB, and/or  
1334 synchrotron assisted X-ray and spectroscopic techniques.

1335 (iv) Studies of stable isotopes chemistry and noble gases from additional UHPM  
1336 diamond localities to increase our knowledge of processes that occur during continental  
1337 crust - mantle interaction.

1338 (v) Coordination of laboratory-assisted researches on microdiamonds with general  
1339 questions of Earth’s dynamics through studies of UHP minerals assemblages associated  
1340 with diamond formations.

1341 (vi) Modelling and calculations of subduction and exhumation rates; and  
1342 understanding of how much crustal materials have reached the “point-of-no-return”  
1343 during deep subduction and remained in the Earth’s deep interior being intermixed with  
1344 the mantle.

1345

1346 **Acknowledgements**

1347 LD research was performed as a part of the International Lithosphere Program,  
1348 Task Force IV, project "Fate of the subducted continental lithosphere: insight through  
1349 analytical mineralogy and microstructures", and were supported in different years by  
1350 NSF grants EAR 0229666, EAR 0107118 and INT-EAR 0329596; Los Alamos National  
1351 Laboratory through Science and Technology Base Programs (grant 9949); the  
1352 Consortium for Materials Properties Research in Earth Sciences (COMPRES); Pacific

1353 Rim Program of the University of California, and the University of California Lab Fee  
1354 Research Grant. EO'B acknowledges that a portion of this work was performed under the  
1355 auspices of the US Department of Energy by Lawrence Livermore National Laboratory  
1356 under Contract No. DE-AC52-07NA27344. HS research was supported by KAKENHI  
1357 Grant Numbers JP20740314, JP23340169, JP24109702, JP26287139, and JP15KK0150  
1358 from MEXT/JSPS, Japan. Helpful discussions of several aspects of UHPM  
1359 microdiamonds origin with C.V. Stan, S.W. Faryad, M. Janák, J. Kotková and K.  
1360 Naemura are acknowledged.

1361

## 1362 REFERENCES

1363 Akaishi M, Yamaoka S (2000) Crystallization of diamond from C–O–H fluids under  
1364 high-pressure and high-temperature conditions. *J Cryst Growth* 209:999-1003

1365

1366 Allègre CJ, Staudacher T, Sarda P, Kurz M (1983) Constraints on evolution of Earth's  
1367 mantle from rare gas systematics. *Nature* 303:762-766

1368

1369 Anthony TR, Banholzer WF (1992) Properties of diamond with varying isotopic  
1370 composition. *Diam Relat Mater* 1:717-26

1371

1372 Ballentine CJ, Burnard PG, (2002) Production, release and transport of noble gases in the  
1373 continental crust. *Rev Mineral Geochem* 47:481-538

1374

1375 Ballentine CJ, Marty B, Lollar BS, Cassidy M (2005) Neon isotopes constrain convection  
1376 and volatile origin in the Earth's mantle. *Nature* 433:33-38

1377

1378 Basu S, Jones AP, Verchovsky AB, Kelley SP, Stuart FM (2013) An overview of noble  
1379 gas (He, Ne, Ar, Xe) contents and isotope signals in terrestrial diamond. *Earth-Sci*  
1380 *Rev* 126:235-249

1381

1382 Bebout GE, Fogel ML (1992) Nitrogen-isotope compositions of metasedimentary rocks  
1383 in the Catalina schist, California: implications for metamorphic devolatilization  
1384 history. *Geochim. Cosmochim. Acta* 56, 2839-2849

1385

1386 Begemann F (1994) Indigenous and extraneous noble gases in terrestrial diamonds. *In*:  
1387 *Noble Gas Geochemistry and Cosmochemistry*. Matsuda J (ed.) Terra Scientific  
1388 Publishing Company, Tokyo, p. 217-227

1389

1390 Bottinga Y (1968) Carbon isotope fractionation between graphite, diamond, and carbon  
1391 dioxide. *Earth Planet Sci Lett* 5:301-307  
1392

1393 Boyd FR, Gurney JJ, Richardson SH (1985) Evidence for a 150–200-km thick Archaean  
1394 lithosphere from diamond inclusion thermobarometry. *Nature* 315:387-389  
1395

1396 Broadley MB, Kagi H, Burgess R, Zedgenizov D, Mikhail S, Almayrac M, Ragozin A,  
1397 Pomazansky B, Sumino H (2018) Plume-lithosphere interaction, and the  
1398 formation of fibrous diamonds. *Geochem Perspect Lett.* 8:26-30.  
1399

1400 Bruguier O, Bosch D, Cabby R, Vitale-Brovarone A, Fernandez L, Hammor D, Laouar R,  
1401 Ouabadi A, Abdallah N, Mechaty M (2017) Age of UHP metamorphism in the  
1402 Western Mediterranean: Insight from rutile and minute zircon inclusions in a  
1403 diamond-bearing garnet megacryst (Edough Massif, NE Algeria). *Earth Planet Sci*  
1404 *Lett* 474:215-225  
1405

1406 Brun J-P, Faccenna C (2008) Exhumation of high-pressure rocks driven by slab rollback.  
1407 *Earth Planet Sci Lett* 272:1-7  
1408

1409 Bundy FP, Kasper JS (1967) Hexagonal diamond—A new form of carbon. *J Chem Phys*  
1410 46:3437–3446

1411 Bundy FP (1980) The P, T phase and reaction diagram for elemental carbon. *J Geophys*  
1412 *Res Solid Earth* 85:6930-6936  
1413

1414 Bureau H, Keppler H (1999) Complete miscibility between silicate melts and hydrous  
1415 fluids in the upper mantle: experimental evidence and geochemical implications.  
1416 *Earth Planet Sci Lett* 165:187-196.  
1417

1418 Busigny V, Cartigny P, Philippot P (2011) Nitrogen isotopes in ophiolitic metagabbros: a  
1419 re-evaluation of modern nitrogen fluxes in subduction zones and implication for  
1420 the early Earth atmosphere. *Geochim. Cosmochim. Acta* 75:7502-7521  
1421

1422 Cabby R, Bruguier O, Fernandez L, Hammor D, Boscha D, Mechaty M, Laouar R,  
1423 Ouabadi A, Abdallah N, Doucheta C (2014) Metamorphic diamonds in a garnet  
1424 megacryst from the Edough Massif (northeastern Algeria). Recognition and  
1425 geodynamic consequences. *Tectonophysics* 637:341-353  
1426

1427 Cartigny P (2005) Stable isotopes and the origin of diamond. *Elements* 1:79–84  
1428

1429 Cartigny P, de Corte K, Shatsky VS, Ader M, De Paepe P, Sobolev NV, Javoy M (2001)  
1430 The origin and formation of metamorphic microdiamonds from the Kokchetav  
1431 massif, Kazakhstan: a nitrogen and carbon isotopic study. *Chem Geol* 176:265-  
1432 281  
1433

1434 Cartigny P, Palot M, Thomassot E, Harris JW (2014) Diamond formation: a stable  
1435 isotope perspective. *Annual Rev Earth Planet Sci* 42:699-732

1436  
1437 Chopin C (1984) Coesite and pure pyrope in high-grade blueschists of the Western Alps:  
1438 a first record and some consequences. *Contrib Miner Petrol* 86:107–118  
1439  
1440 Chopin C, Sobolev NV (1995) Principal mineralogic indicators of UHP in crustal rocks.  
1441 *In: Ultrahigh-Pressure Metamorphism* (Coleman RG, Wang X. eds) Cambridge  
1442 University Press, p. 96-133  
1443  
1444 Ciaoué-Long JC, Sobolev NV, Shatsky VS, Soboiev AV (1991) Zircon response to  
1445 diamond-pressure metamorphism in the Kokchetav massif, USSR. *Geology*  
1446 19:710-713  
1447  
1448 Claoué-Long JC, Sobolev NV, Shatsky VS, Sobolev AV (1991) Zircon response to  
1449 diamond-pressure metamorphism in the Kokchetav massif, USSR. *Geology*  
1450 19:710-713  
1451  
1452 Danilenko VV (2004) Shock-wave sintering of nanodiamonds. *Phys Solid State* 46:711-  
1453 715  
1454  
1455 Daulton TL, Eisenhour DD, Bernatowicz TJ, Lewis RS, Buseck PR (1996) Genesis of  
1456 presolar diamonds: Comparative high-resolution transmission electron  
1457 microscopy study of meteoritic and terrestrial nano-diamonds. *Geochim*  
1458 *Cosmochim Acta* 60:4853-4872  
1459  
1460 de Corte K, Cartigny P, VShatsky VS, Sobolev NV, Javoy M (1998) First evidence of  
1461 fluid inclusions in metamorphic microdiamonds from the Kokchetav massif,  
1462 Northern Kazakhstan. *Geochim. Cosmochim Acta* 62:3765–3777  
1463  
1464 de Corte K, Korsakov A, Taylor WR, Cartigny P, Ader M, de Paepe P (2000) Diamond  
1465 growth during ultrahigh-pressure metamorphism of the Kokchetav Massif,  
1466 northern Kazakhstan. *Island Arc* 9: 428–438  
1467  
1468 de Corte K, Taylor WR, De Paepe P (2002) Inclusion contents of microdiamonds from  
1469 UHP metamorphic rocks of the Kokchetav massif. *In: The Diamond-Bearing*  
1470 *Kokchetav Massif*. Parkinson CD, Katayma I, Liou JG, Maryama S (eds),  
1471 Universal Academy Press Inc, Kazakhstan, p. 115–135  
1472  
1473 Denisov VN, Mavrin BN, Serebryanaya NR, Dubitsky GA, Aksenonov VV, Kirichenko  
1474 AN, Kuzmin NV, Kulnitskiy BA, Perezhugin IA, Blank VD (2011) First-  
1475 principles, UV Raman, X-ray diffraction and TEM study of the structure and  
1476 lattice dynamics of the diamond–lonsdaleite system. *Diam Relat Mater* 20:951-  
1477 953  
1478  
1479 Derjaguin BV, Fedoseev DV (1994) Physico-chemical synthesis of diamond in  
1480 metastable range. *Prog Surf Sci* 45:71-80  
1481

1482 Dobrzhinetskaya LF (2012) Microdiamonds—frontier of ultrahigh-pressure  
1483 metamorphism: a review. *Gondwana Res* 21:207-223  
1484  
1485 Dobrzhinetskaya LF, Eide EA, Larsen RB, Sturt BA, Trønnes RG, Smith DC, Taylor WR  
1486 Posukhova TV (1995) Microdiamond in high-grade metamorphic rocks of the  
1487 Western Gneiss region, Norway. *Geology* 23:597-600  
1488  
1489 Dobrzhinetskaya LF, Green II HW, Mitchell TE, Dickerson RM (2001) Metamorphic  
1490 diamonds: mechanism of growth and inclusion of oxides. *Geology* 29:263-266  
1491  
1492 Dobrzhinetskaya LF, Green II HW, Weschler M, Darus M, Wang YC, Massonne HJ,  
1493 Stöckhert B (2003) Focused ion beam technique and transmission electron  
1494 microscope studies of microdiamonds from the Saxonian Erzgebirge, Germany  
1495 *Earth Planet Sci Lett* 210:399-410  
1496  
1497 Dobrzhinetskaya LF, Renfro AP, Green II HW (2004) Synthesis of skeletal diamonds:  
1498 Implications for microdiamond formation in orogenic belts. *Geology* 32:869-872  
1499  
1500 Dobrzhinetskaya LF, Wirth R, Green HW (2005) Direct observation and analysis of a  
1501 trapped COH fluid growth medium in metamorphic diamond. *Terra Nova* 17:472-  
1502 477  
1503  
1504 Dobrzhinetskaya LF, Wirth R, Green II HW (2006a) Nanometric inclusions of carbonates  
1505 in Kokchetav diamonds from Kazakhstan: A new constraint for the depth of  
1506 metamorphic diamond crystallization. *Earth Planet Sci Lett* 243:85-93  
1507  
1508 Dobrzhinetskaya LF, Liu Z, Cartigny P, Zhang J, Tchkheta D, Hemley RJ, Green II HW  
1509 (2006b) Synchrotron infrared and Raman spectroscopy of microdiamonds from  
1510 Erzgebirge, Germany. *Earth Planet Sci Lett* 248:340-349  
1511  
1512 Dobrzhinetskaya LF, Green HW (2007a) Diamond synthesis from graphite in presence of  
1513 water and SiO<sub>2</sub>: implications for diamond formation in quartzites from  
1514 Kazakhstan. *Int Geol Rev* 49:389–400  
1515  
1516 Dobrzhinetskaya LF, Green II HW (2007b) Experimental studies of mineralogical  
1517 assemblages of metasedimentary rocks at Earth's mantle transition zone  
1518 conditions. *J Metamorph Geol* 25:83-96  
1519  
1520 Dobrzhinetskaya LF, Green II HW, Takahata N, Sano Y, Shirai K (2010) Crustal  
1521 signature of  $\delta^{13}\text{C}$  and nitrogen content in microdiamonds from Erzgebirge,  
1522 Germany: Ion microprobe studies. *J Earth Sci* 21:623-634  
1523  
1524 Dobrzhinetskaya LF, Wirth R, Green II HW, Schreiber A, O'Bannon III EF (2013) First  
1525 find of polycrystalline diamond in ultrahigh-pressure metamorphic terrane of  
1526 Erzgebirge, Germany. *J Metamorph Geol* 31:5-18  
1527

1528 Dobrzhinetskaya LF, Wirth R, Green II HW (2014) Diamonds in Earth's oldest zircons  
1529 from Jack Hills conglomerate, Australia, are contamination. *Earth Planet Sci Lett*  
1530 387:212-218  
1531

1532 Dubinchuk VT, Simakov SK, Pechnikov VA (2010) Lonsdaleite in diamond-bearing  
1533 metamorphic rocks of the Kokchetav Massif. *Dokl Earth Sci* 430:40-42  
1534

1535 Egger, D.H. & Baker, D.R., 1982. Reduced volatiles in the system C-O-H: implications  
1536 to mantle melting, fluid formation and diamond genesis. *In: High Pressure*  
1537 *Research in Geophysics* Akimoto S, Manghnani MH (eds), Center Academic  
1538 Publisher, Tokyo, pp. 237–250.  
1539

1540 Ekimova TE (1992) Diamond inclusions in rock-forming minerals of metamorphic rocks.  
1541 *Dokl Akad Nauk* 322:366-368  
1542

1543 Ernst WG, Liou JG (1999) Overview of UHP metamorphism and tectonics in well-  
1544 studied collisional orogens. *Int Geol Rev* 41:477-493  
1545

1546 Essenov CE, Efimov LA, Shiygin ED, Abducabirova MA, Vedernicov NN, Nuriybaev  
1547 AN (1968) To problem of the diamond deposits of the Northern Kazakhstan.  
1548 *Vestn Akad Nauk Kaz SSR* 1:37-45  
1549

1550 Faure M, Fabbri O, Monie P (1988) The Miocene bending of southwest Japan: new  
1551 <sup>39</sup>Ar/<sup>40</sup>Ar and microtectonic constraints from the Nagasaki schists (western  
1552 Kyushu), an extension of the Sanbagawa high-pressure belt. *Earth Planet Sci Lett*  
1553 91:105-16  
1554

1555 Fedoseev DV, Galimov EM, Varnin VP, Prokhorov VS, Deryagin BV (1971) Carbon  
1556 isotopes fractionation at physical-chemical synthesis of diamond from gas.  
1557 *Doklady Akademii Nauk SSSR*, 201:1149-1150 (In Russian)  
1558

1559 Ferrando S, Frezzotti ML, Dallai L, Compagnoni R (2005) Multiphase solid inclusions in  
1560 UHP rocks (Su-Lu, China): Remnants of supercritical silicate-rich aqueous fluids  
1561 released during continental subduction. *Chem Geol* 233:68-81  
1562

1563 Frezzotti ML (2019) Diamond growth from organic compounds in hydrous fluids deep  
1564 within the Earth. *Nat Comm* 10:1-8  
1565

1566 Frezzotti ML, Ferrando S, Dallai L, Compagnoni R (2007) Intermediate alkali-alumina-  
1567 silicate aqueous solutions released by deeply subducted continental crust: fluid  
1568 evolution in UHP OH-rich topaz-kyanite quartzites from Donghai (Sulu, China). *J*  
1569 *Petrol* 48: 1219-1241  
1570

1571 Frezzotti ML, Selverstone J, Sharp ZD, Compagnoni R (2011) Carbonate dissolution  
1572 during subduction revealed by diamond-bearing rocks from the Alps. *Nat Geosci*  
1573 4:703-706

1574  
1575 Frezzotti ML, Huizenga JM, Compagnoni R, Selverstone J (2014) Diamond formation by  
1576 carbon saturation in C–O–H fluids during cold subduction of oceanic lithosphere.  
1577 *Geochim Cosmochim Acta* 143:68-86  
1578  
1579 Frondel C, Marvin UB (1967) Lonsdaleite, a hexagonal polymorph of diamond. *Nature*  
1580 214:587-589  
1581  
1582 Frost BR, Frost CD (2014) *Essential of Igneous and Metamorphic Petrology*. Cambridge  
1583 University Press  
1584  
1585 Gautheron C, Cartigny P, Moreira M, Harris JW, Allègre CJ (2005) Evidence for a  
1586 mantle component shown by rare gases, C and N isotopes in polycrystalline  
1587 diamonds from Orapa (Botswana). *Earth Planet Sci Lett* 240:559–572  
1588  
1589 Glassley W, Korstgard J, Sorensen K, Platou SW (2014) A new UHP metamorphic  
1590 complex in the ~1.8 Ga Nagssugtoqidian orogen of West Greenland. *Am Mineral*  
1591 99:1315-1334  
1592  
1593 Godard G, Smith DC, Thouvenin C (2003) Microdiamond within zircon in thin section in  
1594 the Straumen coesite-kyanite-eclogite pod, Norway. *In: The Alice Wain*  
1595 *Memorial West Norway Eclogite Field Symposium, abstract volume* (Eide EA  
1596 (ed). *Norges Geologiske Undersøkelse, Rapport 2003.055*. p. 54  
1597  
1598 Godard G, Smith DC, Moreau M (2004) Raman mapping of microdiamonds and other  
1599 carbon phases included in zircons in a Norwegian eclogite. 32nd International  
1600 Geological Congress, Florence, 20-28 August 2004, Abstract 153-2  
1601  
1602 Goryainov SV, Likhacheva AY, Rashchenko SV, Shubin AS, Afanas' ev VP, Pokhilenko  
1603 NP (2014) Raman identification of lonsdaleite in Popigai impactites. *J Raman*  
1604 *Spectrosc* 45:305-13  
1605  
1606 Graham DW (2002) Noble gas isotope geochemistry of mid-ocean ridge and ocean island  
1607 basalts: Characterization of mantle source reservoirs. *Rev Mineral Geochem*  
1608 47:247-317  
1609  
1610 Hanneman RE, Strong HM, Bundy FP (1967) Hexagonal diamonds in meteorites:  
1611 Implications. *Science* 155:997–999  
1612  
1613 Harris JW, Hawthorne JB, Oosterveld MM, Wehmeyer E (1975) A classification scheme  
1614 for diamonds and a comparative study of South African diamond characteristics.  
1615 *In: Physics and Chemistry of the Earth*. Ahrens LH, Dawson JB, Duncan AR,  
1616 Erlank AJ (eds) Pergamon Press, p.765-783  
1617

1618 Hattori H, Shibata K (1982) Radiometric dating of Pre-Neogene granitic and  
 1619 metamorphic rocks in northwestern Kyushu, Japan—with emphasis on  
 1620 geotectonics of the Nishisonogi zone. *Bull Geol Surv Jpn* 33:57–84  
 1621  
 1622 Herchen H, Cappelli MA (1991) First-order Raman spectrum of diamond at high  
 1623 temperatures. *Phys Rev B* 43:11740  
 1624  
 1625 Herman J, Korsakov A (2003) Carbonate melts and diamond formation in subducted  
 1626 continental crust. *GSA Annual Meeting*, 137  
 1627  
 1628 Hermann J, Rubatto D, Korsakov A, Shatsky VS (2006) The age of metamorphism of  
 1629 diamondiferous rocks determined with SHRIMP dating of zircon. *Rus Geol*  
 1630 *Geophys* 47:513-520  
 1631  
 1632 Honda M, Reynolds JH, Roedder E, Epstein S (1987) Noble gases in diamonds:  
 1633 occurrences of solarlike helium and neon. *J Geophys Res* 92:12521  
 1634  
 1635 Honda M, McDougall I, Patterson DB, Doulgeris A, Clague DA (1991) Possible solar  
 1636 noble-gas component in Hawaiian basalts. *Nature* 349:149-151  
 1637  
 1638 Honda M, Phillips D, Harris JW, Yatsevich I (2004) Unusual noble gas compositions in  
 1639 polycrystalline diamonds: preliminary results from the Jwaneng kimberlite,  
 1640 Botswana. *Chem Geol* 203:347–358  
 1641  
 1642 Hong SM, Akaishi M, Yamaoka S (1999) Nucleation of diamonds in the system of  
 1643 carbon and water under very high pressure and temperature. *J Cryst Growth*  
 1644 *200:326–329*  
 1645  
 1646 Hopkins MD, Harrison TM, Manning CE (2008) Low heat flow inferred from > 4 Gyr  
 1647 zircons suggests Hadean plate boundary interactions. *Nature* 456:493-496  
 1648  
 1649 Hopkins MD, Harrison TM, Manning CE (2010) Constraints on Hadean geodynamics  
 1650 from mineral inclusions in > 4 Ga zircons. *Earth Planet Sci Lett* 298:367-376  
 1651  
 1652 Hopkins MD, Harrison TM, Manning CE (2012) Metamorphic replacement of mineral  
 1653 inclusions in detrital zircon from Jack Hills, Australia: Implications for the  
 1654 Hadean Earth: COMMENT. *Geology* 40:e281-e281  
 1655  
 1656 Hwang SL, Shen P, Chu HT, Yui TF (2000) Nanometer-size  $\alpha$ -PbO<sub>2</sub>-type TiO<sub>2</sub> in garnet:  
 1657 A thermobarometer for ultrahigh-pressure metamorphism. *Science* 288:321-324  
 1658  
 1659 Hwang SL, Shen P, Yui TF, Chu HT (2003) Metal-sulfur-COH-silicate fluid mediated  
 1660 diamond nucleation in Kokchetav ultrahigh-pressure gneiss. *Eur J Mineral*  
 1661 *15:503-511*  
 1662

1663 Imamura K, Ogasawara Y, Yurimoto H, Kusakabe M (2013) Carbon isotope  
1664 heterogeneity in metamorphic diamond from the Kokchetav UHP dolomite  
1665 marble, northern Kazakhstan. *Int Geol Rev* 55:453-467  
1666

1667 Ishida H, Ogasawara Y, Ohsumi K, Saito A (2003) Two stage growth of microdiamond  
1668 in UHP dolomite marble from Kokchetav Massif, Kazakhstan. *J Metamorph Geol*  
1669 21:515-522  
1670

1671 Jackson MG, Carlson RW, Kurz MD, Kempton PD, Francis D, Blusztajn J (2010)  
1672 Evidence for the survival of the oldest terrestrial mantle reservoir. *Nature*  
1673 466:853-856  
1674

1675 Jacob DE, Dobrzhinetskaya LF, Wirth R (2014) New insight into polycrystalline  
1676 diamond genesis from modern nanoanalytical techniques. *Earth-Sci Rev* 136:21-  
1677 35  
1678

1679 Jagoutz E, Shatsky VS, Sobolev NV (1990) Sr-Nd-Pb isotopic study of ultra-high PT  
1680 rocks from Kokchetav massif. *EOS* 71:1707  
1681

1682 Jagoutz E, Shatsky VS, Sobolev NV (1991) The origin and history of ultrahigh PT rocks  
1683 from Kokchetav Massif. *Terra Abstracts* 3:83  
1684

1685 Janák M, Froitzheim N, Lupták B, Vrabec M, Ravna EJK (2004) First evidence for  
1686 ultrahigh-pressure metamorphism of eclogites in Pohorje, Slovenia: Tracing deep  
1687 continental subduction in the Eastern Alps. *Tectonics* 23 TC5014  
1688 doi:10.1029/2004TC001641  
1689

1690 Janák M, Froitzheim N, Vrabec M, Krogh Ravna EJ, De Hoog JCM (2006) Ultrahigh-  
1691 pressure metamorphism and exhumation of garnet peridotite in Pohorje, Eastern  
1692 Alps. *J Metamorph Geol* 24:19-31  
1693

1694 Janák M, Krogh Ravna EJ, Kullerud K, Yoshida K, Milovský R, Hirajima T (2013)  
1695 Discovery of diamond in the Tromsø Nappe, Scandinavian Caledonides (N.  
1696 Norway). *J Metamorph Geol* 31:691-703  
1697

1698 Janák M, Froitzheim N, Yoshida K, Sasinková V, Nosko M, Kobayashi T, Hirajima T,  
1699 Vrabec M (2015) Diamond in metasedimentary crustal rocks from Pohorje,  
1700 Eastern Alps: a window to deep continental subduction. *J Metamorph Geol*  
1701 33:495-512  
1702

1703 Kaneoka I (1983) Noble gas constraints on the layered structure of the mantle. *Nature*  
1704 302:698-700  
1705

1706 Kashkarov IF, Polkanov YA (1964) On discovery of diamonds in titanium-zirconium  
1707 sands. *Dokl Akad Nauk SSSR (Proceeding of Academy of Sciences of USSR)*  
1708 157:1129 (in Russian)

1709  
1710 Katayama I, Parkinson CD, Okamoto K, Nakajima Y, Maruyama S (2000) Supersilicic  
1711 clinopyroxene and silica exsolution in UHPM eclogite and pelitic gneiss from the  
1712 Kokchetav massif, Kazakhstan. *Am Mineral* 10:1368–1374  
1713  
1714 Katayama I, Maruyama S, Parkinson CD, Terada K, Sano Y (2001a) Ion micro-probe U–  
1715 Pb zircon geochronology of peak and retrograde stages of ultrahigh-pressure  
1716 metamorphic rocks from the Kokchetav massif, northern Kazakhstan. *Earth  
1717 Planet Sci Lett* 188:185-198  
1718  
1719 Katayama I, Zayachkovsky AA, Maruyama S (2001b) Prograde pressure–temperature  
1720 records from inclusions in zircons from ultrahigh-pressure–high-pressure rocks of  
1721 the Kokchetav Massif, northern Kazakhstan. *Island Arc* 9:417-427  
1722  
1723 Katayama I, Ohta, M, Ogasawara Y (2002) Mineral inclusions in zircon from diamond-  
1724 bearing marble in the Kokchetav massif, northern Kazakhstan. *Eur J Mineral*  
1725 14:1103-1108  
1726  
1727 Katsube A, Hayasaka Y, Santosh M, Li S, Terada K (2009) SHRIMP zircon U–Pb ages  
1728 of eclogite and orthogneiss from Sulu ultrahigh-pressure zone in Yangkou area,  
1729 eastern China. *Gondwana Research* 15:168–177  
1730  
1731 Klonowska I, Janák M, Majka J, Petrik I, Froitzheim N, Gee DG, Sasinková V (2017)  
1732 Microdiamond on Åreskutan confirms regional UHP metamorphism in the Seve  
1733 Nappe Complex of the Scandinavian Caledonides. *J Metamorph Geol* 35:541-564  
1734  
1735 Koeberl C, Masaitis VL, Shafranovsky GI, Gilmour I, Langenhorst F, Schrauder M  
1736 (1997) Diamonds from the Popigai impact structure, Russia. *Geology* 25:967-970  
1737  
1738 Kohn MJ (2010) Carbon isotope compositions of terrestrial C3 plants as indicators of  
1739 (paleo) ecology and (paleo) climate. *Proc Natl Acad Sci USA* 107:19691-5  
1740  
1741 Konzett J, Frost DJ (2009) The high P–T stability of hydroxyl-apatite in natural and  
1742 simplified MORB—an experimental study to 15 GPa with implications for  
1743 transport and storage of phosphorus and halogens in subduction zones. *J Petrol*  
1744 50:2043-2062  
1745  
1746 Konzett J, Rhede D, Frost DJ (2012) The high PT stability of apatite and Cl partitioning  
1747 between apatite and hydrous potassic phases in peridotite: an experimental study  
1748 to 19 GPa with implications for the transport of P, Cl and K in the upper mantle.  
1749 *Contrib Mineral Petrol* 163:277-296  
1750  
1751 Korsakov A, Theunissen K, Smirnova LV (2004) Intergranular diamonds derived from  
1752 partial melting of crustal rocks at ultrahigh-pressure metamorphic conditions.  
1753 *Terra Nova* 16:146-151  
1754

- 1755 Korsakov A, Herman J (2006) Silicate and carbonate melt inclusions associated with  
1756 diamonds in deeply subducted carbonate rocks. *Earth Planet Sci Lett* 241: 104-  
1757 118  
1758
- 1759 Kotková J, O'Brien PJ, Ziemann MA (2011) Diamonds in the Bohemian Massif—  
1760 evidence for ultrahigh-pressure metamorphism. *Geologické výzkumy na Morave*  
1761 *a ve Slezsku* 18:35-38  
1762
- 1763 Kröner A, Willner AP (1998) Time of formation and peak of Variscan HP-HT  
1764 metamorphism of quartz-feldspar rocks in the central Erzgebirge, Saxony,  
1765 Germany. *Contrib Mineral Petrol* 132:1-20  
1766
- 1767 Krueger A (2008) Diamond nanoparticles: Jewels for chemistry and physics. *Adv Mater*  
1768 20:2445-2449  
1769
- 1770 Kumar MS, Akaishi M, Yamaoka S (2001) Effect of fluid concentration on the formation  
1771 of diamond in the CO<sub>2</sub>–H<sub>2</sub>O–graphite system under HP–HT conditions. *J Cryst*  
1772 *Growth* 222:9-13  
1773
- 1774 Kurz MD, Jenkins WJ, Hart SR (1982) Helium isotopic systematics of oceanic islands  
1775 and mantle heterogeneity. *Nature* 297:43-47  
1776
- 1777 Kurz MD (1986) Cosmogenic helium in a terrestrial igneous rock. *Nature* 320:435-439  
1778
- 1779 Kurz MD, Gurney JJ, Jenkins WJ, Lott III DE (1987) Helium isotopic variability within  
1780 single diamonds from the Orapa kimberlite pipe. *Earth Planet Sci Lett* 86:57-68  
1781
- 1782 Kurz MD, Curtice J, Fornari D, Geist D, Moreira M (2009) Primitive neon from the  
1783 center of the Galapagos hotspot. *Earth Planet Sci Lett* 286:23-34  
1784
- 1785 Lal D. (1989) An important source of <sup>4</sup>He (and <sup>3</sup>He) in diamonds. *Earth Planet Sci Lett*  
1786 96:1-7  
1787
- 1788 Langenhorst F, Shafranovsky G, Masaitis VL (1998) A comparative study of impact  
1789 diamonds from the Popigai, Ries, Sudbury, and Lappajarvi craters. *Meteorit*  
1790 *Planet Sci Suppl*, 33:A90  
1791
- 1792 Langenhorst F (2003) Nanostructures in ultrahigh-pressure metamorphic coesite and  
1793 diamond: a genetic fingerprint. *Mitt Österr Miner Ges* 148:401–412  
1794
- 1795 Lavrova LD (1991) New type of diamond deposits. *Priroda (Nature)* 12:62-68 (in  
1796 Russian)  
1797
- 1798 Lavrova LD, Petchnikov VA, Petrova MA, Ekimova TE, Nadezhkina ED (1995) New  
1799 genetic type of diamond deposits-geological peculiarities and origin. *In:*  
1800 *International Kimberlite Conference: Extended Abstracts* 6:311-313

1801  
1802 Lavrova LD, Pechnikov VA, Petrova MA, Ekimova TE, Karpenko SF, Lyalikov AV,  
1803 Spiridonov VG, Bibikova EV, Fugzan MM, Shukolyukov YA (1997) Diamond  
1804 formation in the age succession of geological events on the Kokchetav massif:  
1805 evidence from isotopic geochronology. *Geokhimiya (Geochemistry)* 675-682 (in  
1806 Russian)  
1807  
1808 Leung I, Winston R (2002) Microstructures and Superelasticity in Natural Diamond. *EOS*  
1809 *Trans, Am Geophys Union*, 83, MR61A-1028  
1810  
1811 Letnikov FA (1983) Diamond origin in deep-seated tectonic zones. *Dokl Akad Nauk*  
1812 *SSSR (Proceeding of Academy of Sciences of USSR)* 271:433-435  
1813  
1814 Liati A, Gebauer D, Fanning CM (2011) Geochronology of the Alpine UHP Rhodope  
1815 zone: a review of isotopic ages and constraints on the geodynamic evolution. *In:*  
1816 *Ultrahigh-Pressure Metamorphism: 25 Years After The Discovery of Coesite and*  
1817 *Diamond*. Dobrzhinetskaya LF, Faryad SW, Wallis S, Cuthbert S (eds), Elsevier,  
1818 London, p. 295–316  
1819  
1820 Liou JG, Ernst WG, Zhang RY, Tsujimori T, Jahn BM (2009) Ultrahigh-pressure  
1821 minerals and metamorphic terranes—the view from China. *J Asian Earth Sci*  
1822 35:199-231  
1823  
1824 Liou JG, Tsujimori T, Yang J, Zhang RY, Ernst WG (2014) Recycling of crustal  
1825 materials through study of ultrahigh-pressure minerals in collisional orogens,  
1826 ophiolites, and mantle xenoliths: A review. *J Asian Earth Sci* 96:386-420  
1827  
1828 Lipp MJ, Baonza VG, Evans WJ, Lorenzana HE (1997) Nanocrystalline diamond: Effect  
1829 of confinement, pressure, and heating on phonon modes. *Phys Rev B* 56:5978  
1830  
1831 Liu L, Zhang J, Green, HW, Jin Z, Bozhilov KN (2007) Evidence of former stishovite in  
1832 metamorphosed sediments, implying subduction to >350 km. *Earth Planet Sci*  
1833 *Lett* 263:180-191  
1834  
1835 Majka J, Rosén Å, Janák M, Froitzheim N, Klonowska I, Manecki M, Sasinková V,  
1836 Yoshida K (2014) Microdiamond discovered in the Seve Nappe (Scandinavian  
1837 Caledonides) and its exhumation by the “vacuum-cleaner” mechanism. *Geology*  
1838 42:1107-1110  
1839  
1840 Manning CE (2004) The chemistry of subduction-zone fluids. *Earth Planet Sci Lett*  
1841 223:1-16  
1842  
1843 Massonne H-J (1999) A new occurrence of microdiamonds in quartzofeldspathic rocks of  
1844 the Saxonian Erzgebirge, Germany, and their metamorphic evolution. *Proc. 7<sup>th</sup>*  
1845 *Int. Kimberlite Conf., Cape Town 1998, P.H. Nixon Vol., p. 533-539*  
1846

1847 Massonne H-J (2003) A comparison of the evolution of diamondiferous quartz-rich rocks  
1848 from the Saxonian Erzgebirge and the Kokchetav Massif: are so-called  
1849 diamondiferous gneisses magmatic rocks? *Earth Planet Sci Lett* 216:347-364  
1850

1851 Massonne H-J, O'Brien PJ (2003) The Bohemian massif and the NW Himalaya. *In:*  
1852 *Ultrahigh Pressure Metamorphism*. Carswell DA, Compagnoni R, Rolfo F (eds) p  
1853 145-187  
1854

1855 Massonne H-J, Tu W (2007)  $\delta^{13}\text{C}$  signature of early graphite and subsequently formed  
1856 microdiamond from the Saxonian Erzgebirge, Germany. *Terra Nova* 19:476-480  
1857

1858 Massonne H-J, Kennedy A, Nasdala L, Theye T (2007) Dating of zircon and monazite  
1859 from diamondiferous quartzofeldspathic rocks of the Saxonian Erzgebirge - hints  
1860 at burial and exhumation velocities. *Mineral Mag* 71:371–389  
1861

1862 Massonne H-J, Fockenberg T (2012) Melting of metasedimentary rocks at ultrahigh  
1863 pressure - Insights from experiments and thermodynamic calculations.  
1864 *Lithosphere* 4:269-285  
1865

1866 Mathez EA, Fogel RA, Hutcheon ID, Marshintsev VK (1995) Carbon isotopic  
1867 composition and origin of SiC from kimberlites of Yakutia, Russia. *Geochim*  
1868 *Cosmochim Acta* 59:781-791  
1869

1870 Masaitis VL, Futergendler SI, Gnevushev MA (1972) Diamonds in impactites of the  
1871 Popigai meteorite crater. *All-Union Mineralogical Society Proceedings* 1:108-112  
1872

1873 Masaitis VL, Shafranovsky GL, Grieve RA, Langenhorst F, Peredery W, Balmasov EL,  
1874 Fedorova IG, Therriault A (1997) Discovery of diamonds at the Sudbury  
1875 Structure. *Lunar and Planetary Institute, Contribution*, 922:33  
1876

1877 Masaitis VL, Shafranovsky GI, Fedorova IG, Koivisto M, Korhonen JV (1998)  
1878 Lappajarvi Astrobleme: The first find of impact diamonds on the Fennoscandian  
1879 Shield. *Lunar and Planetary Institute, Contribution*, 1171.  
1880

1881 Mattinson CG, Wooden JL, Liou JG, Bird DK, Wu CL (2006) Age and duration of  
1882 eclogite-facies metamorphism, North Qaidam HP/UHP terrane, western China.  
1883 *Amer J Sci* 306:683–711  
1884

1885 Menneken M, Nemchin AA, Geisler T, Pidgeon RT, Wilde SA (2007) Hadean diamonds  
1886 in zircon from Jack Hills, Western Australia. *Nature* 448:917-920  
1887

1888 Meyers PA (2014) Why are the  $\delta^{13}\text{C}_{\text{org}}$  values in Phanerozoic black shales more  
1889 negative than in modern marine organic matter? *Geochem Geophys.* 15:3085-106.  
1890

- 1891 Mposkos ED, Kostopoulos DK (2001) Diamond, former coesite and supersilicic garnet in  
1892 metasedimentary rocks from the Greek Rhodope: a new ultrahigh-pressure  
1893 metamorphic province established. *Earth Planet Sci Lett* 192:497-506  
1894
- 1895 Mukhopadhyay S (2012) Early differentiation and volatile accretion recorded in deep-  
1896 mantle neon and xenon. *Nature* 486:101-104  
1897
- 1898 Murri M, Smith RL, McColl K, Hart M, Alvaro M, Jones AP, Németh P, Salzmann CG,  
1899 Corà F, Domeneghetti MC, Nestola F. (2019) Quantifying hexagonal stacking in  
1900 diamond. *Sci Reports* 9:1-8  
1901
- 1902 Naemura K, Ikuta D, Kagi H, Otake S, Ueda T, Ohi S, Kobayashi T, Svojtka M,  
1903 Hirajima T (2011) Diamond and other possible ultradeep evidence discovered in  
1904 the orogenic spinel-garnet peridotite from the Moldanubian Zone of the Bohemian  
1905 Massif, Czech Republic. *In: Ultrahigh-Pressure Metamorphism*. Elsevier p. 77-  
1906 111  
1907
- 1908 Nasdala L, Massonne H-J (2000) Microdiamonds from the Saxonian Erzgebirge,  
1909 Germany: in situ micro-Raman characterisation. *Eur J Mineral* 12:495-498  
1910
- 1911 Nasdala L, Grambole D, Wildner M, Gigler AM, Hainschwang T, Zaitsev AM, Harris  
1912 JW, Milledge J, Schulze DJ, Hofmeister W, Balmer WA (2013) Radio-  
1913 colouration of diamond: a spectroscopic study. *Contrib Mineral Petr* 165:843-61  
1914
- 1915 Nasdala L, Steger S, Reissner C (2016) Raman study of diamond-based abrasives, and  
1916 possible artefacts in detecting UHP microdiamond. *Lithos* 265:317-327  
1917
- 1918 Nemchin AA, Whitehouse MJ, Menneken M, Geisler T, Pidgeon RT, Wilde SA (2008) A  
1919 light carbon reservoir recorded in zircon-hosted diamond from the Jack Hills.  
1920 *Nature* 454:92-95  
1921
- 1922 Németh P, Garvie LA, Aoki T, Dubrovinskaia N, Dubrovinsky L, Buseck PR (2014)  
1923 Lonsdaleite is faulted and twinned cubic diamond and does not exist as a discrete  
1924 material. *Nat Comm* 5:1-5  
1925
- 1926 Nishiyama T, Ohfuji H, Fukuba K, Terauchi M, Nishi U, Harada K, Unoki K, Moribe Y,  
1927 Yoshiasa A, Ishimaru S, Mori Y (2020) Microdiamond in a low-grade metapelite  
1928 from a Cretaceous subduction complex, western Kyushu, Japan. *Sci Rep* 10:1-1  
1929
- 1930 Ogasawara Y (2005) Microdiamonds in ultrahigh-pressure metamorphic rocks. *Elements*  
1931 1:91-96  
1932
- 1933 Ogasawara Y, Ohta M, Fukusava K, Katayama I, Maruyama S (2000) Diamond bearing  
1934 and diamond-free metacarbonate rocks from Kumdy-Kol from the Kokchetav  
1935 massif, northern Kazakhstan. *The Island Arc* 9:400-416  
1936

- 1937 Ogasawara Y, Fukasawa K, Maruyama S (2002) Coesite exsolution from supersilicic  
1938 titanite in UHP marble from the Kokchetav Massif, northern Kazakhstan. *Am*  
1939 *Mineral* 87:454-461  
1940
- 1941 Ohfuji H, Irifune T, Litasov KD, Yamachita T, Isobe F, Afanasiev V, Pokhilenko NP  
1942 (2015) Natural occurrence of pure nano-polycrystalline diamond from impact  
1943 crater. *Sci Rep* 5:14702  
1944
- 1945 Ohta M, Mock T, Ogasawara Y, Rumble D (2003) Oxygen, carbon, and strontium  
1946 isotope geochemistry of diamond-bearing carbonate rocks from Kumdy-Kol,  
1947 Kokchetav Massif, Kazakhstan. *Lithos* 70:77-90  
1948
- 1949 Okamoto K, Liou JG, Ogasawara Y (2000) Petrology of the diamond-grade eclogite in  
1950 the Kokchetav Massif, northern Kazakhstan. *Island Arc* 9:379–399  
1951
- 1952 Okay A, Xu ST, Sengor AMC (1988) Coesite from the Dabie Shan eclogite, Central  
1953 China. *Eur J Mineral* 1:595-598  
1954
- 1955 Ozima M, Zashu S (1988) Solar-type Ne in Zaire cubic diamonds. *Geochim Cosmochim*  
1956 *Acta* 52:19–25  
1957
- 1958 Ozima M, Zashu S (1991) Noble gas state of the ancient mantle as deduced from noble  
1959 gases in coated diamonds. *Earth Planet Sci Lett* 105:13–27  
1960
- 1961
- 1962 Ozima M, Podosek FA (2002) *Noble Gas Geochemistry*. Cambridge Univ. Press,  
1963 Cambridge  
1964
- 1965 Pal'yanov Y, Sokol A, Borzdov Y, Khokhryakov A, Sobolev NV (1999) Diamond  
1966 formation from mantle carbonate fluids. *Nature* 400:417–418  
1967
- 1968 Pal'yanov YuN, Sokol AG, Khokhryakov, AF, Pal'yanova GA, Borzdov YuM, Sobolev  
1969 NV (2000) Diamond and graphite crystallization in COH fluid at PT parameters  
1970 of the natural diamond formation. *Doklady Nauk o Zemle (Proceeding of Earth*  
1971 *Sciences)* 375:1395–1399 (in Russian)  
1972
- 1973 Pal'yanov N, Sokol AG, Borzdov M, Khokhryakov AF (2002) Fluid-bearing alkaline  
1974 carbonate melts as the medium for the formation of diamonds in the Earth's  
1975 mantle: an experimental study. *Lithos* 60:145-159  
1976
- 1977 Pal'yanov YN, Bataleva YV, Sokol AG, Borzdov YM, Kupriyanov IN, Reutsky VN,  
1978 Sobolev NV (2013) Mantle–slab interaction and redox mechanism of diamond  
1979 formation. *PNAS* 110:20408-20413  
1980
- 1981 Palot, M., Pearson, D.G., Stern, R.A., Stachel, T., Harris, J.W., (2013) Multiple growth  
1982 events, processes and fluid sources involved in diamond genesis: a micro-

- 1983 analytical study of sulphide-bearing diamonds from Finsch mine, RSA. *Geochim.*  
1984 *Cosmochim. Acta* 106:51–70  
1985  
1986 Parkinson CD (2000) Coesite inclusions and prograde compositional zonation of garnet  
1987 in whiteschist of the HP-UHPM Kokchetav massif, Kazakhstan: a record of  
1988 progressive UHP metamorphism. *Lithos* 52:215-233  
1989  
1990 Parman SW (2007) Helium isotopic evidence for episodic mantle melting and crustal  
1991 growth. *Nature* 446:900-903  
1992  
1993 Pechnikov VA, Kaminsky FV (2008) Diamond potential of metamorphic rocks in the  
1994 Kokchetav Massif, northern Kazakhstan. *Eur J Mineral* 20:395-413  
1995  
1996 Pechnikov VA, Kaminsky FV (2011) Structural and microstructural regularities of the  
1997 distribution of diamond in metamorphic rocks of the Kumdy-Kol and Barchi-Kol  
1998 deposits, Kokchetav Massif, Northern Kazakhstan. *Can Mineral* 49:673-690  
1999  
2000 Pedroza-Montero M, Chernov V, Castañeda B, Meléndrez R, Gonçalves JA, Sandonato  
2001 GM, Bernal R, Cruz-Vázquez C, Brown F, Cruz-Zaragoza E, Barboza-Flores M  
2002 (2005) TL, OSL, Raman spectroscopy and SEM characterization of boron doped  
2003 diamond films. *Phys Status Solidi B* 202:2154-9  
2004  
2005 Perraki M, Proyer A, Mposkos E, Kaindl R, Hoinkes G (2006) Raman micro-  
2006 spectroscopy on diamond, graphite and other carbon polymorphs from the  
2007 ultrahigh-pressure metamorphic Kimi Complex of the Rhodope Metamorphic  
2008 Province, NE Greece. *Earth Planet Sci Lett* 241:672-685  
2009  
2010 Perraki M, Faryad SW (2014) First finding of microdiamond, coesite and other UHP  
2011 phases in felsic granulites in the Moldanubian Zone: Implications for deep  
2012 subduction and a revised geodynamic model for Variscan Orogeny in the  
2013 Bohemian Massif. *Lithos* 202:157-166  
2014  
2015 Platt JP, Behr WM, Johannesen K, Williams JR (2013) The Betic-Rif arc and its orogenic  
2016 hinterland: a review. *Ann Rev Earth Planet Sci* 41:313-357  
2017  
2018 Pleshakov AM, Shukolyukov YA (1994) Isotopic variations of helium in the diamonds of  
2019 the Kokchetav massif's metamorphic rocks, Kazakhstan. in: Matsuda, J. (Ed.),  
2020 Noble Gas Geochemistry and Cosmochemistry, Terra Scientific Publishing  
2021 Company (TERRAPUB), Tokyo, p. 229-243  
2022  
2023 Porcelli D, Ballentine CJ (2002) Models for distribution of terrestrial noble gases and  
2024 evolution of the atmosphere. *Rev Mineral Geochem* 47:411-48  
2025  
2026 Porcelli D, Elliott T (2008) The evolution of He isotopes in the convecting mantle and the  
2027 preservation of high  $^3\text{He}/^4\text{He}$  ratios. *Earth Planet Sci Lett* 269:175-185  
2028

- 2029 Rasmussen B, Fletcher IR, Muhling JR, Wilde SA (2010) In situ U–Th–Pb  
2030 geochronology of monazite and xenotime from the Jack Hills belt: Implications  
2031 for the age of deposition and metamorphism of Hadean zircons. *Precambrian Res*  
2032 180:26-46  
2033
- 2034 Rasmussen B, Fletcher IR, Muhling JR, Gregory CJ, Wilde SA (2011) Metamorphic  
2035 replacement of mineral inclusions in detrital zircon from Jack Hills, Australia:  
2036 Implications for the Hadean Earth. *Geology* 39:1143-1146  
2037
- 2038 Rasmussen B, Fletcher IR, Muhling JR, Gregory CJ, Wilde SA (2012) Metamorphic  
2039 replacement of mineral inclusions in detrital zircon from Jack Hills, Australia:  
2040 Implications for the Hadean Earth: REPLY. *Geology* 40:e282-e283  
2041
- 2042 Rosing MT (1999) <sup>13</sup>C-depleted carbon microparticles in > 3700-Ma sea-floor  
2043 sedimentary rocks from West Greenland. *Science* 283:674-676  
2044
- 2045 Rozen OM (1972) A find of the diamonds linked with eclogites of the Precambrian  
2046 Kokchetav massif. *Dokl Akad Nauk SSSR* 203:674-676  
2047
- 2048 Rozen OM, Zayachkovsky AA, Kljuev YuA, Smirnov VL (1979) Peculiarities of trace-  
2049 minerals composition and conditions of the formation of the North Kazakhstan  
2050 eclogites. *In: A.V. Sidorenko (Editor), Problems of Sedimentary Geology of*  
2051 *Precambrian. Nauka Press, Moscow p. 170-186 (in Russian with English abstract)*  
2052
- 2053 Reutsky V, Borzdov Y, Palyanov Y, Sokol A, Izokh O (2015) Carbon isotope  
2054 fractionation during experimental crystallisation of diamond from carbonate fluid  
2055 at mantle conditions. *Cont Mineral Petrol* 170:41  
2056
- 2057 Rost R, Dolgov YA, Vishnevsky SA (1978) Gases in inclusions of impact glass in the  
2058 Ries Crater, West Germany, and finds of high-pressure carbon polymorphs. *Dokl*  
2059 *Akad Nauk SSSR* 241:695-698  
2060
- 2061 Ruiz-Cruz MD, de Galdeano CS (2012) Diamond and coesite in ultrahigh-pressure–  
2062 ultrahigh-temperature granulites from Ceuta, Northern Rif, northwest Africa.  
2063 *Mineral Mag* 76:683-705  
2064
- 2065 Ruiz-Cruz MD, de Galdeano CS (2013) Coesite and diamond inclusions, exsolution  
2066 microstructures and chemical patterns in ultrahigh pressure garnet from Ceuta  
2067 (Northern Rif, Spain). *Lithos* 177:184-206  
2068
- 2069 Ruiz-Cruz MD, de Galdeano CS (2014) Garnet variety and zircon ages in UHP meta-  
2070 sedimentary rocks from the Jubrique zone (Alpujarride Complex, Betic  
2071 Cordillera, Spain): evidence for a pre-Alpine emplacement of the Ronda  
2072 peridotite. *Int Geol Rev* 56:845-868  
2073

2074 Sarda P, Staudacher T, Allègre CJ (1988) Neon isotopes in submarine basalts. *Earth*  
2075 *Planet Sci Lett* 91:73-88  
2076

2077 Schertl HP, Sobolev NV (2013) The Kokchetav Massif, Kazakhstan: “Type locality” of  
2078 diamond-bearing UHP metamorphic rocks. *J Asian Earth Sci* 63:5-38  
2079

2080 Schönig J, von Eynatten H, Meinhold G, Lünsdorf NK (2019) Diamond and coesite  
2081 inclusions in detrital garnet of the Saxonian Erzgebirge, Germany. *Geology*  
2082 47:715-718  
2083

2084 Schmidt S, Nagel TJ, Froitzheim N (2010) A new occurrence of microdiamond-bearing  
2085 metamorphic rocks, SW Rhodopes, Greece. *Eur J Mineral* 1:189-98  
2086

2087 Schmidt S, Nagel TJ, Froitzheim N, Janák M (2011) The age of UHP metamorphism and  
2088 the exhumation path of microdiamond-bearing rocks (SW Rhodope, Greece).  
2089 European Geophysical Union General Assembly, 13:125  
2090

2091 Seno T, Rehman HU (2011) When and why the continental crust is subducted: Examples  
2092 of Hindu Kush and Burma. *Gondwana Res* 19:327-333  
2093

2094 Shatsky VS, Sobolev NV (1993) Some aspects of origin of diamonds in metamorphic  
2095 rocks. *Doklady Akademii Nauk (Proceeding of Academy of Sciences)* 331: 1217–  
2096 1219 (in Russian)  
2097

2098 Shukolyukov YuA, Pleshakov AM, Lavrova LD (1993) The unprecedentedly high  
2099  $^3\text{He}/^4\text{He}$  ratio in diamonds from a metamorphic rock of the Kokchetav massif,  
2100 Kazakhstan. *Petrologia (Petrology)* 1:110-119 (in Russian)  
2101

2102 Shumilova TG, Mayer E, Isaenko SI (2011) Natural monocrystalline lonsdaleite. *Dokl*  
2103 *Earth Sci* 441:1552-1554  
2104

2105 Simakov SK (2010) Metastable nanosized diamond formation from a CHO fluid system.  
2106 *J Mat Res* 25:2336-2340  
2107

2108 Simakov SK (2015) Different sizes of diamond formation in natural processes. *Dokl*  
2109 *Earth Sci* 461:419-421  
2110

2111 Simakov SK (2018) Nano-and micron-sized diamond genesis in nature: an overview.  
2112 *Geosci Front* 9:1849-1858  
2113

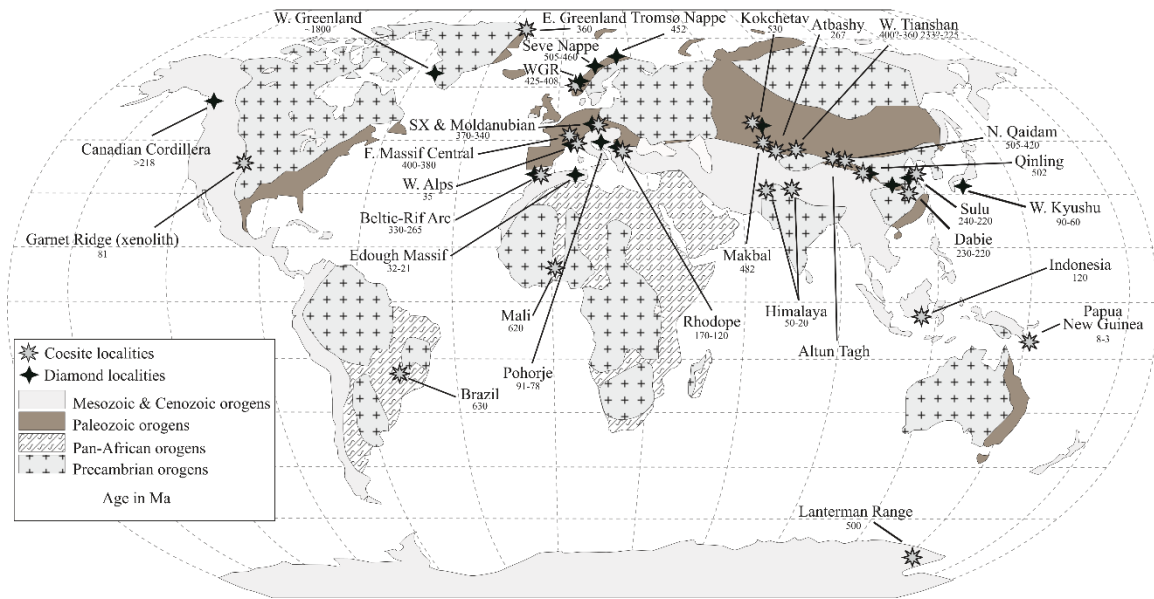
2114 Simakov SK, Dubinchuk VT, Novikov MP, Drozdova IA (2008) Formation of diamond  
2115 and diamond-type phases from the carbon-bearing fluid at PT parameters  
2116 corresponding to processes in the Earth's crust. *Dokl Earth Sci* 421:835  
2117

- 2118 Sitnikova ES, Shatsky VS (2009) New FTIR spectroscopy data on the composition of the  
 2119 medium of diamond crystallization in metamorphic rocks of the Kokchetav  
 2120 Massif. *Russ Geol Geophys* 50:842-849  
 2121
- 2122 Smart, K.A., Chacko, T., Stachel, T., Muehlenbachs, K., Stern, R.A., Heaman, L.M.  
 2123 (2011) Diamond growth from oxidized carbon sources beneath the Northern Slave  
 2124 Craton, Canada: a  $\delta^{13}\text{C}$ -N study of eclogite-hosted diamonds from the Jericho  
 2125 kimberlite. *Geochim. Cosmochim. Acta* 75:6027–47  
 2126
- 2127 Smith DC (1984) Coesite in clinopyroxene in the Caledonides and its implications for  
 2128 geodynamics. *Nature* 310:641-644  
 2129
- 2130 Smith DC (2004) Raman Micromapping of Physical and/or Chemical Transformations of  
 2131 Minerals of Interest in Geology or Archaeology. International Congress  
 2132 GEORAMAN, Univ. Hawaii, Spec. Pub. S.O.E.S.T., Honolulu, 04-02 71–72.  
 2133
- 2134 Smith DC, Godard G (2009) UV and VIS Raman spectra of natural lonsdaleites: Towards  
 2135 a recognised standard. *Spectrochim Acta A* 73:428-35  
 2136
- 2137 Smith DC, Godard G (2013) A Raman spectroscopic study of diamond and disordered  
 2138  $\text{sp}^3$ -carbon in the coesite-bearing Straumen Eclogite Pod, Norway. *J Metamorph*  
 2139 *Geol* 31:19-33.  
 2140
- 2141 Smith DC, Godard G, Dobrzhinetskaya LF, Green HW II, Belleil M (2004) A  
 2142 preliminary comparative Raman mapping study of contrasting  
 2143 zircon/diamond/graphite relations at Kokchetav, Kazakhstan. *In: Proceedings,*  
 2144 *XIXth International Conference on Raman Spectroscopy.* Fredericks P.M., Frost  
 2145 RL, Rintoul L (eds), Goldcoast, Australia, 562–563  
 2146
- 2147 Smith DC, Dobrzhinetskaya LF, Godard G, Green HW II (2011) Diamond–lonsdaleite–  
 2148 graphite relations examined by Raman mapping of carbon microinclusions inside  
 2149 zircon at Kumdy Kol, Kokchetav, Kazakhstan: evidence of the metamictization of  
 2150 diamond. *In: Ultrahigh-Pressure Metamorphism – 25 Years After the Discovery*  
 2151 *of Coesite and Diamond.* Dobrzhinetskaya LF, Faryad SW, Wallis S, Cuthbert S  
 2152 (eds) p. 43-75  
 2153
- 2154 Sobolev NV, Shatsky VS (1987) Inclusions of carbon minerals in garnets of metamorphic  
 2155 rocks. *Geologiya i Geofizika (Geology and Geophysics)* 7:77-80  
 2156
- 2157 Sobolev NV, Shatsky VS (1988) Accessory diamond in high-pressure metamorphic rocks  
 2158 of the Earth crust. *In: Composition and Processes of Deep Seated Zones of*  
 2159 *Continental Lithosphere.* Sobolev NV (ed) Akademy Nauk USSR press,  
 2160 Novosibirsk, p. 182-184  
 2161
- 2162 Sobolev NV, Shatsky VS (1990) Diamond inclusions in garnets from metamorphic rocks:  
 2163 a new environment for diamond formation. *Nature* 343:742-746

2164  
2165 Sokol AG, Tomilenko AA, Pal'yanov Yu, N Borzdov, Yu M, Pal'yanova GA,  
2166 Khokhryakov AF (2000) Fluid regime of diamond crystallization in carbonate-  
2167 carbon systems. *Eur J Mineral*, 12:367–375.  
2168  
2169 Solin SA, Ramdas AK (1970) Raman spectrum of diamond. *Phys Rev B* 1:1687  
2170  
2171 Song S, Zhang L, Niu Y, Su L, Jian P, Liu D (2005) Geochronology of diamond-bearing  
2172 zircons from garnet peridotite in the North Qaidam UHPM belt, Northern Tibetan  
2173 Plateau: a record of complex histories from oceanic lithosphere subduction to  
2174 continental collision. *Earth Planet Sci Lett*, 234:99-118  
2175  
2176 Spengler D, Van Roermund HL, Drury MR, Ottolini L, Mason PR, Davies GR (2006)  
2177 Deep origin and hot melting of an Archaean orogenic peridotite massif in  
2178 Norway. *Nature* 440:913-917  
2179  
2180 Steger S, Nasdala L, Wagner A (2013) Raman spectra of diamond abrasives and possible  
2181 artefacts in detecting UHP microdiamond. CORALS Conference on Raman and  
2182 Luminescence Spectroscopy in the Earth Sciences. Vienna, Austria p. 95-96  
2183  
2184 Stöckhert B, Duyster J, Trepmann C, Massonne H-J (2001) Microdiamond daughter  
2185 crystals precipitated from supercritical COH+ silicate fluids included in garnet,  
2186 Erzgebirge, Germany. *Geology* 29:391-394  
2187  
2188 Stöckhert B, Trepmann CA, Massonne H-J (2009) Decrepitated UHP fluid inclusions:  
2189 about diverse phase assemblages and extreme decompression rates (Erzgebirge,  
2190 Germany). *J Metam Geol* 27:673-684  
2191  
2192 Stuart FM, Lass-Evans S, Fitton JG, Ellam RM (2003) High  $^3\text{He}/^4\text{He}$  ratios in picritic  
2193 basalts from Baffin Island and the role of a mixed reservoir in mantle plumes.  
2194 *Nature* 424:57-59  
2195  
2196 Sumino H, Dobrzhinetskaya LF, Burgess R, Kagi H (2011) Deep-mantle-derived noble  
2197 gases in metamorphic diamonds from the Kokchetav massif, Kazakhstan. *Earth*  
2198 *Planet Sci Lett* 307:439-449  
2199  
2200 Sverjensky DA, Stagno V, Huang F (2014) Important role for organic carbon in  
2201 subduction-zone fluids in the deep carbon cycle. *Nat Geosci* 7:909-913  
2202  
2203 Tirel C, Brun J-P, Burov E, Wortel MJR, Lebedev S (2013) A plate tectonics oddity:  
2204 Caterpillar-walk exhumation of subducted continental crust. *Geology* 41:555–558  
2205  
2206 Trieloff M, Kunz J, Clague DA, Harrison D, Allègre CJ (2000) The nature of pristine  
2207 noble gases in mantle plumes. *Science* 288:1036-1038  
2208

- 2209 Tretiakova LI, Lyukhin AM (2016) Impact-cosmic-metasomatic origin of microdiamonds  
 2210 from Kumdy-Kol deposit, northern Kazakhstan. *National Geology*  
 2211 (*Otechestvennaya Geologiya*) 2:69-77 (in Russian)  
 2212
- 2213 Tretiakova LI, Lyukhin AM (2017) Impact–Cosmic–Metasomatic Origin of  
 2214 Microdiamonds from Kumdy–Kol Deposit, Kokchetav Massiv, N. Kazakhstan.  
 2215 11<sup>th</sup> International Kimberlite Conference Extended Abstract, 11IKC: 4506  
 2216
- 2217 van Roermund HL, Carswell DA, Drury MR, Heijboer TC (2002) Microdiamonds in a  
 2218 megacrystic garnet websterite pod from Bardane on the island of Fjørtoft, western  
 2219 Norway: Evidence for diamond formation in mantle rocks during deep continental  
 2220 subduction. *Geology* 30:959-962  
 2221
- 2222 Verchovsky AB, Ott U, Begemann F (1993) Implanted radiogenic and other noble gases  
 2223 in crustal diamonds from Northern Kazakhstan. *Earth Planet Sci Lett* 120:87-102  
 2224
- 2225 Vrijmoed JC, Van Roermund HL, Davies GR (2006) Evidence for diamond-grade ultra-  
 2226 high pressure metamorphism and fluid interaction in the Svartberget Fe–Ti garnet  
 2227 peridotite–websterite body, Western Gneiss Region, Norway. *Mineral Petrol*  
 2228 88:381-405  
 2229
- 2230 Vrijmoed JC, Smith DC, Van Roermund HLM (2008) Raman confirmation of  
 2231 microdiamond in the Svartberget Fe-Ti type garnet peridotite, Western Gneiss  
 2232 Region, Western Norway. *Terra Nova* 20:295-301  
 2233
- 2234 Wada N, Matsuda J (1998) A noble gas study of cubic diamonds from Zaire: constraints  
 2235 on their mantle source. *Geochim Cosmochim Acta* 62:2335–2345  
 2236
- 2237 Wang H, Wu Y-B, Gao S, Zheng J-P, Liu Q, Liu X-C, Qin Z-W, Yang S-H, Gong H-J  
 2238 (2014) Deep subduction of continental crust in accretionary orogen: Evidence  
 2239 from U–Pb dating on diamond-bearing zircons from the Qinling orogen, central  
 2240 China. *Lithos* 190:420-429  
 2241
- 2242 Wu BR, Xu JA (1998) Total energy calculations of the lattice properties of cubic and  
 2243 hexagonal diamond. *Phys Rev B*, 57:13355  
 2244
- 2245 Xu S, Liu Y, Chen G, Compagnoni R, Rolfo F, He M, Liu H (2003) New finding of  
 2246 micro-diamonds in eclogites from Dabie-Sulu region in central-eastern China.  
 2247 *Chinese Sci Bull* 48:988–994  
 2248
- 2249 Xu S, Okay AI, Ji S, Sengor AMC, Su W, Liu Y, Jiang L (1992) Diamond from the  
 2250 Dabie Shan metamorphic rocks and its implication for tectonic setting. *Science*  
 2251 256:80–82  
 2252

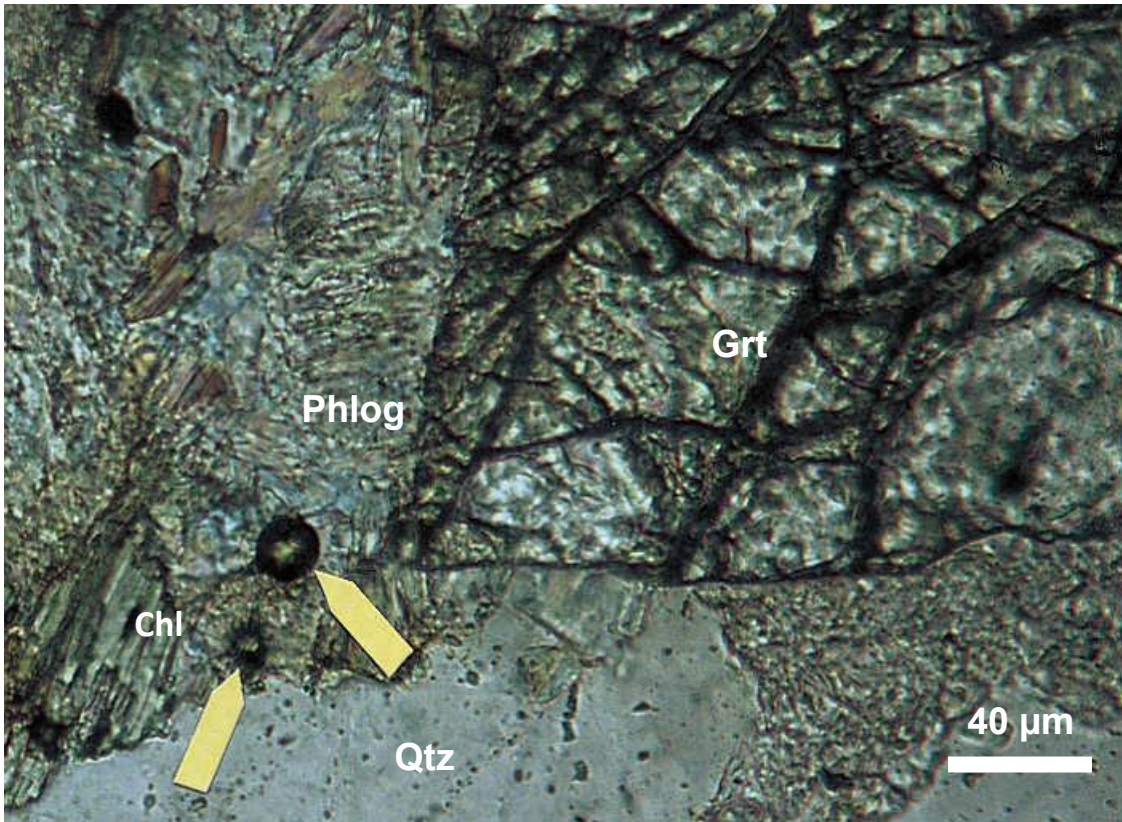
- 2253 Xu S, Liu Y, Chen G, Compagnoni R, Rolfo F, He M, Liu H (2003) New finding of  
 2254 micro-diamonds in eclogites from Dabie-Sulu region in central-eastern China.  
 2255 Chinese Sci Bull 48:988-994  
 2256
- 2257 Yamaoka S, Kumar MS, Akaishi M, Kanda H (2000) Reaction between carbon and water  
 2258 under diamond-stable high pressure and high temperature conditions. *Dia Relat*  
 2259 *Mater* 9:1480-1486  
 2260
- 2261 Yang JS, Xu XZ, Zhang ZM, Rong H, LiY, Xiong FH, Liang FH, Liu Z, Liu F, Li JY, Li  
 2262 ZL, Chen SY, Guo GL, Robinson P (2013) Ophiolite-type diamonds and deep  
 2263 genesis of chromitite. *Acta Geosci Sin* 34: 643–653 (in Chinese with English  
 2264 abstract)  
 2265
- 2266 Yang J, Xu Z, Dobrzhinetskaya LF, Green II, HW, Pei X, Shi R, Wu C, Wooden JL,  
 2267 Zhang J, Wan Y, Li H (2003) Discovery of metamorphic diamonds in Central  
 2268 China: an indication of a >4000 km-long-zone of deep subduction resulting from  
 2269 multiple continental collisions. *Terra Nova* 15:370–379  
 2270
- 2271 Ye K, Cong BL, Ye DN (2000) The possible subduction of continental material to depths  
 2272 greater than 200 km. *Nature* 407:734–736  
 2273
- 2274 Zhang KJ, Cai JX, Zhang YX, Zhao TP (2006) Eclogites from central Qiangtang,  
 2275 northern Tibet (China) and tectonic implication. *Earth Planet Sci Lett* 245:722–  
 2276 729  
 2277
- 2278 Zhang J, Prakapenka V, Kubo A, Kavner A, Green HW II, Dobrzhinetskaya LF (2011)  
 2279 Diamond formation from amorphous carbon and graphite in presence of COH  
 2280 fluids: an in situ high-pressure and-temperature laser-heated diamond anvil cell  
 2281 experiments. *In: Ultrahigh Pressure Metamorphism: 25 Years After the Discovery*  
 2282 *of Coesite and Diamond*, Dobrzhinetskaya LF, Faryad SW, Wallis S, Cuthbert S  
 2283 (eds) Elsevier, London, p.113-124  
 2284
- 2285 Zhang RY, Liou JG, Lo CH (2017) Raman spectra of polycrystalline microdiamond  
 2286 inclusions in zircons, and ultrahigh-pressure metamorphism of a  
 2287 quartzofeldspathic rock from the Erzgebirge terrane, Germany. *Int Geol Rev*  
 2288 59:779-792  
 2289



2290

2291 **Figure 1.** World map of coesite and non-cratonic microdiamond occurrences within  
 2292 Precambrian, Pan-African, Paleozoic and Mezozoic orogens. Numbers indicate age of  
 2293 UHP metamorphism in Ma. Sx- Saxoturingian area of Bohemian massif. Map is modified  
 2294 after Dobrzhinetskaya and Faryad (2011).

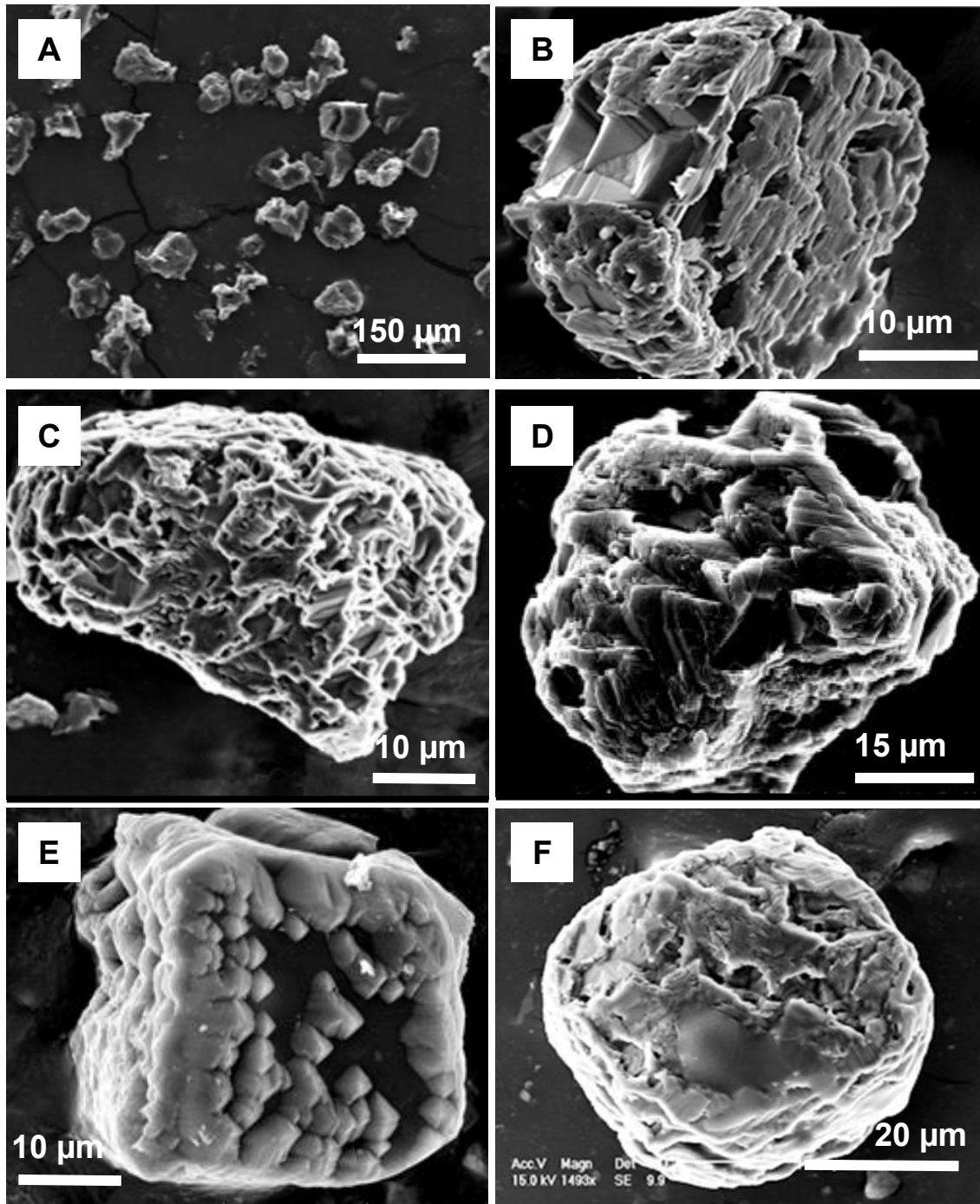
2295



2296

2297 **Figure 2.** Photomicrograph of a standard petrographic thin section showing two diamond  
2298 crystals (*in situ*) in quartz-calc-silicate rocks from Kumdy Kol lake locality, Kokchetav  
2299 massif, Kazakhstan. Photomicrograph taken with a plane polarized transmitted light from  
2300 an optical microscope equipped with a digital camera. Yellow arrowheads point to two  
2301 diamond crystals situated at the phlogopite (Phlog) – chlorite (Chl) boundary; Grt -  
2302 garnet; Qtz- quartz. Sample was collected by L Dobrzhinetskaya from the abandoned  
2303 underground mining gallery which crosses the diamond-bearing rocks of different  
2304 lithologies; the petrographic thin section was prepared at the University of California,  
2305 Riverside without any diamond abrasives.

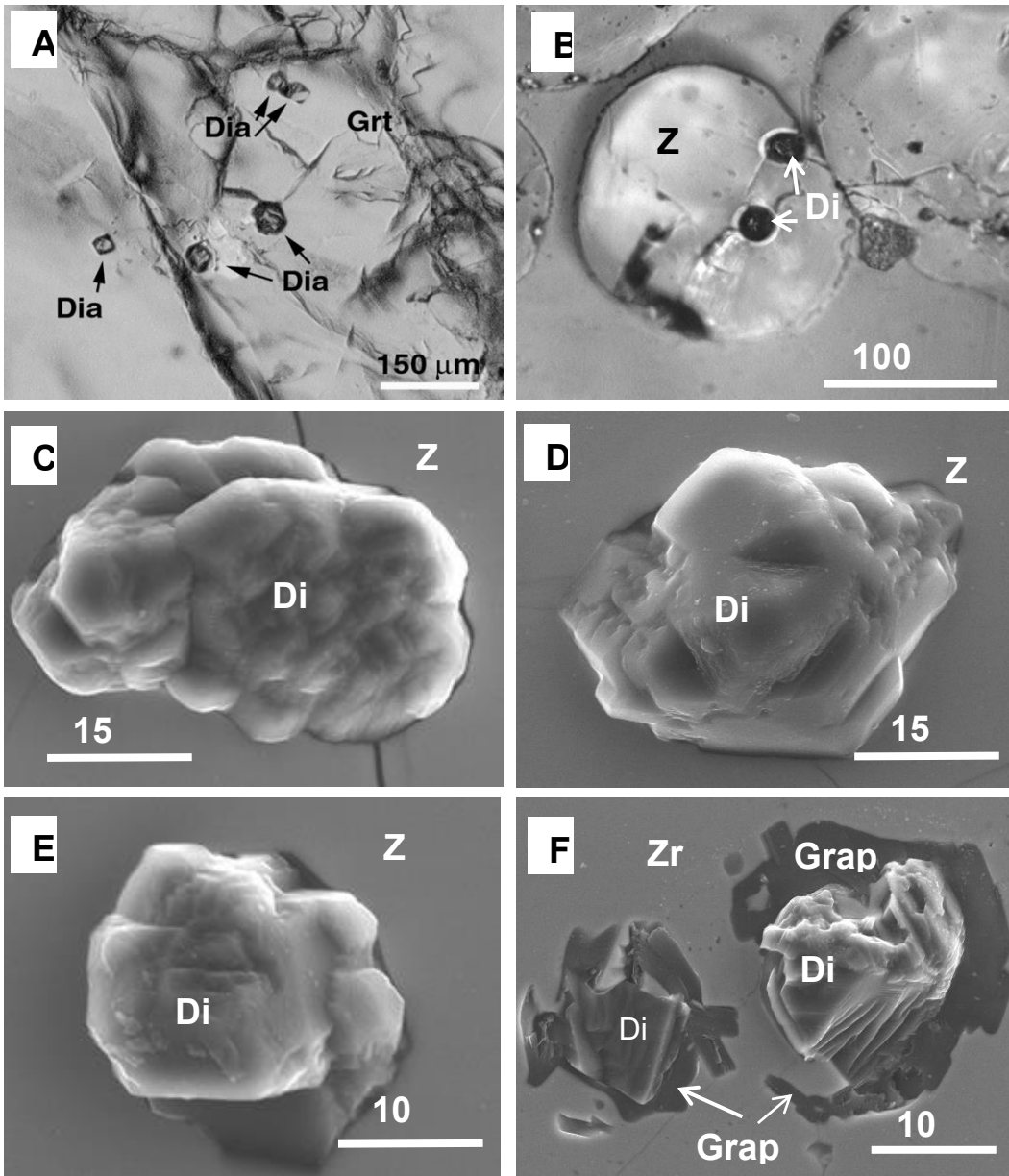
2306



2307

2308 **Figure 3.** Secondary Electron Scanning Electron Microscope images of microdiamonds  
 2309 from Kokchetav massif, Kazakhstan. A – diamonds separated from garnet-biotite gneiss;  
 2310 B – platy skeletal-like diamond single crystal from quartzite; C – shapeless diamond  
 2311 crystal from metacarbonate rocks; D – polycrystalline diamond from marble; E -

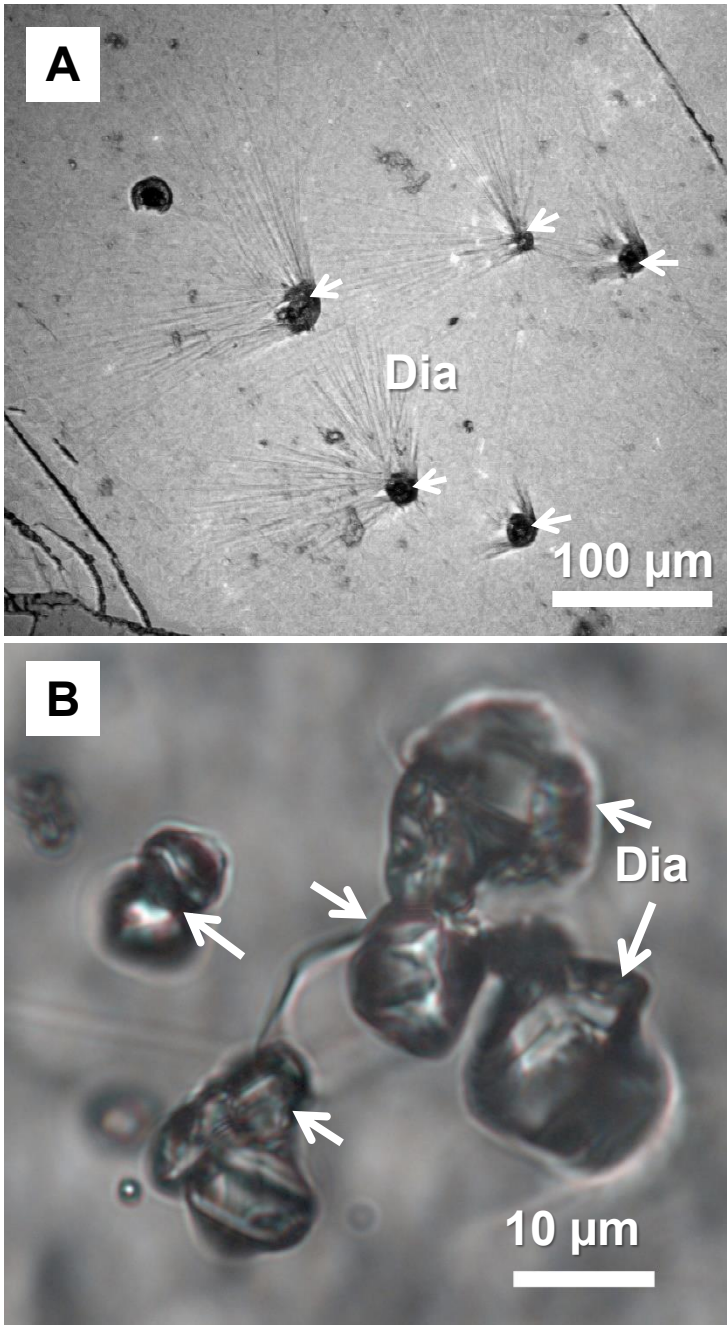
2312 truncated corners cuboid-like diamond with graphite (black contrast) from garnet-biotite  
2313 gneiss; F – cuboidal diamond with truncated corners – from garnet-biotite gneiss.  
2314  
2315



2316

2317 **Figure 4.** Diamonds from Erzgebirge UHPM terrane, Germany. Samples are collected by  
 2318 L. Dobrzhinetskaya from garnet-phengite-quartz-feldspathic gneisses occurred as small  
 2319 outcrops on the eastern shore of the Saidenbach Water Reservoir, Saxonian Erzgebirge,  
 2320 Germany. A – Photomicrograph of diamond inclusions in garnet from garnet-biotite-  
 2321 quartz-feldspathic gneiss (optical microscope equipped with a digital camera, polished  
 2322 thin section, reflected light). B – Photomicrograph of diamond inclusions in zircon  
 2323 separated from garnet-quartz-feldspathic gneiss (optical microscope equipped with a  
 2324 digital camera, zircons are glued on the petrographic glass slide and slightly polished,  
 2325 reflected light mode). C - E – Secondary electron SEM images of diamond inclusions in

2326 zircon (zircon was polished with a special technique using colloidal silica polishing  
2327 compound). F - Secondary electron SEM images of diamond partly replaced by graphite  
2328 included in zircon (sample preparation technique is like C-E).  
2329  
2330



2331

2332 **Figure 5.** Diamonds from Saxony-type granulite of Bohemian massif. Photomicrographs

2333 from optical microscope: A – microdiamond (white arrowheads) inclusions in garnet

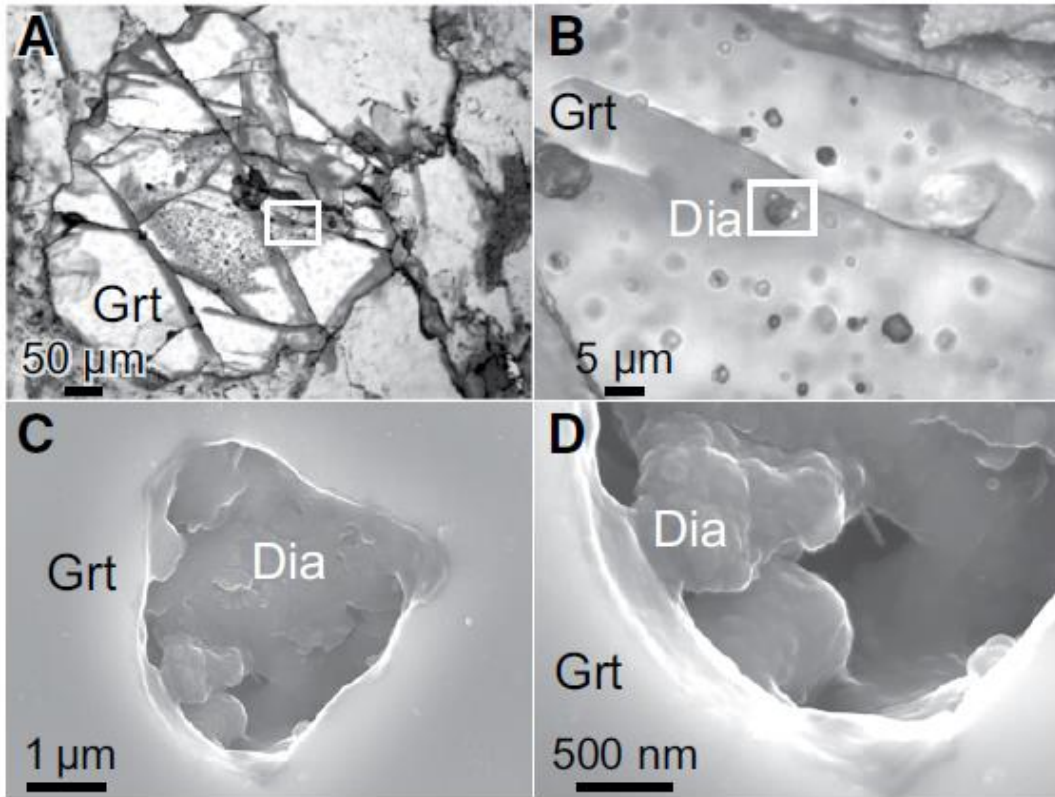
2334 (reflected light mode); polishing striation developed on the garnet surface around the

2335 microdiamonds. B – microdiamond (white arrowheads) inclusions in garnet (plain

2336 parallel light). Photomicrographs are adopted from Kotková et al. (2011).

2337

2338

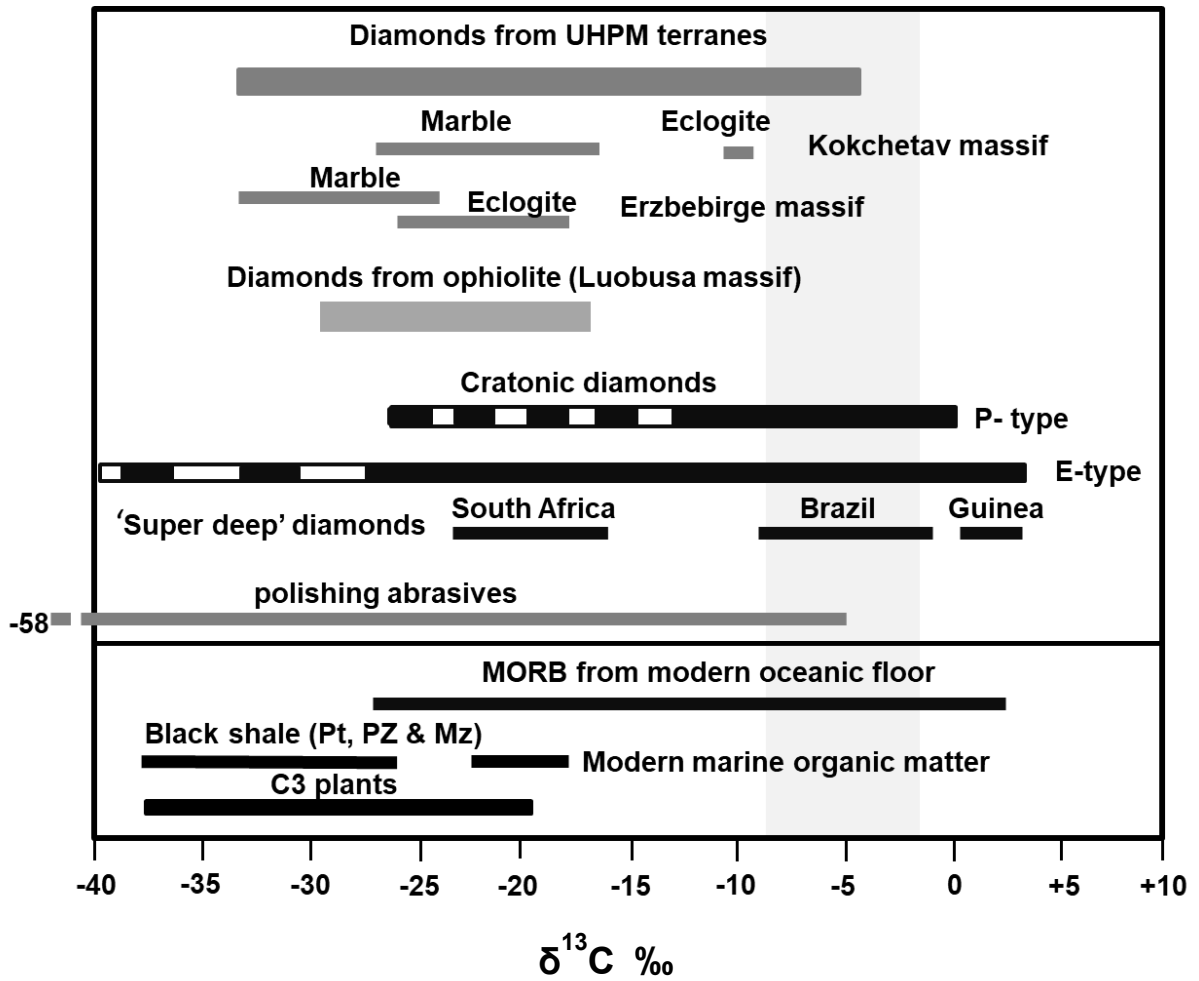


2339

2340 **Figure 6.** Microdiamond inclusions in garnet from garnet-sillimanite-biotite gneiss,  
 2341 Jämtland, Sweden Caledonides (adopted from Majka et al. 2014). A and B – diamond  
 2342 (Dia) inclusion in garnet acquired at different magnifications (optical microscope: plane  
 2343 polarized transmitted light); C and D - SE SEM images of the same diamond shown in  
 2344 plates A and B (acquired at different magnifications).

2345

2346

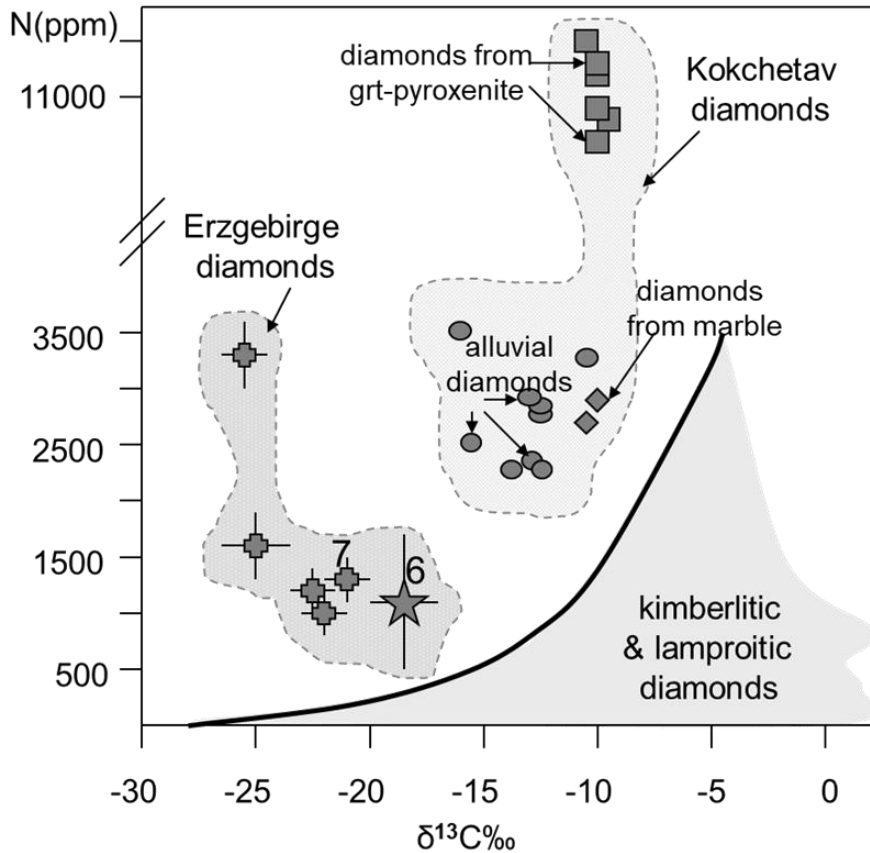


2347

2348 **Figure 7.**  $\delta^{13}\text{C}$  characteristics of diamonds from UHPM terranes, diamonds from  
 2349 ophiolite (Luobasa chromitite massif), E-type and P-type of cratonic diamonds; modified  
 2350 after Liou et al. (2014), see Table 2 for references.  $\delta^{13}\text{C}$  values of MORB, black shale of  
 2351 Proterozoic, Paleozoic, and Mesozoic ages and C3 plants adopted from Kohn 2010 and  
 2352 Myers 2014.

2353

2354

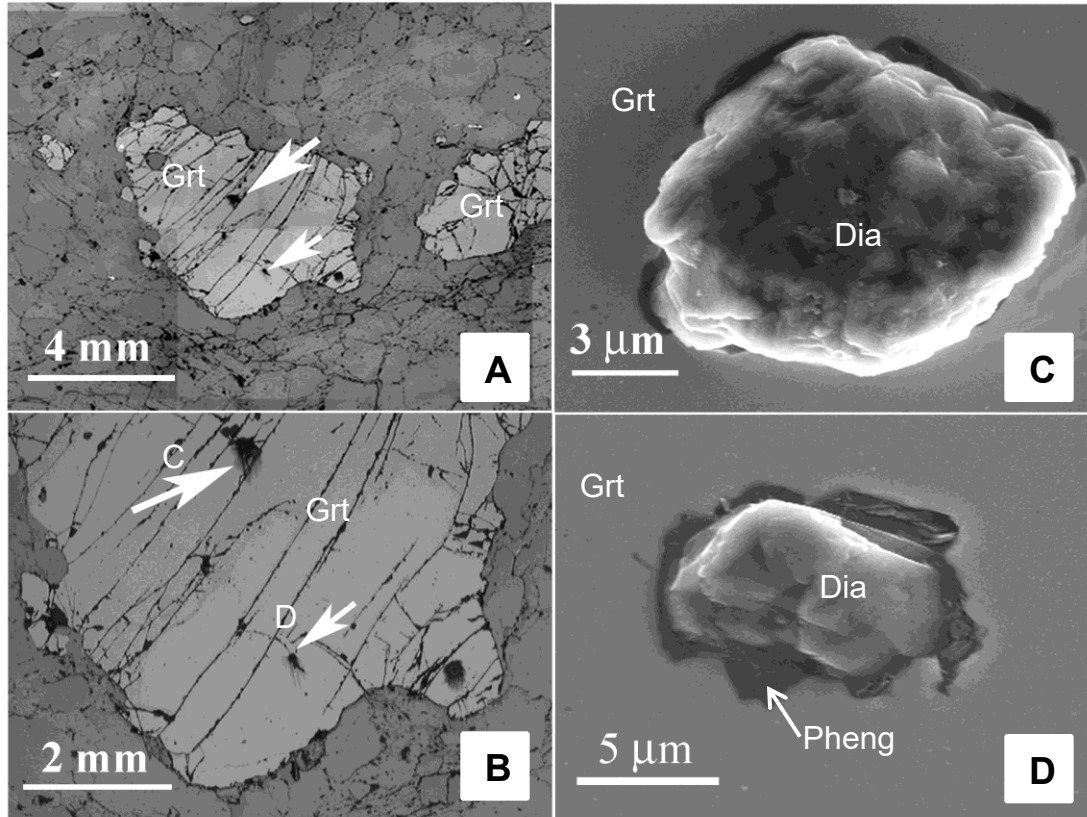


2355

2356 **Figure 8.** Nitrogen content versus  $\delta^{13}C_{PDB}$  in the Erzgebirge microdiamonds included in  
 2357 garnets; modified after Dobrzhinetskaya et al. (2010). Diamonds #6 (star) and #7 (cross)  
 2358 are situated in the same garnet crystal in the core and the rim respectively. The fields of  
 2359 kimberlitic and lamproitic diamonds, and diamonds from garnet pyroxenite (square),  
 2360 marbles (diamond) and from alluvial deposits of the Kokchetav massif, Kazakhstan are  
 2361 adopted from Cartigny et al. (2001; 2003).

2362

2363

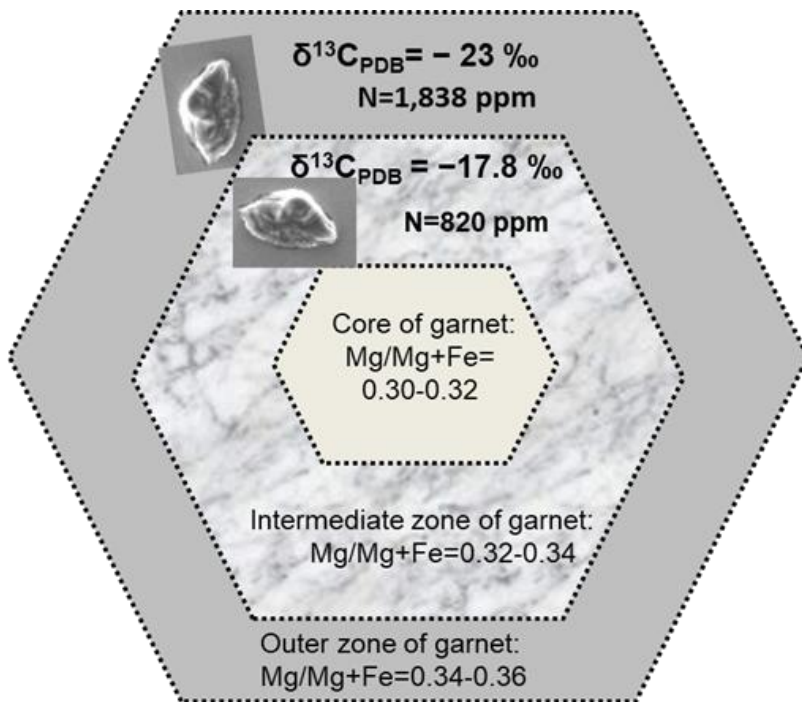


2364

2365 **Figure 9.** A and B - optical microscope digital microphotograph shows (reflected light)  
 2366 the polished slide from Erzgebirge garnet-quartz-feldspathic gneiss. Garnet contains  
 2367 inclusions of microdiamonds (indicated by white arrowheads). Plates C and D -  
 2368 Secondary Electron SEM images of diamonds (shown as C and D in plate B) inclusions  
 2369 in garnet. Diamond in plate C which is situated in the central part of the garnet (see A)  
 2370 has  $\delta^{13}\text{C}_{\text{PDB}} = -17$  to  $-19\%$ , whereas diamond D situated at the outer part of the zoned  
 2371 garnet is characterized by  $\delta^{13}\text{C}_{\text{PDB}} = -22$  to  $-26\%$  (Dobrzhinetskaya et al. 2010).

2372

2373

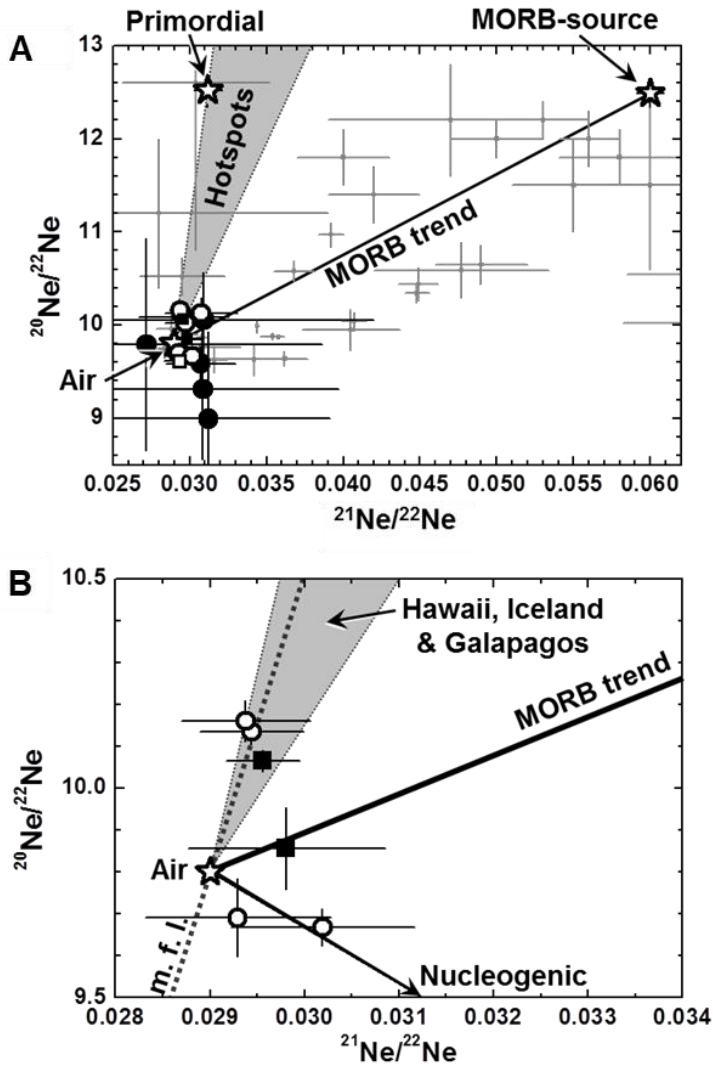


2374

2375 **Figure 10.** Sketch of the slightly zoned garnet with microdiamond inclusions situated  
 2376 within the intermediate zone between the core and the outer rim and close to the outer  
 2377 zone of garnet. Microdiamonds located in the intermediate zone of the garnet  
 2378 ( $\text{Mg}/\text{Mg}+\text{Fe} = 0.32-0.34$ ) are characterized by “heavier” isotopes of carbon  $\delta^{13}\text{C}_{\text{PDB}} =$   
 2379  $-17.8 \text{ ‰}$  and a N concentration of 820 ppm, whereas diamonds from outer garnet zone  
 2380 ( $\text{Mg}/\text{Mg}+\text{Fe} = 0.34-0.36$ ) are characterized by “lighter” isotopes of carbon  $\delta^{13}\text{C}_{\text{PDB}} = -23$   
 2381  $\text{‰}$  and a N content of 1838 ppm (data are adopted from Dobrzhinetskaya et al. 2010).

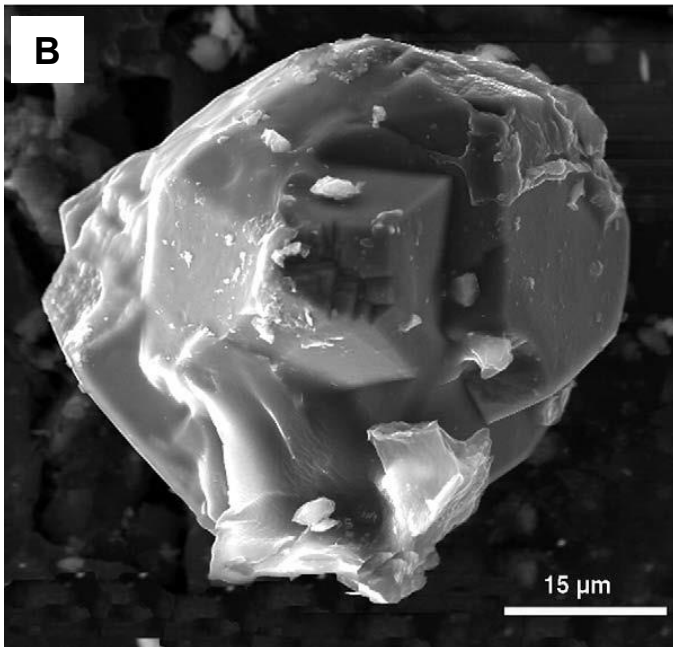
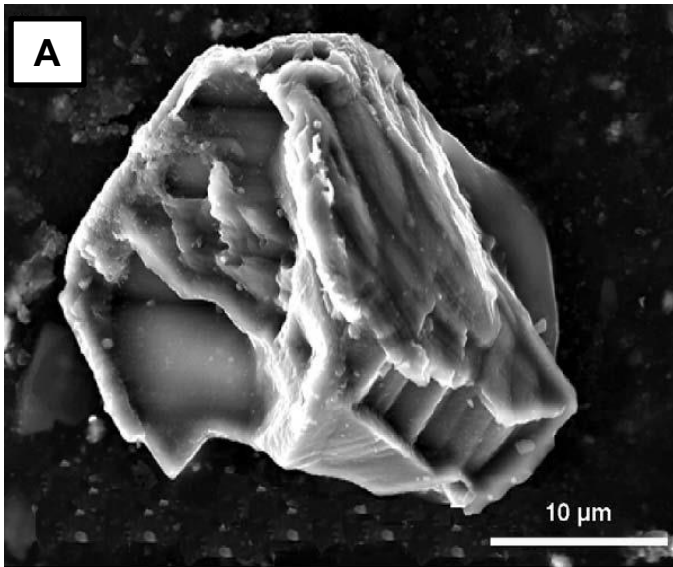
2382

2383



2385 **Figure 11.** A - Neon three-isotope plot for the Kokchetav microdiamond, and plate B is a  
 2386 magnification of plate A (adopted from Sumino et al. 2011). Solid and open circles were  
 2387 obtained by crushing and heating of the Kokchetav microdiamonds, respectively. Total  
 2388 isotope ratios of the heating steps (solid squares) and that of the crushed-powder heating  
 2389 (open square) are also shown. Reported data for kimberlitic diamonds (solid small  
 2390 squares, Gautheron et al. 2005; Honda et al. 1987; 2004; Ozima and Zashu 1988; 1991;  
 2391 Wada and Matsuda 1998; Broadley et al. 2018) are shown for comparison. End-member  
 2392 compositions (air, primordial, and MORB-source mantle) are shown as designated stars.  
 2393 Primordial and MORB-source mantle compositions and a trend which is formed by the  
 2394 data for hotspots (Hawaii, Iceland and Galapagos) enriched in the primordial component

2395 are taken from Trieloff et al. (2000), Sarda et al. (1998) and Kurz et al. (2009). Data point  
2396 uncertainties are 1 sigma. Reference lines for nucleogenic production assuming the  
2397 average crustal composition and F/O = 0.02 (Ballentine and Burnard, 2002) and mass  
2398 fractionation line (m.f.l.) of atmospheric Ne (Ozima and Podosek 2002) are shown as  
2399 solid and dotted lines, respectively  
2400  
2401

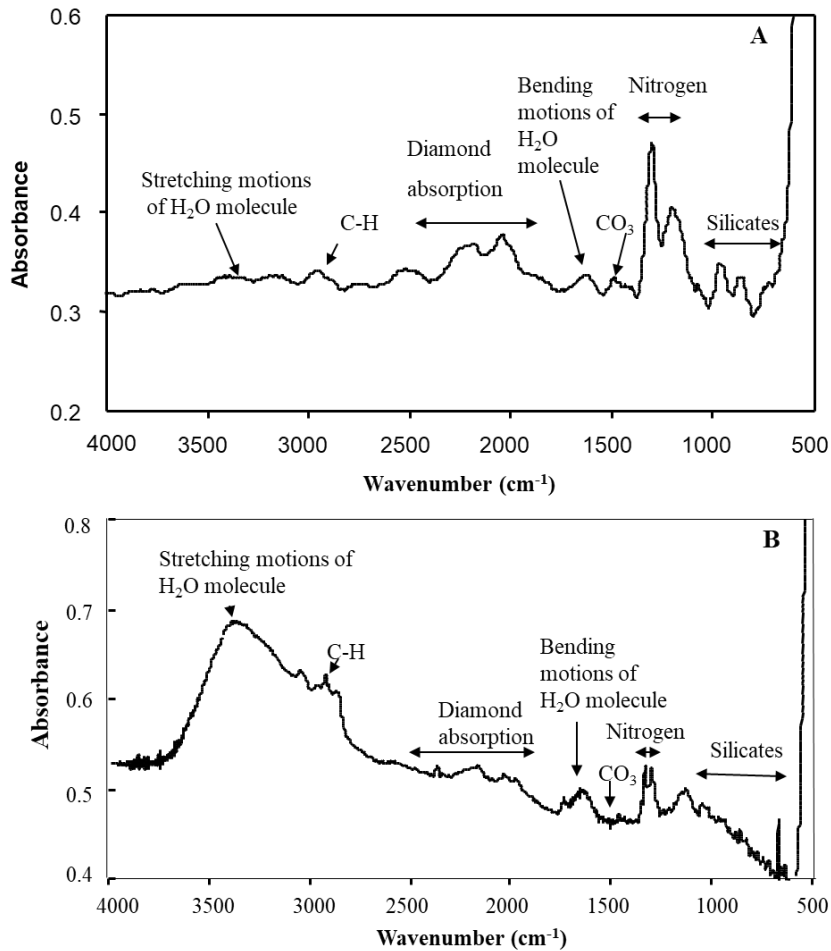


2402

2403 **Figure 12.** Secondary electron SEM images of diamonds extracted from garnet–  
2404 phengite–quartz–feldspathic gneiss from the Erzgebirge massif, Germany: (A) diamond  
2405 #1, (B) diamond #2 (adopted from Dobrzhinetskaya et al. 2006b).

2406

2407

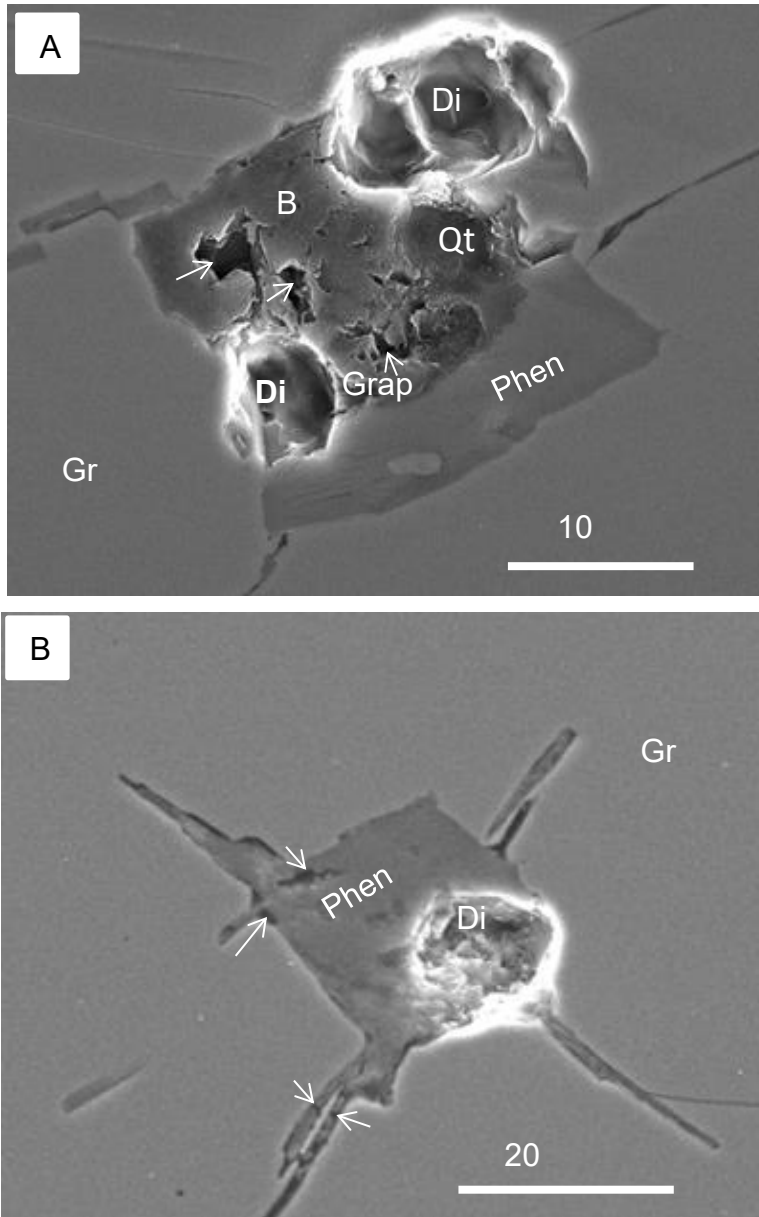


2408

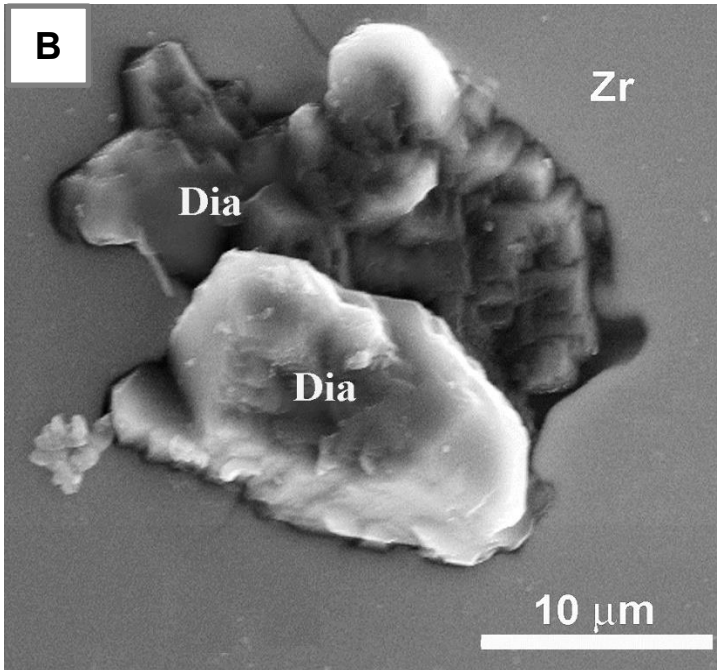
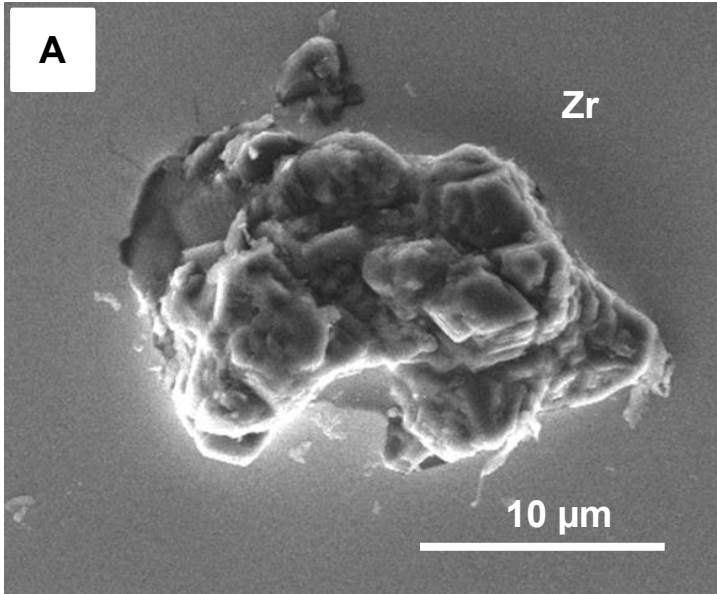
2409 **Figure 13.** Synchrotron IR spectra (beam line U2A, Brookhaven National Laboratory,  
 2410 USA) obtained from Erzgebirge diamond #1 (A) and diamond #2 (B); diamonds are  
 2411 shown in plates A and B of Fig.12 (Spectra are adopted from Dobrzhinetskaya et al.  
 2412 2006b).

2413

2414



2415  
 2416 **Figure 14.** SEM Secondary Electron images of multiphase pockets in garnet from garnet-  
 2417 phengite-quartz-feldspathic gneiss, Erzgebirge, Germany. A – the multiphase pocket  
 2418 contains biotite (Bt), diamond (Dia), phengite (Pheng), quartz (Qtz), and graphite (Graph)  
 2419 shown by arrowheads (adopted from Dobrzhinetskaya et al. 2010); B – the phengite-  
 2420 diamond pocket contains abundant tiny cavities (arrowheads), e.g. traces of fluid  
 2421 inclusions decrepitated during sample preparation.  
 2422

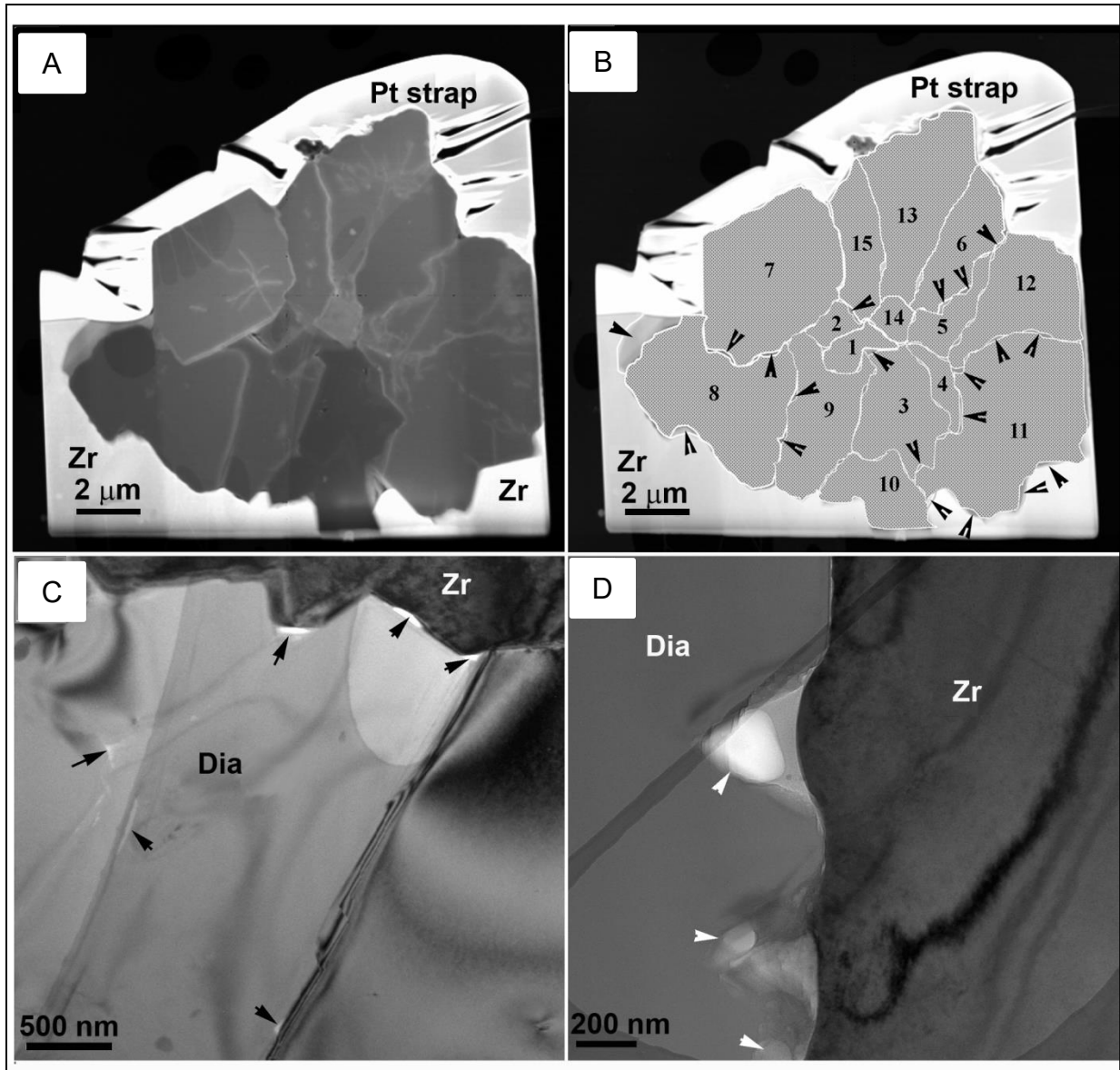


2423

2424 **Figure 15.** A and B - Polycrystalline diamond inclusions in zircons from garnet-  
2425 phengite-quartz-feldspathic gneiss, Erzgebirge, Germany (Secondary Electron SEM  
2426 images).

2427

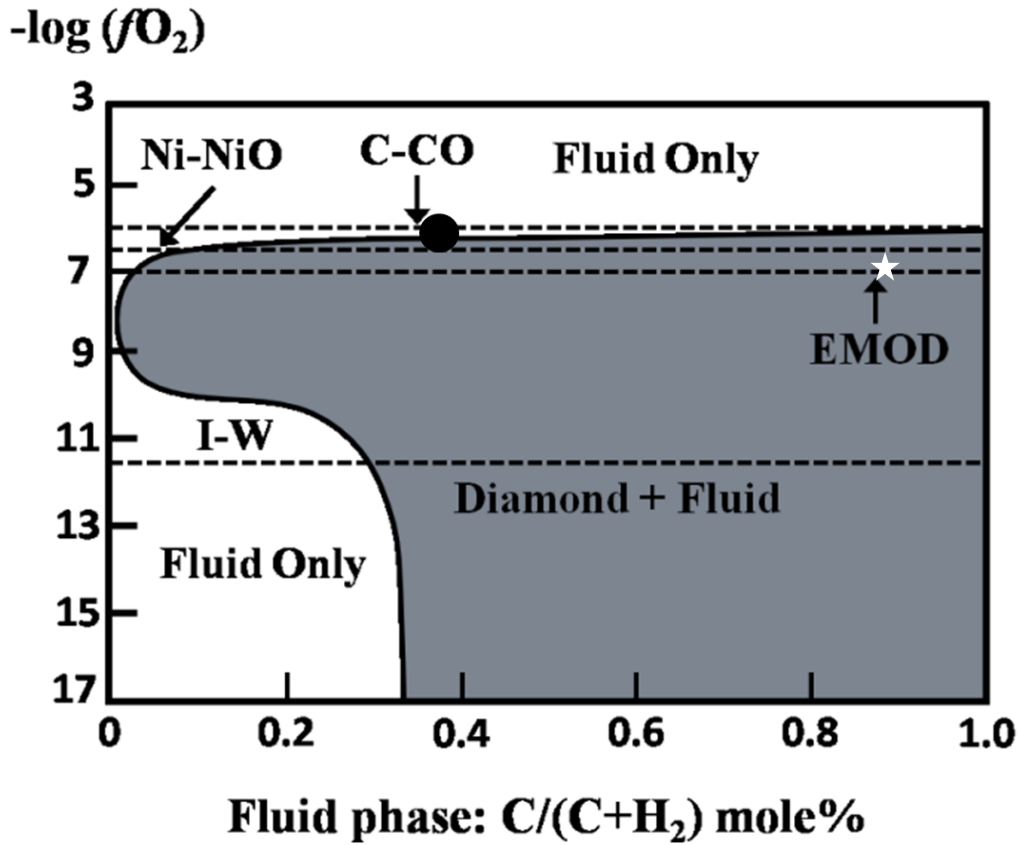
2428



2429

2430 **Figure 16.** Bright Field TEM images of polycrystalline diamond inclusions in zircon  
 2431 (adopted from Dobrzhinetskaya et al. 2013). A - a FIB foil cut through the central part of  
 2432 a diamond shows that the polycrystalline diamond consists of at least 15 individual  
 2433 monocrystals situated closely together; B - a sketch of the individual monocrystals shows  
 2434 that the smaller crystals (#1, 2, and 14) are situated in the central part of the diamond  
 2435 whereas the large crystals have curved boundaries with each other and with the  
 2436 surrounding zircon. Plate C shows the “zig-zag” character of the diamond-zircon and  
 2437 diamond-diamond interfaces containing fluid pockets and a fluid film which are shown

2438 by the black arrowheads. Plate D shows triangle-like cavities at the diamond-zircon  
2439 interface which are filled with fluid; these fluid pockets are marked by white arrowheads.  
2440  
2441

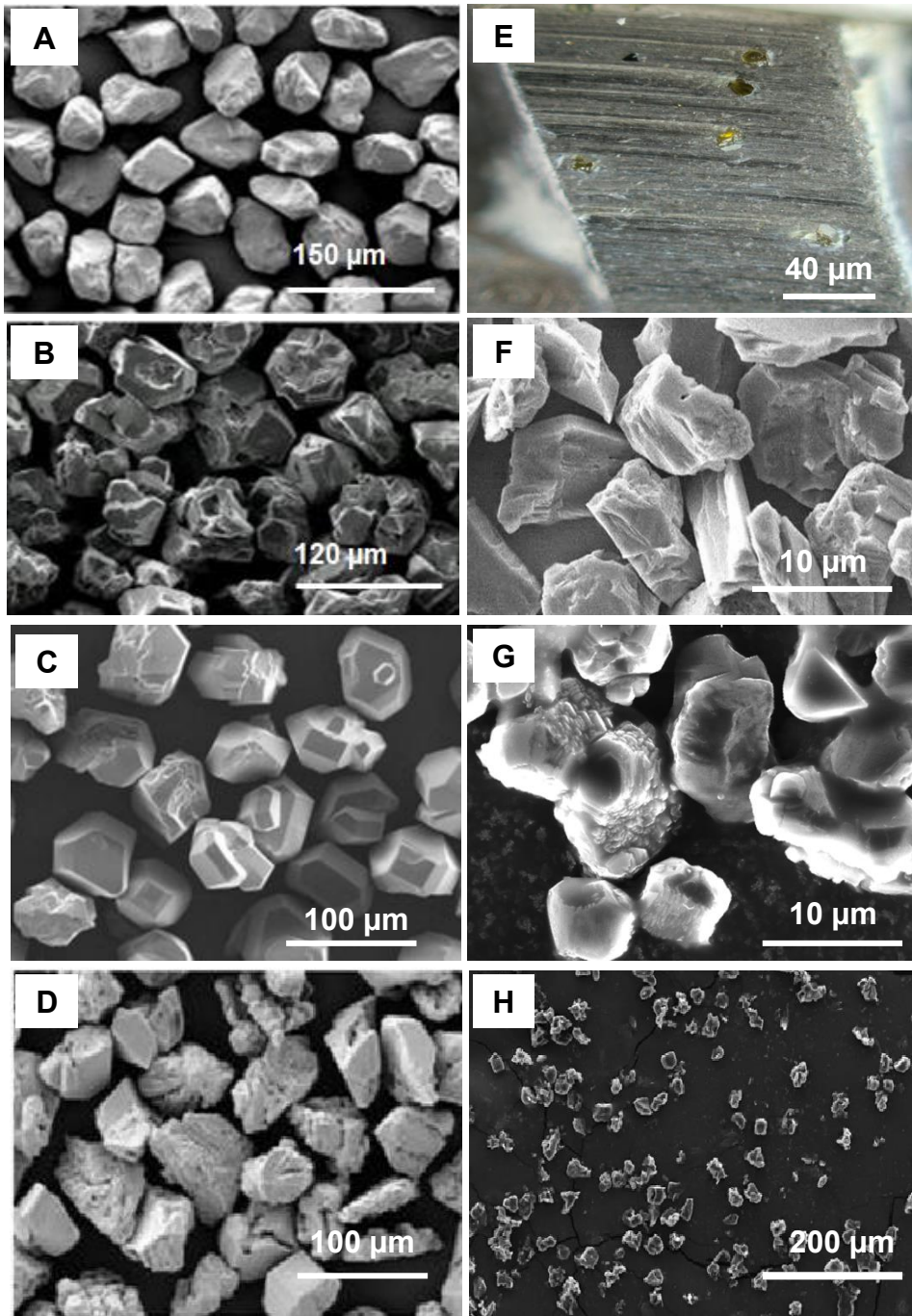


2442

2443 **Figure 17.** Diagram of  $-\log fO_2$  v. fraction of  $(C/C + H_2)$  mole % for C–O–H fluids in  
 2444 equilibrium with diamond at 5 GPa and 1400 K (adopted from Jacob et al., 2011 ,Taylor,  
 2445 1990 and Dobrzhinetskaya et al. 2013). C– CO, Ni-NiO, EMOD (enstatite + magnesite +  
 2446 olivine + diamond), and IW (iron-wustite) are known buffer curves adopted from Eggler  
 2447 & Baker 1982 and Sokol et al. (2000). Gray field corresponds to conditions at which  
 2448 diamond coexists with a fluid (**Diamond + Fluid**); blank fields above and outside of the  
 2449 left part of the black curve, marked as **Fluid Only**, correspond to that oxidation state and  
 2450 concentrations of C and H<sub>2</sub> where diamond is not stable. The black dot corresponds to the  
 2451 position of the Erzgebirge diamonds within the C–CO buffer curve; white star – fluid  
 2452 oxidation state for diamonds from Lago di Cignana, Western Alps (Frezzotti et al. 2014).

2453

2454



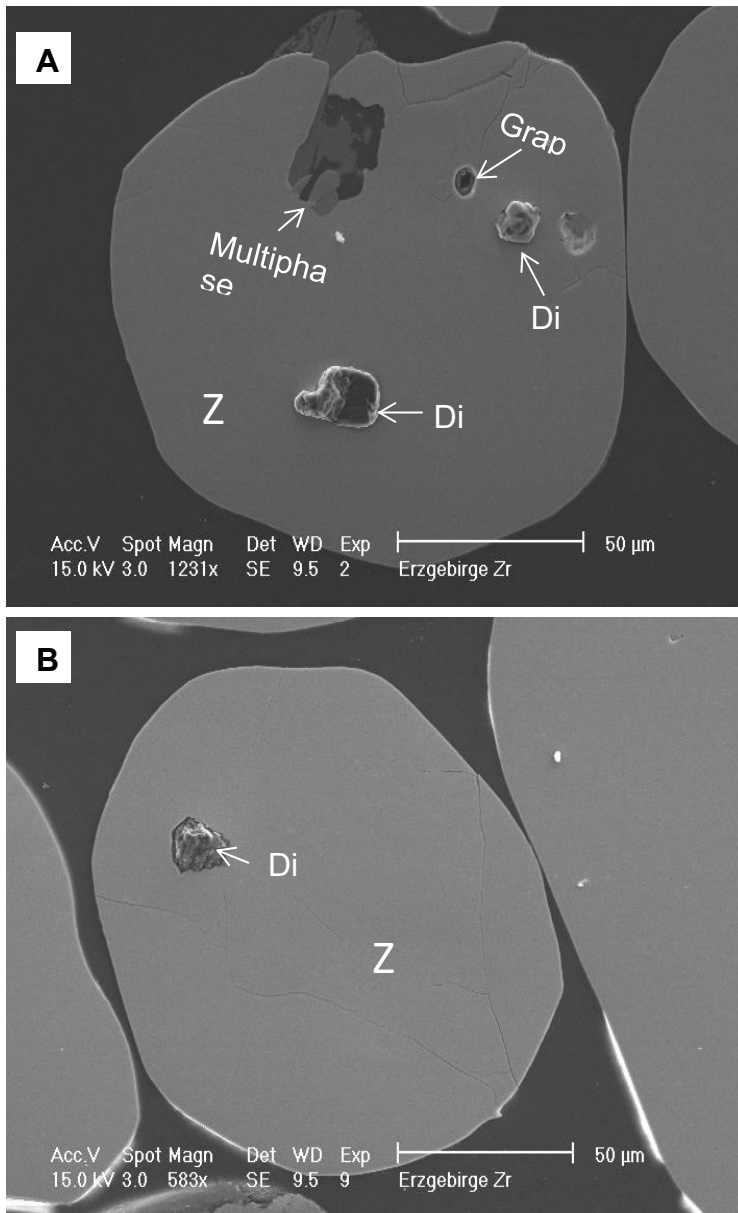
2455

2456 **Figure 18.** A-B – synthetic diamond abrasive powder, courtesy of Henan Baililai  
 2457 Superhard Material Co., Ltd; C-D -synthetic diamond grit, courtesy of Hiperion Materials  
 2458 & Technologies, France; E - a segment of a diamond saw blade, (Wiki Commons), F –  
 2459 synthetic diamond abrasive, TradeIndia Ltd ([www.tradeindia.com](http://www.tradeindia.com)), G – natural  
 2460 microdiamonds separated from Erzgebirge garnet-quartz-feldspathic gneiss

2461 (Dobrzhinetskaya's collection); H –natural microdiamonds separated from Kokchetav  
2462 garnet-biotite gneisses (Dobrzhinetskaya's collection).

2463

2464



2465

2466

2467

2468

2469

2470

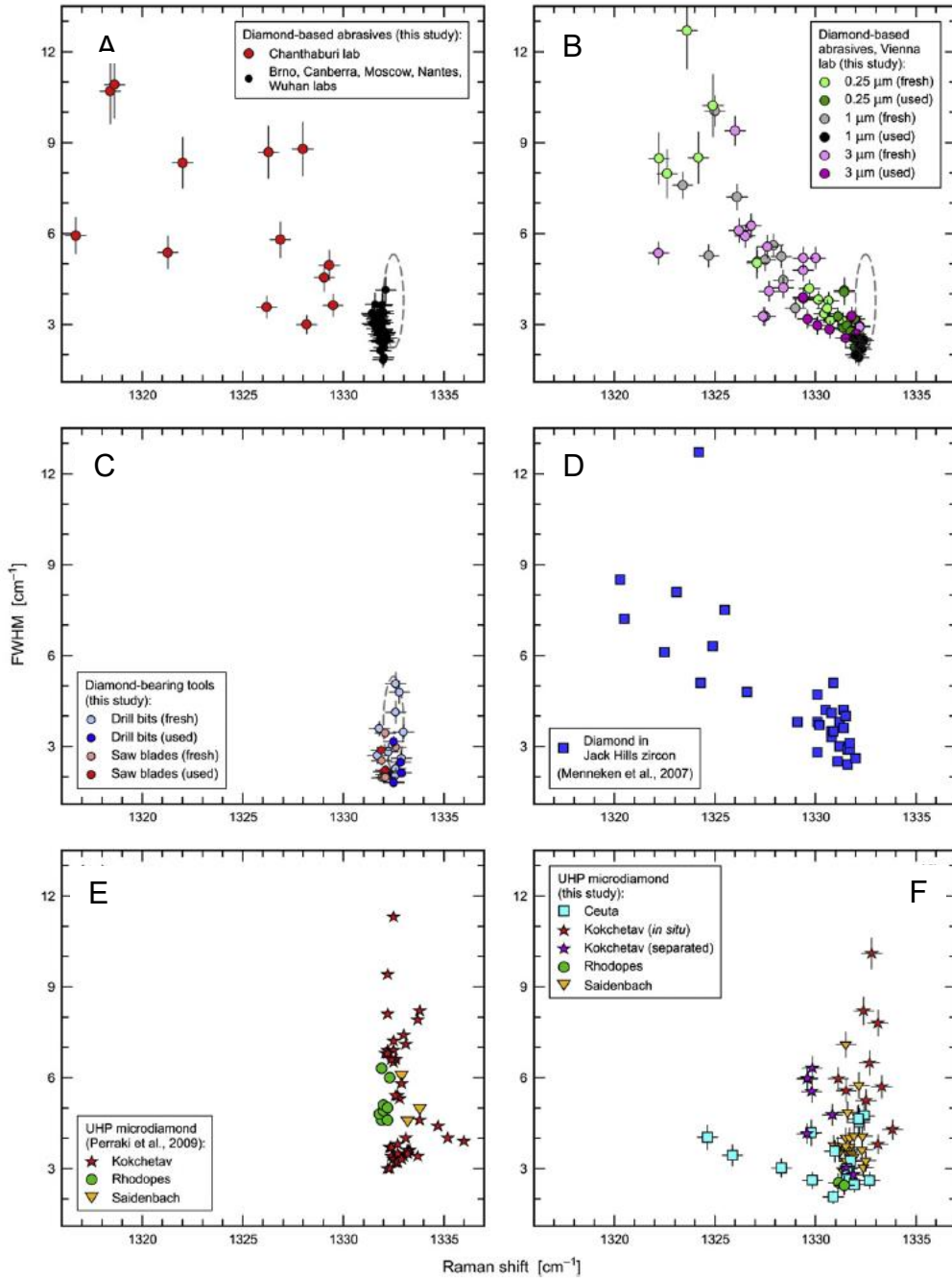
2471

2472

2473

2474

**Figure 19.** SE SEM images of zircon grains separated from the garnet-quartz-feldspathic gneiss from the Erzgebirge, Germany; zircons are mounted with Petropoxy on a standard petrographic glass slide and polished with SiC grit, Al<sub>2</sub>O<sub>3</sub> and SiO<sub>2</sub>-colloidal abrasive liquid (see polishing procedure protocol described in Dobrzhinetskaya et al. 2001). A- diamond inclusions are standing above the perfectly polished zircon surface, whereas graphite and multiphase inclusions (phengite + SiO<sub>2</sub>+ KAlSi<sub>3</sub>O<sub>8</sub>) remain flat; lattice parameters of SiO<sub>2</sub> and KAlSi<sub>3</sub>O<sub>8</sub> are not measured due to the small size of inclusions. B - diamond inclusion in zircon; phengite (black contrast) occurs at the diamond-zircon interface.

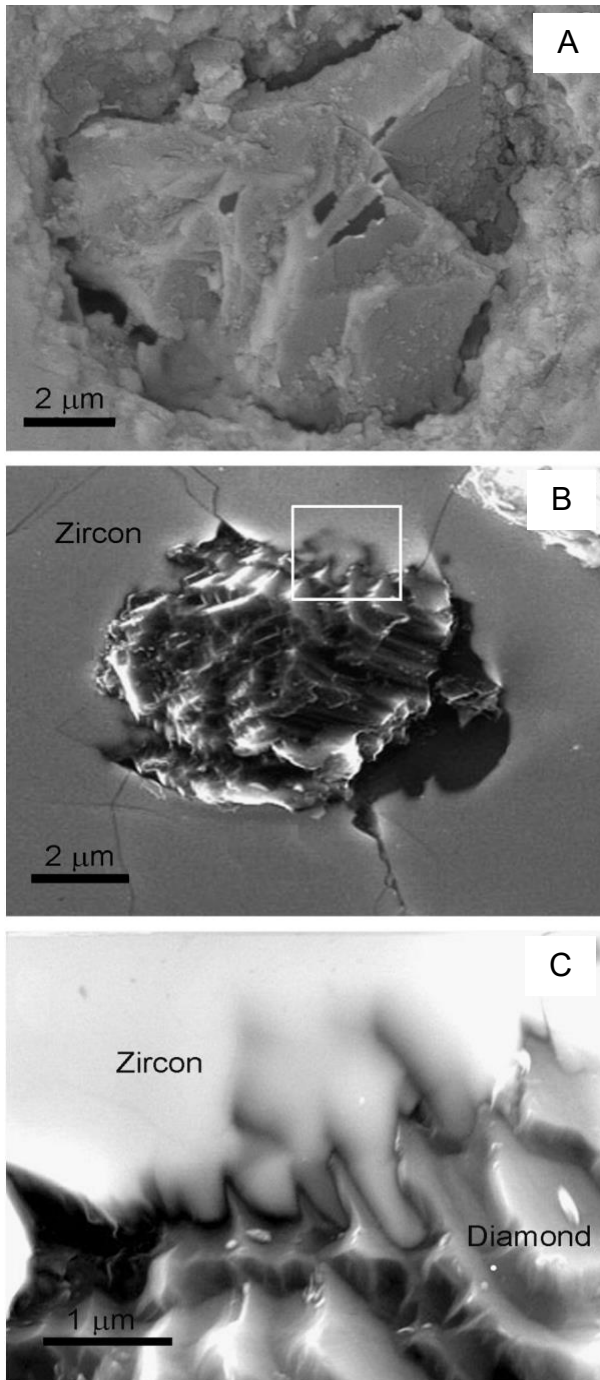


2475

2476

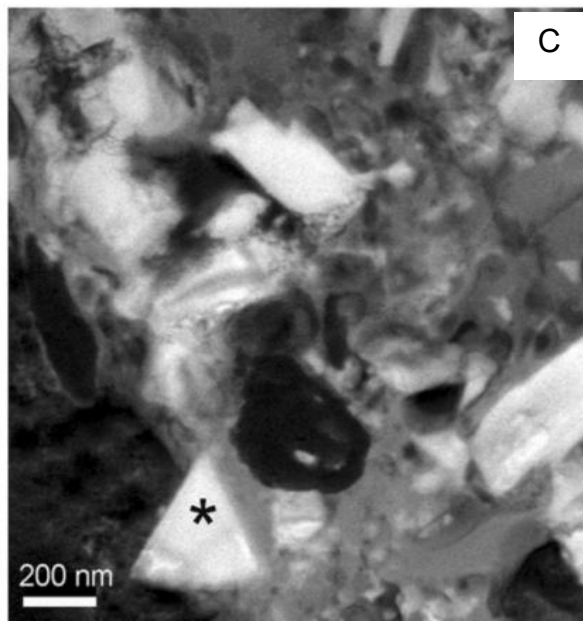
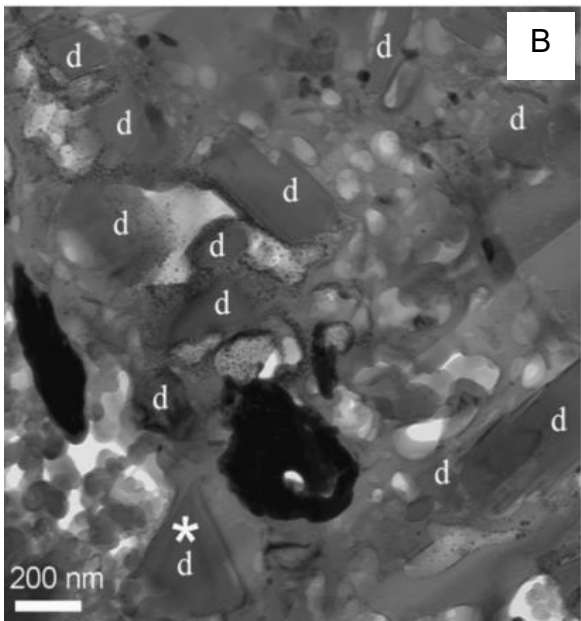
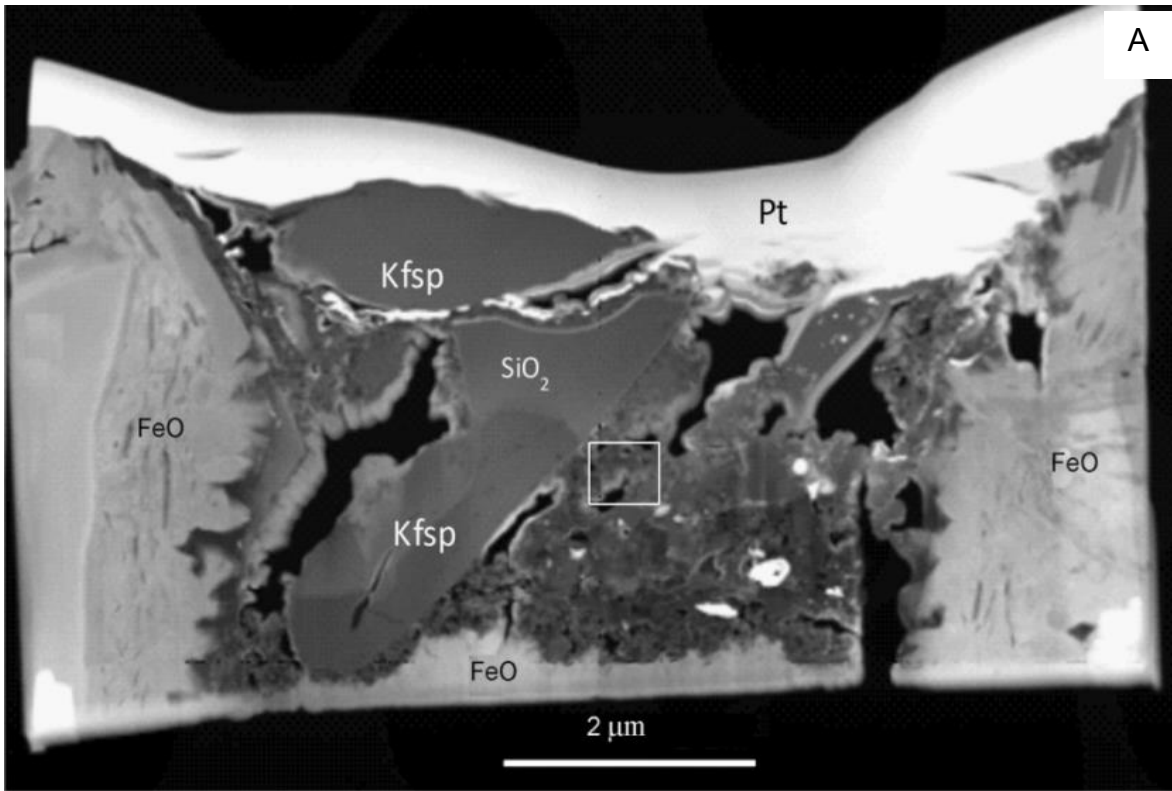
2477 **Figure 20.** Plots of the FWHM as a function of peak position of the first-order Raman  
 2478 mode of diamond (LO=TO mode at 1332 cm<sup>-1</sup> for ideal ambient single-crystal diamond),  
 2479 adopted from Nasdala et al. 2016 - Fig 5. A – C - data from diamond-based abrasive and  
 2480 diamond tools (Nasdala et al. 2016's studies), dashed oval - data from Perraki et al. 2009;  
 2481 D - Jack Hills diamonds in zircon (Menneken et al. 2007 Fig 2); E - diamonds from

2482 UHPM terranes from Perraki et al. 2009; F – diamonds from UHPM terranes (Nasdala et  
2483 al. 2016's studies).  
2484



2485  
2486 **Figure 21.** SEM images of microdiamonds included in zircons (adopted from  
2487 Dobrzhinetskaya et al. 2014). A – diamond inclusion in zircon from Jack Hills  
2488 conglomerates (image is from Fig. 3(e) of Menneken et al. 2007). B - diamond inclusion  
2489 in zircon from Kokchetav massif, Kazakhstan, black contrast in the right lower corner of  
2490 diamond is chlorite (Dobrzhinetskaya et al. 2001). C – a portion of the diamond–zircon

2491 interface (white boxed area on plate B) shows that diamond is intricately intergrown with  
2492 its host zircon.  
2493



2494

2495

2496 **Figure 22.** STEM - TEM images of FIB foils cut through inclusions identified by Raman

2497 spectroscopy as diamond (adopted from Dobrzhinetskaya et al. 2014). A - STEM image-

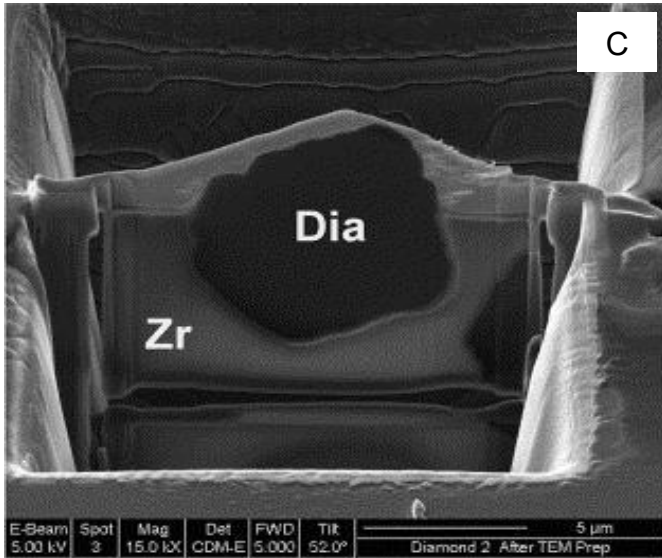
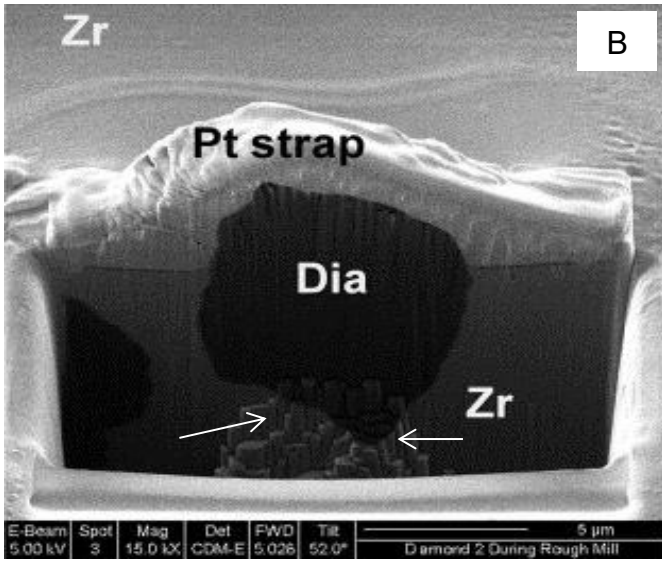
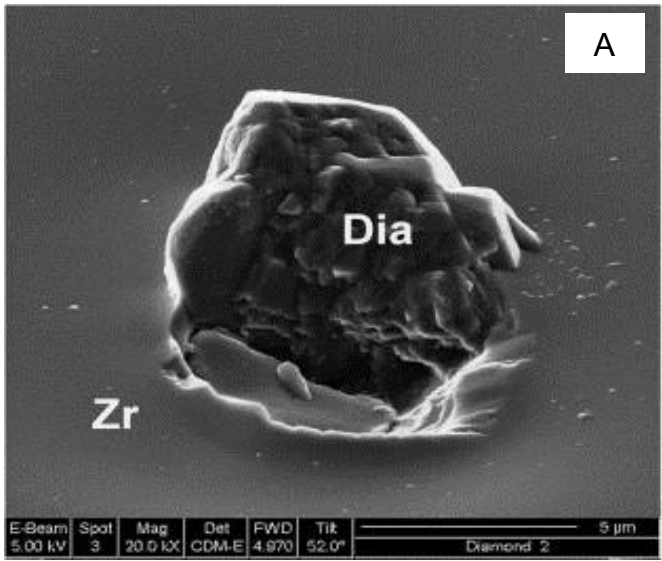
2498 overview of the place where diamond was identified with Raman spectroscopy (1<sup>st</sup> order

2499 diamond Raman mode observed at:  $1332\text{ cm}^{-1}$ ) shows the presence of Kfsp and

2500 amorphous SiO<sub>2</sub> inclusions. The platinum (Pt) film (white contrast) was deposited on the  
2501 surface of the inclusion prior to the FIB foil preparation and it has a concave-upward  
2502 surface indicating that the material from the surface was preferentially eroded during the  
2503 primary mechanical polishing, because the Kfsp inclusion is softer than the zircon. The  
2504 black contrast areas between Kfsp and SiO<sub>2</sub> represent holes that were probably filled with  
2505 volatile-rich solid materials or fluids that “evaporated” to the vacuum chamber during  
2506 FIB milling. B - Bright Field TEM image of boxed area shown in plate (A) showing  
2507 abundant diamond fragments (labeled as ‘d’); the dark contrasted grains with irregular  
2508 shapes and surfaces are gold (from the previous gold sputtering). Note the unusual sharp-  
2509 angle morphology of the diamond. The round bubble-like bright-grey contrast area is an  
2510 epoxy resin mixed with the polishing debris. C - Image taken of the same area as (B) with  
2511 characteristic X-rays of Carbon (carbon-element map). Bright contrast indicates  
2512 essentially pure carbon; \* is labeled for an easy comparison with the diamond fragments  
2513 shown on plates B and C.

2514

2515



2516

2517 **Figure 23.** Secondary electron images (FIB-duobeam) of diamond included in zircon  
2518 form Erzgebirge, Germany (adopted from Dobrzhinetskaya et al. 2003) showing the FIB  
2519 milling sequence. A – polished cross-section of zircon host with a diamond inclusion. B -  
2520 FIB section through the diamond crystal; vertical ‘column-like’ patterns (white  
2521 arrowheads) are due to the initial ‘rough’ milling step. Pt strap covers top of the diamond  
2522 crystal. C - FIB foil shows two-dimensional geometry of diamond inclusion and  
2523 demonstrates the indigenous grain boundary between diamond and zircon host.  
2524  
2525

<b>UHPM terrane/locality</b>	<b>Available data on diamond specific features</b>	<b>Age in MA</b>	<b>P (GPa) &amp; T (°C) estimate, and UHP index minerals associated with diamond</b>	<b>Data source</b>
Kokchetav massif, Kazakhstan (Kumdy-Kol, Barchi-Kol)	size of crystals: 10 –100 $\mu\text{m}$ (average $\sim 40 \mu\text{m}$ ); skeletal, imperfect; cubes with truncated corners single crystals, and polycrystalline diamonds	531 (UHPM) 2100-2700 (protolith)	P=6-9; T=980-1200 coesite, titanatite with exsolution lamella of coesite; diamonds with inclusions of aragonite + $\text{MgCO}_3$	Sobolev and Shatsky 1990; Claoué-Long et al. 1991; Ogasawara et al. 2000; 2002; Okamoto et al. 2000; Katayama et al. 2001a; Dobrzhinetskaya et al. 2001; 2003; 2006
China, Dabie-Sulu	Diamonds ( $\sim 60$ -150 $\mu\text{m}$ size) included in garnet from eclogite; in situ in polished thick sections	220–240 (Dabie-Sulu), South Dabie	P>2.7-5; T=600-930 (Dabie-Sulu) coesite, diamond	Xu et al. 1992; 2003;
China, North Qaidam	Diamond inclusion in Zr recovered from garnet peridotite	420-450 (N. Qaidam UHPM belt)	>2.8-4; 620-740 (N. Qaidam) coesite, diamond, majoritic garnet, relicts of stishovite	Song et al. 2005; Mattisson et al. 2006; Zhang et al. 2006; Liu et al. 2007; Liou et al. 2009; Katsube et al. 2009
China, North Qinling	Diamond ( $\leq 1 \mu\text{m}$ size) inclusions in zircon extracted from eclogite body	507 (North Qinling)	P>2.6; T=590-760 (North Qinling) diamond	Yang et al. 2003
Central China, North Qinling	Diamond inclusion in zircon extracted from amphibolite body	$490.4 \pm 5.8$	P $\sim 4.0 \pm 0.5$ ; T=670-750	Wang et al. 2014
Bohemian massif, Erzgebirge, Saldenbach, Germany	Diamonds (5-50 $\mu\text{m}$ size) imperfect cubes, rose-like single crystals, and polycrystalline diamonds	360 (UHPM)	P>7; T=900-1200 coesite, diamond, $\text{TiO}_2$ with $\alpha\text{PbO}_2$ structure	Massonne 1999; Massone and Nasdala 2000; Hwang et al. 2000; Massonne and O'Brien 2003; Massonne et al. 2007
Bohemian massif, Moldanubian Zone, České Stredohorí, Stráž nad Ohří, Plesovice (Czech Republic)	Diamonds ( $\sim 5$ – 30 $\mu\text{m}$ size) <i>in situ</i> graphitized diamond < 2 $\mu\text{m}$	340 -380 (UHPM)	P>3.5; T=1100 diamond	Kotková et al. 2011 Naemura et al. 2011
Bohemian	Diamonds of $\sim 7$ -8 $\mu\text{m}$	$\sim 360$	P >4.5; T $\sim 680$	

massif, Moldanobian Zone, Kutna Gora area, (Czech Republic)	Gföhl kyanite-bearing granulites	Ma (UHPM)	Diamond, coesite, moissanite	Perraki and Faryad 2014
Western Gneiss Region, Norway (Fjortoft, Svartberget)	Diamonds (1 nm -20 $\mu$ m size) round-like crystals with "striation" and imperfect cubes with truncated edges	408–425 (UHPM)	P>3.2 - 4; T=800 coesite, majoritic garnet, diamond	Smith 1984; Dobrzhinetskaya et al. 1995; van Roermund et al. 2002; Spengler et al. 2006; Vrijmoed et al. 2006; 2008
Northern Norway, Tromso Nappe Caledonides	Diamond inclusions in grt from kyanite-garnet-biotite-gneisses	452	P=3.5+/-0.5; T=800	Janák et al. 2013
Western Gneiss Region, Norway, Straumen	Diamond inclusion in zircon from eclogite	408–425	P=3.75+/-0.75; T=750+/-150	Smith and Godard 2013
Rhodope, Greece (Kimi & Sideronero)	Diamonds of 3-9 mm size inclusions in garnet (Kimi and Xanthi area) and in garnet from garnet-kyanite-mica schist, Sideranero area	202 (UHPM) 39 - 186	P=2.2; T=750	Mposkos and Kostopoulos 2001; Perraki et al. 2006; Schmidt et al. 2010; 2011; Liati et al., 2011.
Western Alps (Lago di Cignana)	Diamond (1-2 $\mu$ m size) inclusions in Mn-rich garnet; associates with fluid inclusions of HCO <sub>3</sub>	35	P $\geq$ 3.2; T $\leq$ 600 (cold subduction)	Frezzotti et al. 2011; 2014; Frezzotti 2019
Eastern Alps, Pohorje	Diamond + SiC inclusions in garnet	92-95	P $\geq$ 3.5 GPa, T =800-850	Janák et al. 2015
Betic Rif Cordilleras, Ceuta (NW Africa and SE Spain )	Diamond ( 5-15 $\mu$ m size) intergrown with coesite; diamond inclusions in garnet, kyanite, apatite	330	P>4.3-7; T=>1150	Ruiz Cruz and Sanz de Galdeano, 2012; 2013; 2014
Snasahögarna Mt., Seve Nappe	Diamond (~1 $\mu$ m size) diam+carbonate+graphite inclusions in garnet	441-445	P=4.1-4.2; T=830-840	Majka et al. 2014, Klonowska et al. 2017

Sweden,				
Nagssugtoqidi an Orogen West Greenland	Diamond is partly replaced by graphite, majorite, reconstructed ringwoodite	1800	P ~7; T ~970	Glassley et al. 2014

2526

2527

2528 **Table 1.** Microdiamonds occurrences in worldwide ultrahigh-pressure metamorphic

2529 terranes. This table contains part of information adopted from Table 1 (Dobrzhinetskaya

2530 2012).

2531

Locality	Minerals/rocks type	$\delta^{13}\text{C}_{\text{PDB}}$ value	$\delta^{15}\text{N}$ value	N content in ppm	References
Kokchetav massif, Kazakhstan	diamonds - bulk measurements	-10.2 ‰ to -26.9 ‰			Chopin and Sobolev 1995; Lavrova et al. 1997;
	diamond from garnet-clinopyroxene rocks;	-10.5 ‰	+5.9 ‰		De Corte et al. 2000
	diamonds from marble	-10.2 ‰	+8.5 ‰		De Corte et al. 2000
	diamond from garnet – clinopyroxene rock;	-10 ‰ to -11 ‰	+5.9 ‰ (mean)	11,150	Cartigny et al. 2001
	diamond from marble	-8.5 ‰ to -10.19 ‰		2,650	Cartigny et al. 2001
S-diamond (outer rim) inclusion in garnet from dolomitic marble;		-17 ‰ to -27 ‰			Imamura et al. 2013
	S-diamond (core) inclusion in garnet from dolomitic marble;	-9 ‰ to -13 ‰			Imamura et al. 2013
	R-diamond inclusion in garnet from dolomitic marble	-8 ‰ to -15 ‰			Imamura et al. 2013
dolomite mineral from dolomitic marble;		-4 ‰ to -7 ‰			Ohta 2003
dolomitic marble (bulk)		-2‰			Ohta 2003
Erzgebirge Massif, Germany	diamond inclusions in zircon (bulk analysis) from garnet-phengite gneiss;	-24 ‰ to -33‰			Massonne and Tu 2007
	diamond inclusions in zoned garnet (outer rim) from garnet-phengite-quartz-feldspathic gneiss;	-22 ‰ to -26 ‰		740 - 3,370	Dobrzhinetskaya et al. 2010
	diamond inclusions in zoned garnet (core zone) from garnet-phengite-quartz-feldspathic gneiss	-17 ‰ to -19 ‰			Dobrzhinetskaya et al. 2010
Worldwide UHPM terranes	UHPM metamorphic rocks	-3 ‰ to -30‰	-1.8 ‰ to +12.4 ‰		Cartigny 2005
Kimberlitic xenoliths	E-type	-26.4 ‰ to +0.2‰	-12.4 ‰ to +18 ‰		Cartigny 2005
	P-type	-38.5 ‰ to +2.7 ‰	-20 ‰ to +12 ‰		Cartigny 2005

Ophiolitic massif (Luobusa)	chromitite	-18 ‰ to -28 ‰		20 - 670	Yang et al. 2013
-----------------------------------	------------	----------------	--	----------	------------------

2532

2533 **Table 2.** Carbon ( $\delta^{13}\text{C}_{\text{PDB}}$ ) and Nitrogen ( $\delta^{15}\text{N}$ ) characteristics of diamonds, bulk rocks  
 2534 and carbon-bearing minerals from Kokchetav massif, Kazakhstan and Erzgebirge massif,  
 2535 Germany, kimberlitic xenoliths and ophiolitic chromitites.

2536

Diamond locality	Rock types	Inclusions in diamonds	Identification method	References
Kokchetav massif, Kazakhstan	Garnet clinopyroxenite	$\text{CO}_3^{2-}$ ; $\text{H}_2\text{O}$ ; $\text{OH}^-$	Infrared spectroscopy	de Corte et al. 1998
	Garnet-biotite-gneiss	crystalline inclusions (40-80 nm)*: $\text{Fe}_2\text{Si}_2\text{O}_6$ ; $\text{TiO}_2$ ; $\text{Cr}_2\text{O}_3$ ; $\text{Fe}_x\text{O}_y$ ; $\text{SiO}_2$ ; $\text{MgCO}_3$ ; $\text{ZrSiO}_4$ ; $\text{BaSO}_4$ ; $\text{Th}_x\text{O}_y$ ; almost all inclusions show trace components of: Si, Cr, Fe, Ti, Mg, Ca, Al, K, Na, S, P, Nb, Cl, Zn, Ni	FIB-TEM, SEM, and EDS	Dobrzhinetskaya et al. 2001; 2003a
	Garnet-biotite-gneiss	Si, K, P, Cl glass (1-5 nm)	AEM, EDX	Hwang et al. 2006
	Dolomite marble	Ultrapotassic fluid inclusions (<500 nm); low in $\text{SiO}_2$	AEM, EDX	Hwang et al. 2006
	Garnet-quartz-clinopyroxene	K rich Si poor fluid/melt in intergranular pockets within a microdiamond aggregate	AEM, EDX	Hwang et al. 2006
	Dolomite marble	$\text{CaCO}_3$ (Fe, Mg) aragonite (10-100 nm) along with COH fluid inclusions	FIB-TEM, EDS	Dobrzhinetskaya et al. 2005
	Dolomite marble	$\text{CaCO}_3$ (aragonite), $\text{CaCO}_3$ , $\text{MgCO}_3$ ; N-bearing phase (5-250 nm)	FIB-TEM, EDS, and EELS	Dobrzhinetskaya et al. 2006b
Erzgebirge, Germany	Gneiss lenses within migmatites of gneiss-eclogite	Silicates, apatite, rutile and diamond, altogether are included in a former fluid/melt pocket	SEM, EDS, EBSD	Stöckhert et al. 2001
	Quartz-feldspathic gneiss	Solid inclusions (20-60 nm)*: $\text{SiO}_2$ , $\text{Al}_2\text{SiO}_5$ , $\text{KH}_2\text{PO}_4$ , $\text{Pb}_x\text{O}_y$ or $\text{PbCO}_3$ ; unknown stoichiometry phases*: Si, K, P, Ti, O or Si, O; Si, Fe and O	FIB-TEM, SEM, and EDX	Dobrzhinetskaya et al. 2003a
	Quartz-feldspathic gneiss	P/K rich silica glass	AEM, EDS	Hwang et al. 2005
	Quartz-feldspathic gneiss	Molecular $\text{H}_2\text{O}$ , $\text{OH}^-$ , $\text{CO}_3^{2-}$ and $\text{SiO}_2$ ; $\text{Pb}_x\text{O}_y$ or $\text{PbCO}_3$ ; $\text{Al}_2\text{SiO}_5$	Synchrotron infrared spectroscopy	Dobrzhinetskaya et al. 2006a
	Quartz-feldspathic gneiss	Silicates, apatite, rutile and diamond are included in former fluid/melt pockets located inside of garnet	SEM, EBSD, EDS	Stöckhert et al. 2009
	Garnet-phengite-quartz-feldspathic gneiss	Solid inclusions (5-20 nm)*: $\text{KAlSi}_3\text{O}_8$ ; $\text{Na}_2\text{SO}_4$ ; $\text{SiO}_2$ ; $\text{KAlSi}_3\text{O}_8$ ; $\text{CaCO}_3$ ; $\text{ZrSiO}_4$ ; $\text{BaCO}_3$ occurring inside of the diamond or at the diamond-diamond interface, almost all inclusions show trace amounts of some of these elements: Fe, Al, Cl, Mg, Ti, Pb, K, Ca, P, Cr	FIB-TEM, SEM, EDS and EELS	Dobrzhinetskaya et al. 2013
Lago di Cignana, Italian Western Alps	Oceanic metasedimentary rocks	Mg-calcite, rutile, graphite like amorphous carbon, $\text{SO}_4^{2-}$ ; $\text{HCO}_3^-$ ; $\text{CO}_3^{2-}$ ; $\text{Si}(\text{OH})_4$ monomer; deprotonated monomers $\text{SiO}(\text{OH})_3^-$ and $\text{SiO}_2(\text{OH})_2^{2-}$	Raman and electron microprobe	Frezzotti et al. 2011

2537

2538 **Table 3.** Inclusions reported in microdiamonds from different UHPM terranes (\* - crystal  
2539 structure is not determined due to extremely small size of inclusions).